Renewable polymer materials from bicyclic sugar derivatives

A Dissertation
SUBMITTED TO THE FACULTY OF
UNIVERSITY OF MINNESOTA
BY

James J. Gallagher

IN PARTIAL FULFILLMENT OF THE REQUIREMENTS
FOR THE DEGREE OF
DOCTOR OF PHILOSOPHY

Marc A. Hillmyer, Theresa M. Reineke

May, 2016

Acknowledgements

Many thanks to all those who helped along the way.
Marc, Theresa, John, Lidia, Laura, Debbie, Ralm, Will B., Haley, Jeff, Alex, Tessie, Leon, Will S., Angelika, Joe, Yaoying, and Zach.

To Michael and Renée

Abstract

Sugar derivatives are excellent candidates for the building blocks of biobased plastics. This thesis focuses on the preparation of new monomers derived from bicyclic sugar derivatives and the polymerization thereof to afford useful polymer materials. The first area of research presented is the preparation of two new monovinyl monomers acetylated methacrylic isosorbide and acetylated acrylic isosorbide (AMI and AAI). PAMI and PAAI prepared by radical polymerization of were found to have high T_g and good thermal stability. Reversible Addition Fragmentation chain Transfer polymerization was used to prepare PAMI and PAAI block copolymer samples with low T_g polyacrylates. These block copolymers were investigated as pressure sensitive adhesives and were found to exhibit desirable adhesive properties consistent with high shear removable pressure sensitive adhesives.

The second area of research focuses on the synthesis and polymerization of two new dimethacrylate monomers from glucarodilactone and mannarodilactone (GDMA and MDMA). Thermally initiated free radical polymerization of these monomers in the bulk afforded highly crosslinked and rigid thermoset materials. Tensile testing of PGDMA demonstrated mechanical properties similar to those reported for commercially available poly(dimethacrylates) from rigid monomers. PGDMA was found to degrade to water-soluble components after 17 days in the presence of base, but remained stable under acidic and neutral conditions. Applications investigated were P(GDMA-*co*-MDMA) coatings and copolymer microspheres from GDMA and methyl methacrylate.

Table of Contents

Chapter 1: Introduction 1

1.1 Introduction 2

1.2 Isosorbide 4

1.2.1 Structure of isosorbide and related dianhydrohexitols 4

1.2.2 Isosorbide production 6

1.2.3 Isosorbide derivatives 7

1.2.4 Step growth polymers incorporating isosorbide 9

1.2.5 Bifunctional isosorbide derivatives as crosslinking agents in thermoset polymers 12

1.2.6 Linear chain growth polymers from isosorbide 14

1.3 Glucarodilactone, mannarodilactone, and polymers thereof 15

1.3.1 Dilactone structure and preparation 15

1.3.2 Polymers derived from dilactones 17

1.4 Thesis outline 20

1.5 References 21

Chapter 2: Isosorbide-derived polymethacrylates 25

2.1 Introduction 26

2.2 Results and Discussion 28

2.2.1 Synthesis of AMI 28

2.2.2 Free radical polymerization of AMI 34

2.2.3 PAMI-CTA via RAFT polymerization 37

2.2.4 PAMI-*b*-PnBA 45

2.3 Conclusion 48

2.4 Experimental 48

2.5 References 53

Chapter 3: Acrylic triblock copolymers incorporating isosorbide for pressure sensitive adhesives 57

3.1 Introduction 58

3.2 Results and Discussion 61

3.2.1 Synthesis of AAI 61

3.2.2 Free radical polymerization of AAI 65

3.2.3 PAAI-PnBA-PAAI and PAAI-PEHA-PAAI via RAFT polymerization 67

3.2.4 Thermal, morphological, and mechanical characterization of triblock copolymers. 79

3.2.5 Adhesive performance of triblock copolymers 84

3.2.6 Dynamic mechanical analysis 88

3.3 Conclusion 93

3.4 Experimental 93

3.5 References 99

Chapter 4: Degradable Thermosets from Sugar-Derived Dilactones ..105

4.1 Introduction 106

4.2 Results and Discussion 109

4.2.1 Synthesis of GDMA and MDMA 109

4.2.2 Bulk polymerization of GDMA 110

4.2.3 Degradation of PGDMA 113

4.2.4 PGDMA and P(GDMA-*co*-MDMA) films 116

4.2.5 PGDMA microspheres by precipitation polymerization 122

4.3 Conclusion 128

4.4 Experimental 129

4.5 References 133

Bibliography 136

Appendix 145

List of Figures

Chapter 1

1.1 Structure of isosorbide and illustration of intermolecular hydrogen bonding of the *endo* hydroxyl. 5

1.2 Dianhydrohexitols isosorbide, isomannide, and isoidide. 5

1.3 A) Twofold dehydration of sorbitol to isosorbide; B) One pot approach to converting cellulose to isosorbide. 6

1.4 Isosorbide derivatives. 8

1.5 Selective acetylation of isosorbide. (a) dicyclocarbodiimide, dimethylamino pyridine, acetic acid; (b) PbO, acetic anhydride. 9

1.6 PEIT produced from isosorbide, ethylene glycol, and terephthalic acid. 11

1.7 PIC product Durabio™ and property comparison to poly(methyl methacrylate) and traditional polycarbonate. 12

1.8 Bifunctional isosorbide derivatives isosorbide bismethacrylate and isosorbide diglycidyl ether. 13

1.9 A) Synthesis of VDT monomers B) polyVDT polymers prepared via RAFT. 15

1.10 (A) Structures of glucarodilactone and mannarodilactone; (B) Simplified pathways to isosorbide and glucarodilactone from glucose via reduction and oxidation, respectively. 16

1.11 Synthesis of (A) mannarodilactone and (B) glucarodilactone. 17

1.12 Polyhydroxy polyamide synthesis from dilactones. 18

1.13 Polyurethanes derived from dilactones. 19

1.14 Preparation of glucarodilactone undecenoate and polymerization via ADMET. 20

Chapter 2

2.1 ^{1}H NMR spectrum of crude product mixture of $Sc(OTf)_3$ catalyzed acetylation of isosorbide with acetic anhydride. 30

2.2 ATR-FTIR of neat A-*exo*-MI. 32

2.3 ^{1}H NMR spectrum of A-*exo*-MI in $CDCl_3$. 32

2.4 ^{1}H NMR spectrum of A-*endo*-MI in $CDCl_3$. 33

2.5 ^{1}H NMR spectra in $CDCl_3$ of the vinyl region for a) A-*endo*-MI, b) A-*exo*-MI, and c) 4:1 mixture of A-*exo*-MI : A-*endo*-MI. 34

2.6 Conversion vs time for the free radical polymerization of AMI in $CHCl_3$. 35

2.7 TGA in air at 180 °C of PAMI prepared by free radical polymerization. 36

2.8 DSC of PAMI (M_n = 88.9 kg mol^{-1}) in N_2. 36

2.9 M_n and $Đ$ as a function of conversion for RAFT polymerization of AMI. 41

2.10 ^{1}H NMR spectrum of PAMI-CTA (14) in $CDCl_3$. 42

2.11 ^{1}H NMR spectrum of a) PAMI-CTA (14) and b) ene-PAMI-CTA (14) in $CHCl_3$. 43

2.12 DSC of PAMI-CTA. 45

2.13 Plot of T_g vs. 1/M_n for PAMI-CTA, PAMI, and PA-*endo*-MI. 45

2.14 THF-SEC of PAMI-*b*-PnBA (19-60) and PAMI-CTA (19) prepared by RAFT polymerization. 47

2.15 DSC of PAMI-*b*-PnBA in N_2. 47

Chapter 3

3.1	^{1}H NMR of AAI in $CDCl_3$.	63
3.2	^{13}C NMR of AAI in $CDCl_3$.	63
3.3	ATR FTIR of AAI.	64
3.4	TGA of AAI.	65
3.5	DSC of AAI.	65
3.7	DSC of PAAI prepared by free radical polymerization.	67
3.8	RAFT polymerization of AAI.	68
3.9	^{1}H NMR of PnBA 27k in $CDCl_3$.	71
3.10	^{1}H NMR of PEHA 45k in $CDCl_3$. End group resonances in insert.	72
3.11	THF SEC of PnBA 27k macro-CTA and PAAI-PnBA-PAAI (63k, 54%).	75
3.12	^{1}H NMR of PAAI-PnBA-PAAI (63k, 54%) in $CDCl_3$.	76
3.13	THF SEC with differential refractive index (dRI) detector of A) PAAI-PnBA-PAAI and B) PAAI-PEHA-PAAI triblock copolymers.	77
3.14	^{1}H NMR in $CDCl_3$ of PAAI-PnBA-PAAI (60k, 17%) after alcoholysis.	78
3.15	THF SEC of PAAI-PnBA-PAAI (60k, 17%) before and after alcoholysis.	79
3.16	TGA of PAAI-PnBA-PAAI (60k, 17%).	80
3.17	TGA of PAAI-PEHA-PAAI (54k, 14%).	80
3.18	DSC of PAAI-PnBA-PAAI and PAAI-PEHA-PAAI triblock copolymers	81
3.19	SAXS patterns for PAAI-PnBA-PAAI and PAAI-PEHA-PAAI triblock copolymers.	82

3.20 Representative stress vs. strain curves for PAAI-PnBA-PAAI (60k, 17%) and PAAI-PEHA-PAAI (54k, 14%). 84

3.21 Adhesive performance of PAAI-PnBA-PAAI and PAAI-PEHA-PAAI triblock copolymers. A) 180° peel test; B) loop tack test; C) shear test. 86

3.22 DSC of PAAI-PEHA-PAAI (54k, 14%) with rosin ester tackifier. 88

3.23 Adhesion testing of PAAI-PEHA-PAAI (54k, 14%) plus rosin ester tackifier. A) loop tack test; B) 180° peel test. 88

3.24 Time temperature superposition and William–Landel–Ferrey fit for DMA of PAAI-PEHA-PAAI (54k, 14%). 90

3.25 Time temperature superposition and William–Landel–Ferrey fit for DMA of PAAI-PnBA-PAAI (60k, 17%). 90

3.26 Attempted time temperature superposition for DMA of PAAI-PEHA-PAAI (54k, 14%). 91

3.27 Attempted time temperature superposition for DMA of PAAI-PnBA-PAAI (60k, 17%). 91

3.28 A) DMA of PAAI-PnBA-PAAI (60k, 17%) and PAAI-PEHA-PAAI (54k, 14%). 92

Chapter 4

4.1 TGA data for GDMA. 111

4.2 FT-IR spectra of GDMA and PGDMA 112

4.3 Tensile testing for various samples of PGDMA. 113

4.4 Commercially available rigid dimethacrylates bis-GMA and UDMA. 113

4.5 Stability of PGDMA and PUDMA in aqueous media. 114

4.6 ^{1}H-NMR spectra of A) crude PGDMA degradation products; B) high MW degradation products isolated by dialysis. 115

4.7 DSC traces of GDMA/MDMA mixtures. 118

4.8 Isothermal DSC trace of GDMA:MDMA (3:2) mixture with 1.5 wt% BPO at 95 °C. 120

4.9 Contact angle measurements for P(GDMA-*co*-MDMA) films. 120

4.10 Image of a salt plate containing a PGDMA film. 121

4.11 P(GDMA-*co*-MDMA) films with Sudan III dye before and after being immersed in an aqueous solution for 14 hours. 122

4.12 SEM images of P(GDMA-*co*-MMA) microparticles. 125

4.13 SEM images of P(GDMA-*co*-MMA) (10:3) microspheres formed at different monomer concentrations. 127

4.14 DSC of P(GDMA-*co*-MMA) microspheres. 128

List of Tables

Chapter 2

2.1 Comparison of molar mass and thermal properties of PAMI vs PA-*endo*-MI. 37

2.2 RAFT polymerization of AMI with different CTAs. 39

2.3 PAMI-CTA and PAMI-*b*-PnBA sample information. 44

Chapter 3

3.1 Screening RAFT agents for PAAI polymerization 68

3.2 PAAI-PnBA-PAAI and PAAI-PEHA-PAAI molar mass data. 73

Chapter 4

4.1 Formulations and characterization of P(GDMA-*co*-MMA) microspheres formed by precipitation polymerization. 126

Chapter 1: Introduction

1.1 Introduction

The modern era is perhaps best described as the plastic age. Plastics are ubiquitous and imagining a developed world without them is an arduous mental exercise. Since the advent of synthetic polymer chemistry in the 19th and early 20th century, polymer materials (plastics) have come to occupy an impressively wide range of applications. As such the global market for plastics large, with an estimated global consumption of 3×10^8 t in 2013.[1] Major application areas for polymers are packaging, construction, automotive, and electronics; all pillars upon which modern society is built. As the global population continues to increase, so too will the demand for plastics. Demand will be driven further by an increase in per capita consumption as more of the global population enters the developed world. Currently plastics are almost entirely derived from non-renewable resources, namely petroleum. Given the essential role of plastics in the modern era, their non-renewability is cause for concern.

Recently bio-sourced raw materials have garnered significant attention as alternatives to conventional petroleum resources. In addition to being renewable, biobased resources are also abundant with Earth's annual production of renewable biomass estimated to be 1.8×10^{11} t.[2] For comparison, the total production of petroleum was approximately 3.9×10^9 t in 2010.[3] The three main classes of biomass raw materials are carbohydrates, lignin, and triglycerides. Carbohydrates include small molecule sugars and natural polymers thereof, namely cellulose and starch, and account for ~75% of total biomass.[2] While they are arguably underutilized as raw materials, sugars are a major component of the current chemical industry. Sucrose (i.e., table sugar) is the most produced

sugar with global production in 2014 of 1.75×10^8 t.[4] This is approximately the same size as the annual production capacity of ethylene, which was estimated to be 1.76×10^8 t in 2015.[5] Additionally, sugars offer functionality such as high heteroatom content and stereochemistry not typically afforded by petroleum derivatives. Therefore, when looking to biobased resources for the chemical feedstocks of the future, carbohydrates are a lead candidate for investigation. It should be noted that the chemical industry as a whole relies heavily on petroleum and that the interest in renewable alternatives is not limited to plastics.

Although renewable plastics currently make up a relatively small share of the market, there are a few successful examples worth noting. One approach to incorporating renewable feedstocks into polymers is via a drop-in replacement strategy, whereby an existing petroleum derived building block is replaced with the same chemical but derived from a renewable source. A premier example of this approach is the PlantBottle™ from Coca-Cola which is up to 30% renewably sourced. PlantBottle™ is a poly(ethylene terephthalate) (PET) product that uses ethylene glycol derived from plants as a drop in replacement for traditional ethylene glycol. Another important example of a drop-in replacement strategy is using ethylene from bio-sourced ethanol in the production of green polyethylene. Increasing the renewability of PET and polyethylene are significant achievements as they are two of the highest volume polymers.[6] An alternative strategy is to use a renewable feedstock to make a new-to-the-world plastic. A key advantage of this approach is the ability to impart unique properties not typically afforded by petroleum derived polymers. Polylactide (PLA) is by far the most successful example of a new-to-

the-world plastic from a renewable resource. This polyester comes from the polymerization of lactide, which is a dimer of lactic acid produced by fermentation of sugars. The global demand for PLA was estimated to be 3.6×10^5 t in 2013.[7] PLA is most often compared to polystyrene due to its rigidity and optical clarity, and finds use in biomaterials, fibers, and packaging applications.[8] PLA is compostable, a unique feature relative to conventional polymers and offers an alternative end-of-use option to conventional recycling.

The research in this thesis is motivated by the need for renewably sourced plastics and the promise of sugars as raw materials. The work described herein focuses on the production of new monomers based on known bicyclic sugar derivatives and the incorporation thereof in to new polymer materials. The following sections of this chapter will introduce the bicyclic sugar derivatives of interest and provide a summary of their properties, methods of production, and applications in the field of polymer chemistry.

1.2 Isosorbide

1.2.1 Structure of isosorbide and related dianhydrohexitols

Isosorbide is a rigid bicyclic diol consisting of two fused furan rings (Figure 1.1). The fused rings adopt a puckered conformation resulting in an *endo* face (interior to the pocket) and *exo* face (exterior to the pocket). Each furan ring contains a hydroxyl group with one being in the *endo* position and one being in the *exo* position. The *exo* hydroxyl group is relatively unencumbered, while the *endo* hydroxyl rests above the fused ring system and is more sterically restricted. The position of the *endo* hydroxyl group allows for intramolecular hydrogen bonding with the ethereal oxygen of the opposing furan. As a

result, the *endo* hydroxyl is more nucleophilic. The distance of the *exo* hydroxyl group from its opposing furan ring precludes intermolecular hydrogen bonding.

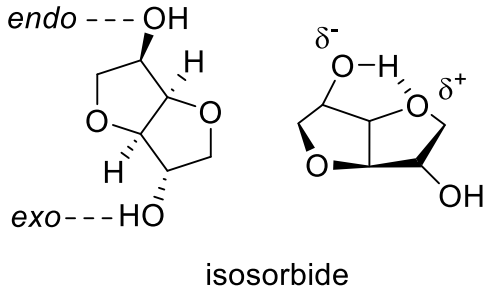

isosorbide

Figure 1.1. Structure of isosorbide (left) and illustration of intermolecular hydrogen bonding of the *endo* hydroxyl (right).

Isosorbide belongs to the family of dianhydrohexitols, of which there are two other members: isomannide and isoidide (Figure 1.2). All three share the same fused bicyclic core with different hydroxyl stereochemistry. Isomannide has both hydroxyl groups in the *endo* position, while isoidide has both hydroxyl groups in the *exo* position. While the parent sugars of isosorbide and isomannide are naturally abundant (glucose and mannose, respectively), isoidide can only be obtained synthetically by isomerization of either isosorbide or isomannide. These dianhydrohexitols have been studied for over a century and continue to garner significant attention for use in a variety of applications. Currently isosorbide is the only one that is commercially relevant.

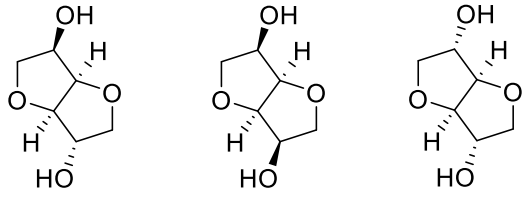

isosorbide isomannide isoidide

Figure 1.2. Dianhydrohexitols isosorbide, isomannide, and isoidide.

1.2.2 Isosorbide production

The most well-known method for producing isosorbide is the twofold dehydration of sorbitol (Figure 1.3A). Sorbitol is produced on a large scale globally via the hydrogenation of glucose and is relatively inexpensive (~1.7×10^6 t and ~$1/kg in 2011).[9] A common approach for the conversion of sorbitol to isosorbide is via strong mineral acid catalysts.[10] Heterogeneous catalysts such as zeolites or polymer bound acids have been reported as alternatives.[11–13] These types of catalysts carry significant advantages by allowing for continuous production and facile separations. The current global leader in isosorbide production is the French agricultural company Roquette, which recently completed construction of the world's largest isosorbide production plant.[14] The facility can produce high purity polymer grade isosorbide with an annual capacity of 2.0×10^4 t. This isosorbide product is marketed under the brand name Polysorb for use in a variety of polymer applications.

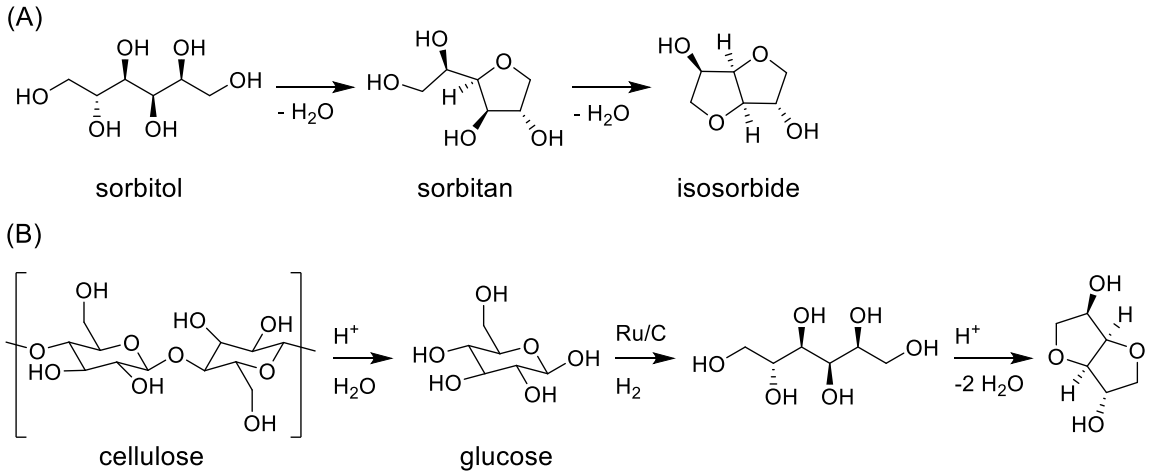

Figure 1.3. A) Twofold dehydration of sorbitol to isosorbide; B) One pot approach to converting cellulose to isosorbide.

While the conversion of sorbitol to isosorbide has clearly proven to be a viable process, the intimate connection of sorbitol to the global food supply is cause for concern. Sorbitol is currently produced from corn, and the major end use for sorbitol is as a food sweetener. Thus the direct conversion of non-edible cellulose to isosorbide is an appealing alternative. A notable recent example in this area is the work of Yamaguci et al which described the one pot conversion of cellulose to isosorbide in yields up to 56% in the presence of amberlyst 70 and Ru/C (Figure 1.3B).[15] In this case, sorbitol is formed *in situ* via acid catalyzed hydrolysis of cellulose to glucose followed by metal catalyzed hydrogenation. Subsequent acid catalyzed dehydration of sorbitol affords the desired isosorbide product. A key aspect of this approach is the ability of amberlyst 70 to serve as an acid catalyst for both hydrolysis of cellulose and dehydration of sorbitol. The use of heterogeneous catalysts makes this approach particularly appealing for scalable production.

1.2.3 Isosorbide derivatives

Derivatives of isosorbide have been investigated for a wide range of applications (Figure 1.4). Perhaps the most well-known examples are the isosorbide di and mono nitrates which are commonly prescribed as vasodilators to prevent chest pain. Use of isosorbide dinitrate as a vasodilator was first reported in 1939[16] and is currently on the World Health Organization's List of Essential Medicines.[17] Another notable isosorbide derivative is dimethyl isosorbide which is high boiling solvent that finds use in personal care and pharmaceutical applications.[18,19] Interestingly, a green method for producing dimethyl isosorbide was recently reported, whereby isosorbide was methylated using

dimethyl carbonate in the presence of a base to afford the desired product in nearly quantitative yield.[19] Diesters of isosorbide can be readily formed by esterification between isosorbide and carboxylic acids and are marketed as green alternatives to phthalate-based plasticizers for polyvinyl chloride. Diacids, diisocyanates, and diamines derived from isosorbide have also been reported.[18,20] Although the last three examples are not yet commercially available, their potential impact is considerable given the utility of diacids, diisocyanates, and diamines as polymer building blocks.

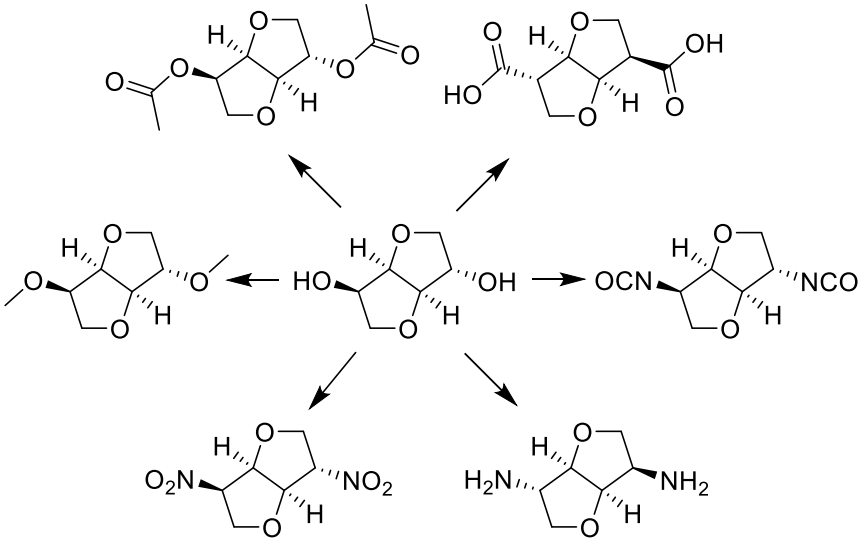

Figure 1.4. Isosorbide derivatives.

The unique environment of each hydroxyl group of isosorbide results in differences in reactivity that can be exploited synthetically. For example, esterification of isosorbide via a Steglich esterification occurs predominantly at the *exo* position due to the steric bulk of the O-acyl isourea intermediate (Figure 1.5).[21] By contrast, esterification with an anhydride in the presence of a Lewis acid catalyst occurs predominantly at the more nucleophilic (albeit more sterically hindered) *endo* position.[22] In addition to differences in reactivity, monofunctional isosorbide derivatives can possess different physiochemical

properties depending on regiochemistry that allow for separation. For example, the isosorbide monoacetate regioisomers can be separated relatively easily based on differences in polarity via column chromatography or distillation. The ability to selectively functionalize and isolate regioisomers allows for preparation of asymmetric isosorbide derivatives and elucidation of structure property relationships. The robust and active synthetic literature surrounding isosorbide provides a solid foundation on which to build a next generation platform chemical.

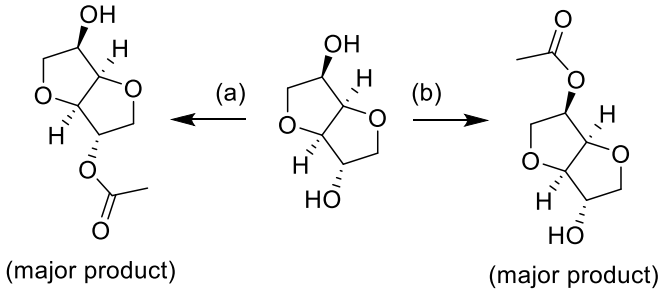

Figure 1.5. Selective acetylation of isosorbide. (a) dicyclocarbodiimide, dimethylamino pyridine, acetic acid; (b) PbO, acetic anhydride.

1.2.4 Step growth polymers incorporating isosorbide

The diol structure of isosorbide makes it directly applicable as a monomer for step growth polymerizations. The use of isosorbide in this context is well known and has been reviewed extensively.[10,18,20,23–27] Examples for nearly every major class of step growth polymer incorporating isosorbide exist, including polyesters, polycarbonates, polyethers, polyurethanes and polyamides. Rather than an exhaustive review, a few illustrative examples will be discussed here. Poly(ethylene-*co*-isosorbide terephthalate) (PEIT) is one of the most studied isosorbide polymers (Figure 1.6). The amount of isosorbide

incorporated into PEIT has a dramatic impact on glass transition temperature (T_g) and crystallinity. Storbick and Ballauff prepared samples of PEIT with 0–100 mol% isosorbide as the diol component and reported T_g ranging from 85–197 °C, respectively. The increase in T_g is due to the bicyclic structure of isosorbide which is significantly more rigid than ethylene glycol. They also determined that the melting point (T_m) decreased from 261 to 221 °C for samples with 0–20 mol% isosorbide, while samples with 34–100 mol% isosorbide were amorphous. The asymmetry of isosorbide results in a regioirregular polymer and suppresses crystallinity. Indeed, poly(isoidide terephthalate) was reported to be crystalline. Furthermore, poly(isosorbide terephthalate) (PIT) was reported to be thermally stable at temperatures up to 360 °C indicating that incorporating isosorbide does not negatively impact thermal stability. The ability to vary T_g and crystallinity over such a wide range means PEIT could be utilized in a variety of different applications. The high T_g and thermal stability of PIT are comparable to known high performance polymers such as poly(ether imide) and poly(phenylene ether).[20] At ~30 mol% isosorbide composition, PEIT is amorphous with a T_g ~ 115 °C and could therefore serve as an alternative to polymers with similar properties such as polycarbonates and poly(methyl methacrylate). At ~10 mol% isosorbide, the relatively modest increase in T_g means PEIT outperforms PET in hot-fill packaging applications. Hot-fill packaging, wherein a liquid (e.g. juice, beverage etc.) is sterilized with heat and bottled while hot to improve shelf life and avoid the need for added preservatives, is the most often cited application for PEIT.

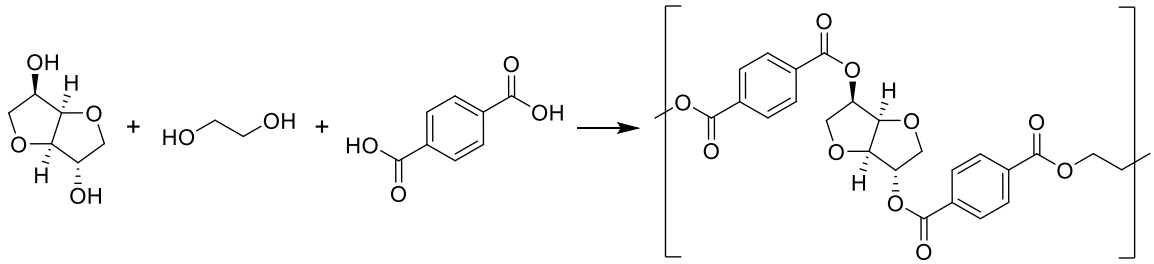

Figure 1.6. PEIT produced from isosorbide, ethylene glycol, and terephthalic acid.

Poly(isosorbide carbonate) (PIC) is another important isosorbide containing step growth polymer (Figure 1.7). The interest in polycarbonates from isosorbide is in part driven by demand for alternatives to bisphenol A. Isosorbide is an appealing candidate for a bisphenol A substitute as both chemicals are rigid diols capable of producing polycarbonates with high T_g (~150 °C).[20] PIC is produced by Teijin Chemical and Mitsubishi Chemical with the latter's product market under the trade name Durabio™ (Figure1.7). As with PEIT, PIC is often comprised of isosorbide and another diol. A wide variety of comonomer diols have been reported for PIC in both the academic and patent literature.[20,28–30] As opposed to PEIT where the overall isosorbide content is typically low, isosorbide content for PIC is usually > 65 mol%. The choice of comonomer can significantly impact the performance of PIC. For example, judicious selection of diol comonomer can afford PIC that is relatively hydrophobic and shows excellent resistance to boiling water.[30] A notable advantage of PIC over traditional polycarbonate is desirable optical properties. Mitsubishi advertises Durabio™ as having high performing optical properties comparable to poly(methyl methacrylate) while maintaining the thermal stability of conventional polycarbonate (Figure 1.7).[31,32] These qualities make PIC useful for electronic display applications such as in automotive interiors and cell phones.

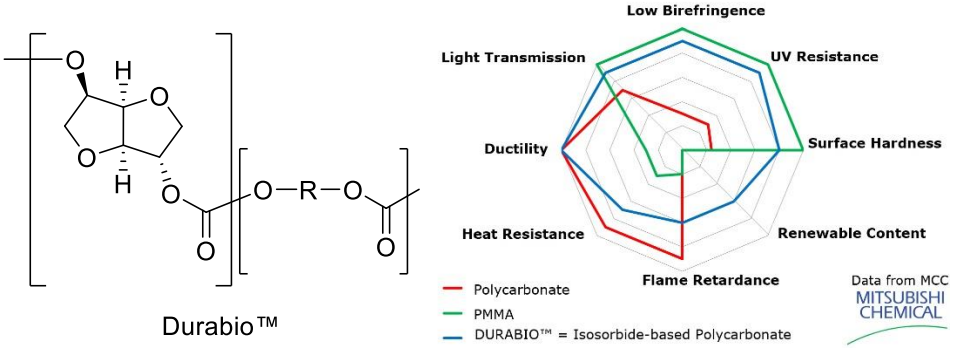

Figure 1.7. PIC product Durabio™ and property comparison to poly(methyl methacrylate) and traditional polycarbonate.[33]

PEIT and PIC are to date the most successful applications of isosorbide in polymer chemistry. Along with a myriad of other examples covered in several reviews, the role of isosorbide as a useful building block in step growth polymerizations is firmly established. Given the desirable properties such as high T_g, thermal stability, and optical clarity, one would expect isosorbide to be a useful component in chain growth type polymerizations as well. Incorporation into chain growth polymers will provide access to new applications for isosorbide and therefore add value to this inexpensive biobased feedstock.

1.2.5 Bifunctional isosorbide derivatives as crosslinking agents in thermoset polymers

Isosorbide has also been incorporated into chain growth type polymers. This requires additional functionalization to install an appropriate functional group. The most common approach has been to functionalize both alcohols to generate a bifunctional structure. This has the benefit of synthetic simplicity, however it limits the applicability to thermosetting applications. For example, isosorbide bismethacrylate was used in a vinyl ester resin formulation as a crosslinking agent with styrene as the comonomer (Figure 1.8).[34] The authors noted a significantly lower viscosity for the resin derived from isosorbide bismethacrylate than that of an analogous commercial vinyl ester resin. After

curing, the resultant thermoset materials were observed to have excellent thermal stability and comparable flexural strength and modulus to commercial high performance vinyl ester resin materials.

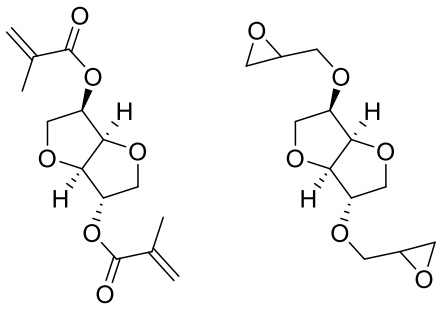

Figure 1.8. Bifunctional isosorbide derivatives isosorbide bismethacrylate (left) and isosorbide diglycidyl ether (right).

Another example of a bifunctional isosorbide crosslinking agent is isosorbide diglycidyl ether which has been used in amine cured epoxy resins (Figure 1.8).[35,36] A notable challenge associated with this bisexpoxide is its synthesis. Ideally the product could be produced by reaction with epichlorohydrin, analogous to commercial bisexpoxides such as bisphenol A diglycidyl ether. However, relatively harsh reaction conditions are required resulting in undesirable coloration and oligomeric products. Currently the most efficient route for obtaining pure monomeric isosorbide diglycidyl ether is first forming the bisallyl isosorbide derivative with allyl bromide followed by oxidation with *m*-chloroperbenzoic acid.[36] The cured isosorbide bisepoxy amine resins exhibited a T_g of ~70 °C which was significantly lower than analogous cured resins from bisphenol A glycidyl ether (~130 °C). The tensile strength, flexural modulus, and impact strength for the cured isosorbide bisepoxy resins were all significantly higher than the cured resins from bisphenol A

glycidyl ether, suggesting that these materials could provide superior mechanical performance if the lower operating temperature is acceptable.

1.2.6 Linear chain growth polymers from isosorbide

Linear chain growth polymers incorporating isosorbide have only recently been reported in the literature. The ability to incorporate isosorbide into a polymer by such a mechanism is appealing since controlled chain growth polymerization methods can be used to construct polymers with well-defined molar mass and architectures. The first example of such polymers in the open literature is the work of Beghdadi et al. which reports the synthesis and polymerization of N-vinyl triazole dianhydrohexitol (VDT) monomers from isosorbide, isomannide, and isoidide (Figure 1.9).[37] The monomers were prepared by alkylation of a dianhydrohexitol with propargyl bromide followed by chromatographic separation to isolate the desired monoallyl products (Figure 1.9A). A copper catalyzed click reaction with mesyl azidoethanol followed by reductive elimination afforded the final VDT monomers. The researchers then used Reversible Addition Fragmentation chain Transfer (RAFT) polymerization to prepare a series of polyVDT polymers with different dianhydrohexitol pendant groups (Figure 1.9B). Interestingly, significant differences were observed between the two isosorbide derived polymers depending on whether the *endo* or *exo* hydroxyl group was exposed. Samples with the *exo* hydroxyl group exposed had T_g = 71 °C and were soluble in water, while those with the *endo* hydroxyl group exposed had a T_g = 118 °C and were insoluble in water. Monovinyl isosorbide derivatives bearing the more conventional acrylic and methacrylic moieties have also been reported recently.

Detailed description of these monomers and their respective polymers are covered in chapters 2 and 3.

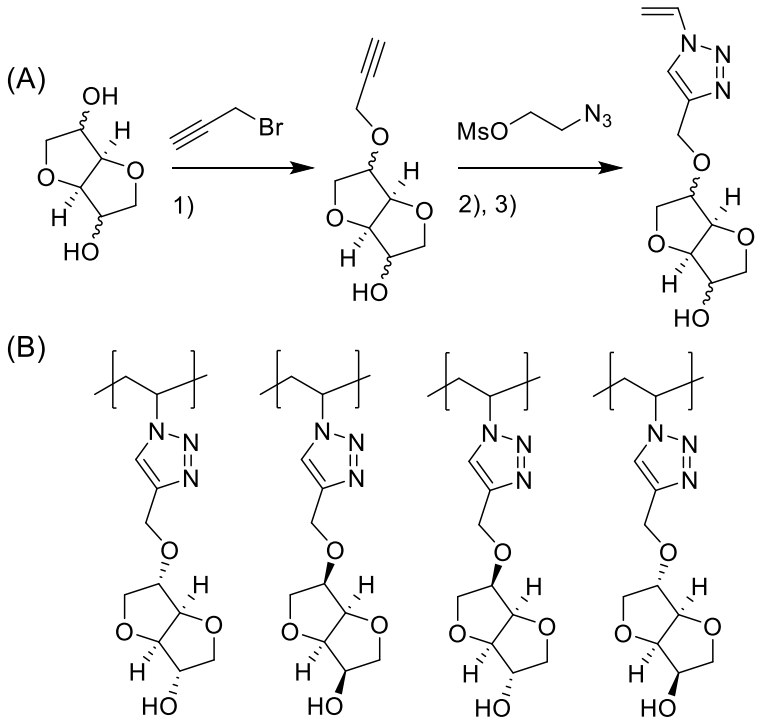

Figure 1.9. A) Synthesis of VDT monomers 1) NaOH, column chromatography; 2) copper iodide triethylphosphite, diisopropylamine; 3) NaI, 1,8-diazabicycloundec-7-ene, column chromatography. B) polyVDT polymers prepared via RAFT.

1.3 Glucarodilactone, mannarodilactone, and polymers thereof

1.3.1 Dilactone structure and preparation

Glucarodilactone and mannarodilactone are the lactone analogues of isosorbide and isomannide, respectively (Figure 1.10A). Whereas the dianhydrohexitols are synthesized by reduction of the respective sugars followed by twofold dehydration, the dilactones are prepared by oxidation of the parent sugar followed by twofold dehydration (Figure 1.10B). The result is a fused bicyclic structure composed of two dilactone rings. Similar to the

dianhydrohexitols, the identity of the parent sugar determines the stereochemistry of the hydroxyl groups. Glucarodilactone has one hydroxyl group in the *endo* position and one in the *exo* position, while mannarodilactone has both hydroxyl groups in the *endo* position. The hypothetical isoiododilactone with both hydroxyl groups in the *exo* position has not been reported in the open literature.

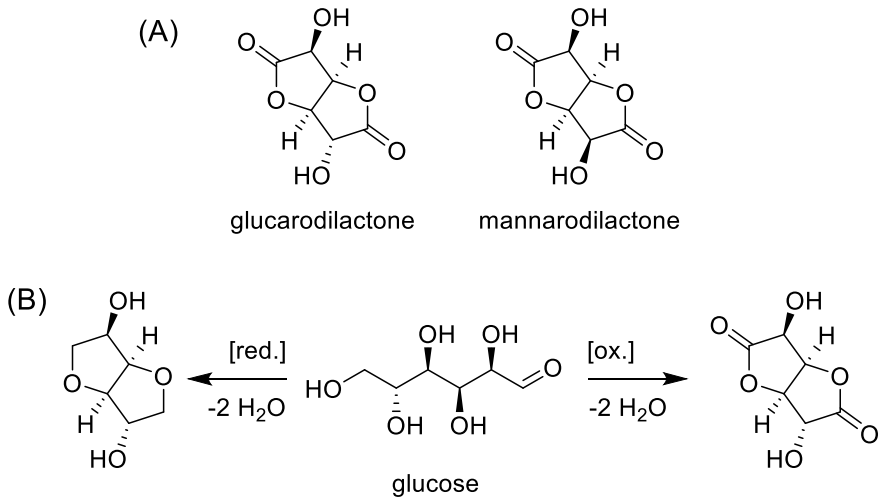

Figure 1.10. (A) Structures of glucarodilactone and mannarodilactone; (B) Simplified pathways to isosorbide and glucarodilactone from glucose via reduction and oxidation, respectively.

While the literature surrounding the dianhydrohexitols is rather robust, the dilactones are relatively underexplored. The lack of commercial availability of the dilactones has limited their application in polymer materials. Mannarodilactone can be prepared by treating mannitol with nitric acid to afford a crude mixture of oxidized products (Figure 1.11A).[38–40] The desired dilactone is then isolated via crystallization. The initial stage of the reaction is accompanied by the evolution of large volumes of noxious gasses and the overall yield is typically low (~10–30%). Recently a facile and scalable method for preparing glucarodilactone was reported by Gehret et al.[41] The first step is the

acidification of calcium glucarate followed by intramolecular esterification of glucaric acid driven by azeotropic removal of the water byproduct (Figure 1.11B). After evaluating different acid catalysts and azeotrope solvents, it was found that sulfuric acid and methyl isobutyl ketone afforded the best combination of overall yield and purity, with up to 73% yield on a 22 kg scale reaction. Notably, glucarodilactone has been considered as a potentially useful biobased feedstock. Glucaric acid was listed as a top 12 value added chemical from biomass by the US Department of Energy in 2004, with glucarodilactone highlighted as a key derivative.[42]

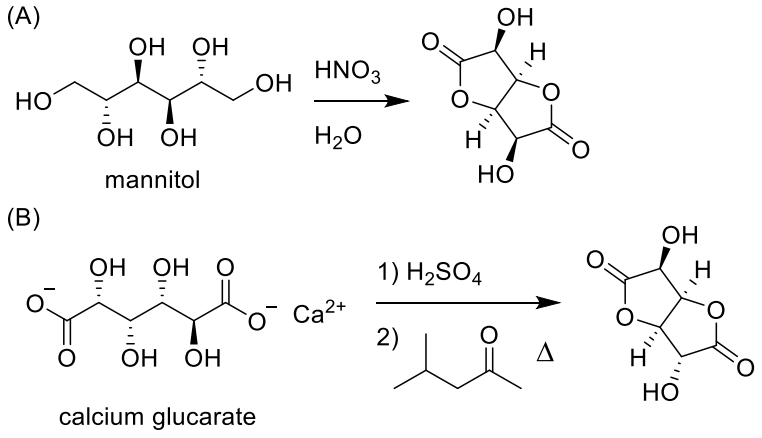

Figure 1.11. Synthesis of (A) mannarodilactone[38–40] and (B) glucarodilactone.[41]

1.3.2 Polymers derived from dilactones

The presence of two lactone rings affords another layer of functionality in addition to the hydroxyl groups of the dilactones. As a result, the dilactones have the unique ability to function as both a bis-electrophile via the lactones and a bis-nucleophile via the alcohols. An example of the former function is the polymerization with a diamine to form a family of polymers known as polyhydroxy polyamides (Figure 1.12).[38–40,43,44] These polymers can

be water soluble depending on the hydrophilicity of the diamine and are reported to degrade in aqueous environments in the presence of acid. Notably, the polyhydroxy polyamides do not melt or cross a T_g without first undergoing thermal decomposition which limits their potential application as thermoplastics. Liu et al have investigated a potential application of polyhydroxy polyamides as gene delivery agents and noted that the hydroxyl stereochemistry has an effect on gene expression.[39]

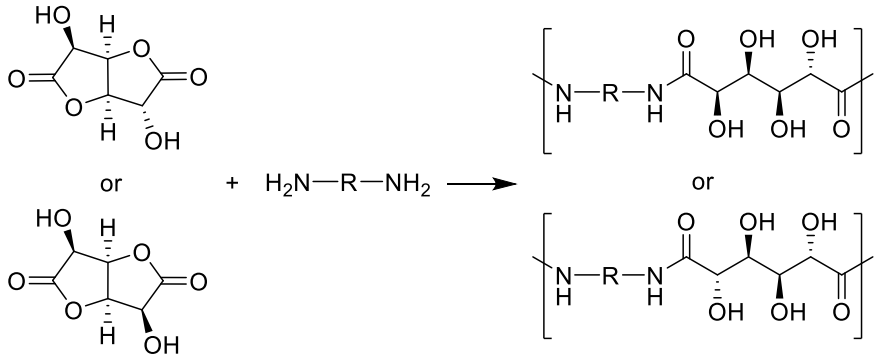

Figure 1.12. Polyhydroxy polyamide synthesis from dilactones.

An example of utilizing the diol functionality of the dilactones in polymer synthesis was reported by Hashimoto et al. in the tin catalyzed polymerization of glucarodilactone and mannarodilactone with different diisocyanates (Figure 1.13).[45,46] The resulting polymers consisted of dilactone structures within the polymer backbone. As with the polyhydroxy polyamides, the polyurethanes were found to have inaccessible melting transitions due to the premature onset of thermal decomposition at about 165 °C. Solution cast films of the polyurethanes were found to be degradable in phosphate buffered saline solutions at pH 4–8, with degradation being significantly faster in basic conditions. The researchers proposed a degradation mechanism of hydrolytic ring opening of the lactones followed by cleavage of the urethane bonds.

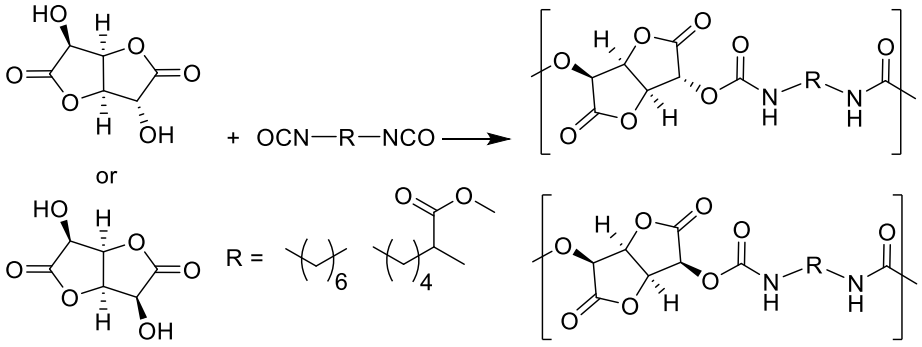

Figure 1.13. Polyurethanes derived from dilactones.

Polyesters incorporating the dilactone structural unit in the polymer backbone have also been reported.[47] Instead of direct condensation between the dilactone and a diacid, glucarodilactone was first reacted with undecenoyl chloride to afford an α-ω diene type monomer (Figure 1.14). The diene was then polymerized via ruthenium catalyzed acyclic diene metathesis (ADMET). Unlike the polyhydroxy polyamides and polyurethanes described above, poly(glucarodilactone undecene) exhibited a melting point of 59 °C, well below the onset of thermal degradation at 206 °C. As a result these polymers could be melt processed and their mechanical properties investigated. Degradation studies revealed rapid degradation in acidic conditions. By contrast to the degradation observed for the polyurethanes above, poly(glucarodilactone undecene) was stable in neutral and basic aqueous environments. Interestingly, copolyesters of the glucarodilactone α-ω diene and the analogous isosorbide α-ω diene exhibited shape memory properties, while no such behavior was observed for either homopolymer.

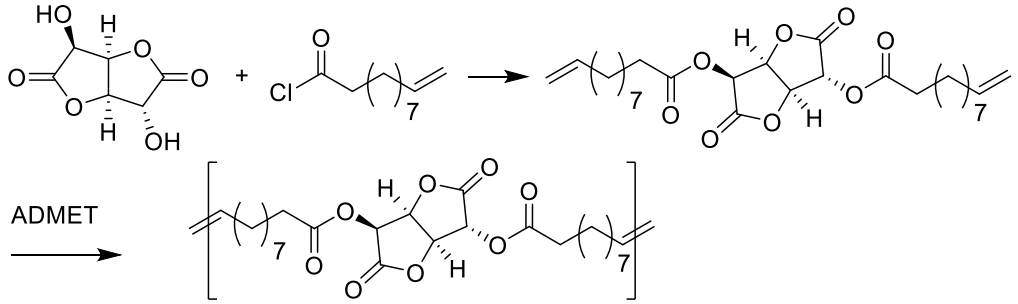

Figure 1.14. Preparation of glucarodilactone undecenoate and polymerization via ADMET.

Similar to examples listed for isosorbide above, it is expected that derivatization of the dilactones with appropriate functional groups should afford bifunctional monomers for use in thermoset applications. These thermoset polymers should be useful in the realm of degradable materials given the known degradability of the liner polymers incorporating the dilactones. To date only one report, which is covered in detail in chapter 4, describes the application of dilactones in thermoset materials.

1.4 Thesis outline

The following three chapters detail work focused on expanding the utility of bicyclic sugar derivatives for use in polymer materials. Chapter 2 describes the synthesis of a new isosorbide monomer acetylated methacrylic isosorbide (AMI). Both AMI regioisomers were prepared by straightforward esterification chemistry and the effect of regiochemistry on polymer properties was investigated. The ability to incorporate AMI into block polymers was demonstrated via RAFT polymerization to afford PAMI-poly(*n*-butyl acrylate) diblock copolymers. Chapter 3 covers the scalable synthesis of acetylated acrylic isosorbide (AAI) and the incorporation thereof into PAAI-poly(*n*-butyl acrylate)-

PAAI and PAAI-poly(2-ethylhexyl acrylate)-PAAI triblock copolymers. These triblock copolymers were then investigated as thermoplastic elastomers in pressure sensitive adhesive applications. Chapter 4 details the synthesis of bismethacrylates derived from glucarodilactone and mannarodilactone. These new monomers were then polymerized to form degradable thermoset materials and potential applications in coatings and polymer microspheres were investigated.

1.5 References

(1) Elias, H.-G.; Mülhaupt, R. In *Ullmann's Encyclopedia of Industrial Chemistry*; Wiley-VCH Verlag GmbH & Co. KGaA: Weinheim, Germany, 2015; Vol. 38, pp 1–70.

(2) Lichtenthaler, F. *Ullmann's Encyclopedia of Industrial Chemistry*; 2010; pp 583–616.

(3) Kola, R.; von Elsner, O.; Riepe, W.; Reuter, K. In *Ullmann's Encyclopedia of Industrial Chemistry*; Wiley-VCH Verlag GmbH & Co. KGaA: Weinheim, Germany, 2000; pp 1–14.

(4) Blauer, R. *Sugar : World Markets and Trade*; 2014.

(5) Global Ethylene Capacity and Capital Expenditure Outlook http://www.acutemarketreports.com/report/global-ethylene-capacity-and-capital-expenditure-outlook-rosneft-and-shell-lead-ethylene-capacity-growth (accessed Mar 23, 2016).

(6) Plastics the Facts http://www.plasticseurope.org/Document/ plastics-the-facts-2013 (accessed Mar 23, 2016).

(7) Lactic Acid And Poly Lactic Acid (PLA) Market Analysis By Application (Packaging, Agriculture, Transport, Electronics, Textiles) And Segment Forecasts To 2020 http://www.grandviewresearch.com/industry-analysis/lactic-acid-and-poly-lactic-acid-market (accessed Mar 23, 2016).

(8) Natureworks. Product and Applications http://www.natureworksllc.com/Product-and-Applications (accessed Mar 23, 2016).

(9) Global Sorbitol Market http://www.transparencymarketresearch.com/sorbitol-market.html (accessed Mar 23, 2016).

(10) Flèche, G.; Huchette, M. *Starch - Stärke* **1986**, *38* (1), 26–30.

(11) Kobayashi, H.; Yokoyama, H.; Feng, B.; Fukuoka, A. *Green Chem.* **2015**, *17* (5), 2732–2735.

(12) Ahmed, I.; Khan, N. A.; Mishra, D. K.; Lee, J. S.; Hwang, J. S.; Jhung, S. H. *Chem. Eng. Sci.* **2013**, *93*, 91–95.

(13) Zhang, J.; Wang, L.; Liu, F.; Meng, X.; Mao, J.; Xiao, F.-S. *Catal. Today* **2015**, *242*, 249–254.

(14) Roquette. *ROQUETTE reinforces its position as world leader in ISOSORBIDE for the performance plastics and chemistry markets ROQUETTE*; 2015.

(15) Yamaguchi, A.; Sato, O.; Mimura, N.; Shirai, M. *Catal. Commun.* **2015**, *67* (2), 59–63.

(16) Krantz, J. C.; Carr, J. C.; Forman, S.; Ellis, F. W. *J. Pharmacol. Exp. Ther.* **1939**, *67*, 187–190.

(17) The International Pharmacopoeia. 19th WHO Model List of Essential Medicines http://www.who.int/medicines/organization/par/edl/expcom13/eml13_en.pdf (accessed Mar 23, 2016).

(18) Rose, M.; Palkovits, R. *ChemSusChem* **2012**, *5* (1), 167–176.

(19) Tundo, P.; Aricò, F.; Gauthier, G.; Rossi, L.; Rosamilia, A. E.; Bevinakatti, H. S.; Sievert, R. L.; Newman, C. P. *ChemSusChem* **2010**, *3* (5), 566–570.

(20) Fenouillot, F.; Rousseau, A.; Colomines, G.; Saint-Loup, R.; Pascault, J. P. *Prog. Polym. Sci.* **2010**, *35* (5), 578–622.

(21) Cekovic, Z.; Tokic, Z. *Synthesis* **1989**, 610–612.

(22) Stoss, P.; Merrath, P.; Schlüter, G. *Synthesis* **1987**, *1987* (2), 174–176.

(23) Delidovich, I.; Hausoul, P. J. C.; Deng, L.; Pfützenreuter, R.; Rose, M.; Palkovits, R. *Chem. Rev.* **2016**, *116* (3), 1540–1599.

(24) Isikgor, F. H.; C. Remzi Becer. *Polym. Chem.* **2015**, *6*, 4497–4559.

(25) Feng, X.; East, A. J.; Hammond, W. B.; Zhang, Y.; Jaffe, M. *Polym. Adv. Technol.* **2011**, *22* (1), 139–150.

(26) Gandini, A. *Green Chem.* **2011**, *13* (5), 1061–1083.

(27) Galbis, J. A.; García-Martín, M. G. *Top. Curr. Chem.* **2010**, *295* (1), 147–176.

(28) Fuji, M.; Akita, M.; Tanaka, T. Polycarbonate copolymer and method of producing the same. US20100190953 A1, 2010.

(29) Ono, A.; Toyohara, K.; Minematsu, H.; Kageyama, Y. Polycarbonate and process for producing the same. US 7,365,148 B2, 2008.

(30) Motoyoshi, T.; Imazato, K.; Yamanaka, K. Polycarbonate resin. US 9096710 B2, 2015.

(31) Mitsubishi Chemical. New biobased engineering plastic "DURABIO" http://www.m-kagaku.co.jp/english/products/business/polymer/sustainable/details/1194667_3255.html (accessed Mar 23, 2016).

(32) Mitsubishi Chemical. World-First — DURABIO™, Bio-based Engineering Plastic from Mitsubishi Chemical, Used on the Front Panel of Sharp's New AQUOS CRYSTAL 2 Smartphone http://www.m-kagaku.co.jp/english/newsreleases/00258.html (accessed Mar 23, 2016).

(33) Roquette. Polycarbonates http://www.roquette-performance-plastics.com/polycarbonate/ (accessed Mar 23, 2016).

(34) Sadler, J. M.; Nguyen, A. P. T.; Toulan, F. R.; Szabo, J. P.; Palmese, G. R.; Scheck, C.; Lutgen, S.; La Scala, J. J. *J. Mater. Chem. A* **2013**, *1* (40), 12579–12586.

(35) Chrysanthos, M.; Galy, J.; Pascault, J. P. *Polymer* **2011**, *52* (16), 3611–3620.

(36) Hong, J.; Radojčić, D.; Ionescu, M.; Petrović, Z. S.; Eastwood, E. *Polym. Chem.* **2014**, *5*, 5360–5368.

(37) Beghdadi, S.; Miladi, I. A.; Ben Romdhane, H.; Bernard, J.; Drockenmuller, E. *Biomacromolecules* **2012**, *13* (12), 4138–4145.

(38) Hashimoto, K.; Wibullucksanakul, S.; Matsuura, M.; Okada, M. *J. Polym. Sci. Part A Polym. Chem.* **1993**, *31* (12), 3141–3149.

(39) Liu, Y.; Reineke, T. M. *J. Am. Chem. Soc.* **2005**, *127* (9), 3004–3015.

(40) Kiely, D. E.; Chen, L.; Lin, T. *J. Polym. Sci. Part A Polym. Chem.* **2000**, *38*, 594–603.

(41) Gehret, T. C.; Frobese, A. S.; Zerbe, J. S.; Chenault, H. K. *J. Org. Chem.* **2009**, *74* (21), 8373–8376.

(42) Werpy, T.; Petersen, G. *Top Value Added Chemicals from Biomass. Volume I—Results of Screening for Potential Candidates from Sugars and Synthesis Gas*; 2004.

(43) Kiely, D.; Chen, L.; Lin, T. *J. Am. Chem. Soc.* **1994**, *116*, 571–578.

(44) Hashimoto, K.; Okada, M.; Honjou, N. *Die Makromol. Chemie, Rapid Commun.* **1990**, *11*, 393–396.

(45) Wibullucksanakul, S.; Hashimoto, K.; Okada, M. *Macromol. Chem. Phys.* **1997**, *198*, 305–319.

(46) Hashimoto, K.; Wibullucksanakul, S.; Okada, M. *J. Polym. Sci. Part A Polym. Chem.* **1995**, *33*, 1495–1503.

(47) Shearouse, W. C.; Lillie, L. M.; Reineke, T. M.; Tolman, W. B. *ACS Macro Lett.* **2015**, *4* (3), 284–288.

Chapter 2: Isosorbide-derived polymethacrylates*

* Reproduced in part with permission from Gallagher, J. J.; Hillmyer, M. A.; Reineke, T. M. *ACS Sustainable Chem. Eng.* **2015**, *3* (4), 662–667. © 2015 American Chemical Society.

2.1 Introduction

Renewable chemical feedstocks are becoming increasingly cost competitive with petroleum based analogs as a result of advances in synthetic methods and production processes. For example, recent improvements in the conversion of the glucose derivative sorbitol to isosorbide have made the latter a viable building block for biobased polymers on the commercial scale.[1,2] Often compared to bisphenol A due to its rigid bicyclic structure and diol functionality, isosorbide has been incorporated into a wide variety of step growth polymers, including polyesters, polycarbonates, polyethers, polyurethanes, and polytriazoles.[3–5] These polymers generally exhibit high glass transition temperatures (T_g) due to the rigid bicyclic structure of isosorbide. Additionally, various difunctional derivatives of isosorbide have been employed in the synthesis of crosslinked, thermoset polymers for use in high performance composites.[6–11]

Despite the numerous examples of isosorbide-based polymers, there are only a few examples of monovinyl isosorbide derivatives for use in linear chain growth polymerizations.[12–15] A monovinyl isosorbide monomer is an appealing building block since the construction of polymers with designed architectures is more easily accomplished via chain growth mechanisms. Beghdadi *et al.* have described the synthesis and Reversible Addition-Fragmentation chain Transfer (RAFT) polymerization of isosorbide derived vinyl dianhydrohexitol triazoles (VDTs).[12] Interestingly, the authors found that the placement of the vinyl triazole moiety at either the *endo* or *exo* position of isosorbide had a significant effect on the solubility and T_g of poly(VDT)s. Polymers prepared from monomer with the vinyl triazole group in the *endo* position had a $T_g \approx 71$ °C and were water

soluble, while those prepared from monomer with the vinyl triazole in the *exo* position had a $T_g \approx 118$ °C and were insoluble in water. The authors noted that the RAFT polymerization of VDTs required about 48 h to reach 50–70% conversion, presumably due to the bulky nature of VDT monomers and modest reactivity of the N-vinyl triazole moiety.

Various options for functionalizing the hydroxyl groups of isosorbide have been reported in the literature (*e.g.* esterification, etherification, carbonylation, tosylation).[4] Due to the relatively poor reactivity of the secondary alcohols, esterification methods typically employ the use of auxiliary reactants. For example, a routine procedure for acetylating isosorbide uses acetic acid, N,N dicylcohexylcarbodiimide, and catalytic 4-dimethylaminopyridine (*i.e.*, Steglich esterification).[16,17] Acetylation by this method occurs predominantly at the less sterically encumbered *exo* position (~60% of product mixture) due to the steric bulk of the O-acyl isourea intermediate (for structure of isosorbide, see Scheme 1). An alternative approach for acetylation uses acetic anhydride and catalytic lead (II) oxide (~2 mol% relative to isosorbide).[18–21] This method favors acetylation at the *endo* position (~80% isolated yield). Although more sterically hindered due to being on the interior of the puckered bicyclic structure, the alcohol in the *endo* position is more nucleophilic due to intramolecular hydrogen bonding with the ethereal oxygen of the opposite tetrahydrofuran ring.[22] Unfortunately, this strategy requires the use of a toxic heavy metal salt. Likewise, synthesis of methacrylic isosorbide has been reported via Steglich esterification methods,[23] use of methacrylic anhydride and stoichiometric equivalent of an amine base,[6] or methacryloyl chloride and an equivalent of triethylamine.[7]

Although these approaches are effective, the use of relatively large amounts of auxiliary reactants is less than ideal from a green chemistry point of view.

In this work we sought to enable the development of advanced materials such as block copolymers using isosorbide by efficiently synthesizing a new monovinyl isosorbide derivative. To this end, we report the (i) synthesis and characterization of acetylated methacrylic isosorbide (AMI); (ii) use of scandium (III) triflate ($Sc(OTf)_3$) as an active and *endo*-selective esterification catalyst for the functionalization of isosorbide; (iii) polymerization of AMI via conventional free radical polymerization to afford linear high T_g polymers (PAMI); (iv) synthesis and use of a new, efficient hydroxy functional chain transfer agent (HO-CPAD) for the RAFT polymerization of AMI to give PAMI-CTA; and (v) synthesis of block copolymer PAMI-*b*-PnBA by chain extension of PAMI-CTA with *n*-butyl acrylate.

2.2 Results and Discussion

2.2.1 Synthesis of AMI

AMI was prepared in two steps according to Scheme 2.1. In both steps $Sc(OTf)_3$ was used to catalyze the esterification of isosorbide with the corresponding anhydride. Compared to alternative Lewis acid catalysts, $Sc(OTf)_3$ and other lanthanide triflates have unusual stability towards air and water.[24,25] As a result, they can be handled under ambient atmosphere, do not require anhydrous reaction conditions, and can be easily recycled and reused without loss of activity. While $Sc(OTf)_3$ is known to be an effective Lewis acid catalyst for the esterification of various alcohols,[26–28] this is the first report to our knowledge employing this catalyst for the esterification of isosorbide. Notably, $Bi(OTf)_3$

has also been reported as an effective water tolerant catalyst for the acylation of isosorbide with acetic anhydride.[29]

In the first step of AMI synthesis, $Sc(OTf)_3$ was found to be an exceptionally active catalyst. Full consumption of acetic anhydride (1 mol eq.) occurred in less than 10 min at room temperature using a catalyst loading of 0.05 mol%. By comparison, reported reaction times for acetylation with acetic anhydride and 2 mol% lead (II) oxide range from 2–20 h. Analysis of the crude product mixture by ^{1}H NMR spectroscopy indicated that the *endo* hydroxyl was the preferred site for acetylation ([*endo*-acetate]:[*exo*-acetate] = 4.2:1.0; See Figure 2.1).

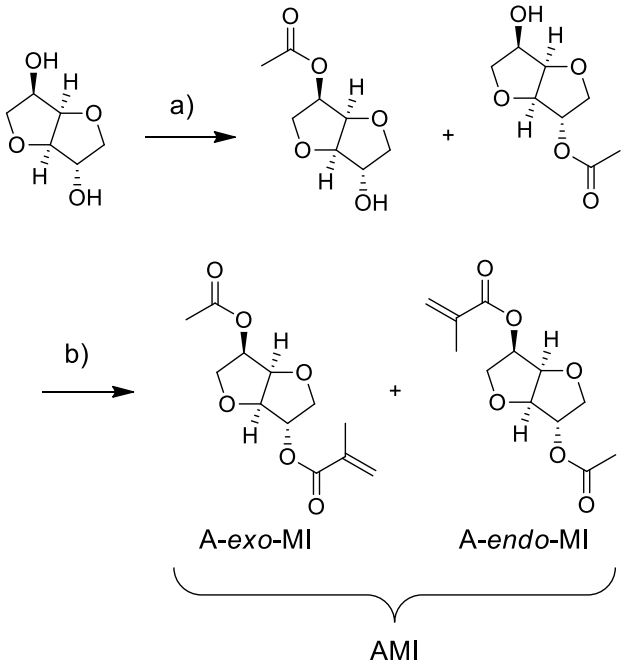

Scheme 2.1. Synthesis of AMI. a) 1 mol eq. acetic anhydride, 0.05 mol% $Sc(OTf)_3$, acetonitrile, room temperature, 10 min; b) 0.97 mol eq. methacrylic anhydride, 1 mol% $Sc(OTf)_3$, acetonitrile, room temperature, 4 h.

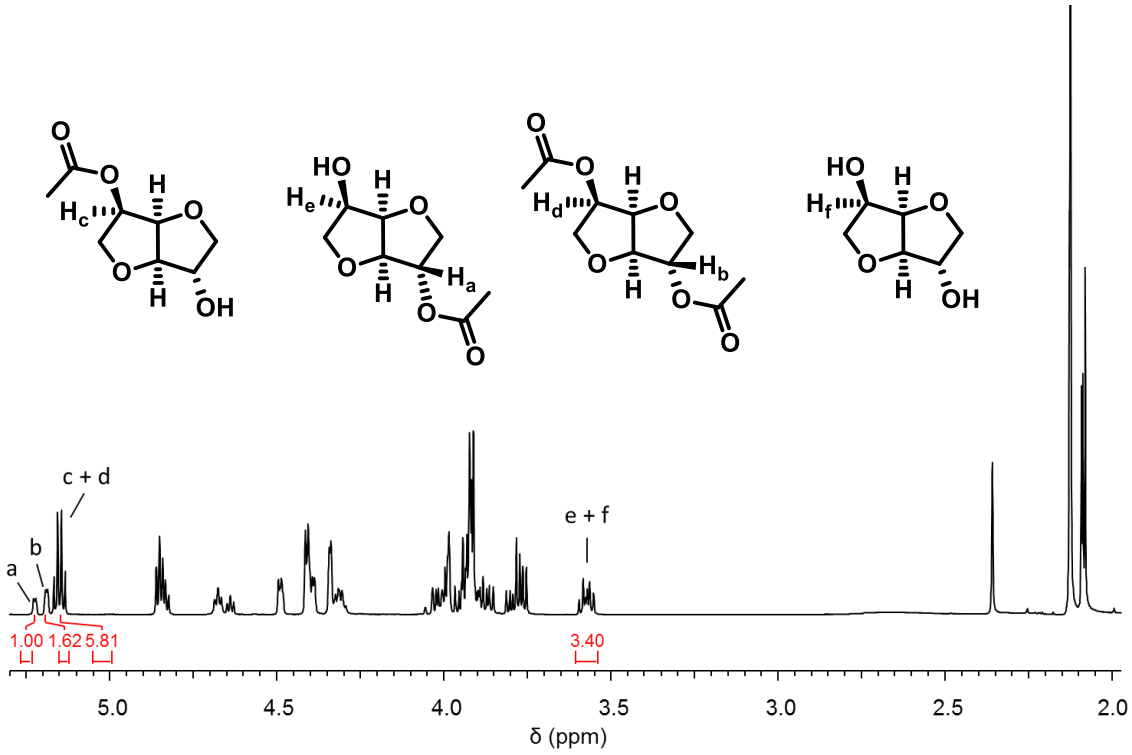

Figure 2.1. ^{1}H NMR spectrum of crude product mixture of $Sc(OTf)_3$ catalyzed acetylation of isosorbide with acetic anhydride.

After isolating the monoacetylated isosorbide products by column chromatography (54% yield), $Sc(OTf)_3$ was again used as a catalyst in the second step to install the methacrylate moiety (Scheme 2.1b). Complete conversion of methacrylic anhydride (0.97 mol eq.) was reached after 4 h at 1 mol% catalyst loading. The reduced reactivity relative to the first step is attributed to the difference in sterics between acetic anhydride and methacrylic anhydride. Additionally, the majority of hydroxyl groups available for functionalization in the second step are located in the less active (but more sterically accessible) *exo* position ($Sc(OTf)_3$ catalyzed methacrylation of isosorbide with methacrylic anhydride also occurs preferentially at the *endo* position).

To characterize each isomer individually, pure samples of A-*exo*-MI and A-*endo*-MI were prepared by isolating select fractions from column chromatography of the first step containing only isosorbide *endo*-acetate or isosorbide *exo*-acetate, respectively, before installing the methacrylate moiety. Both A-*exo*-MI and A-*endo*-MI were clear viscous liquids at room temperature. Differential scanning calorimetry (DSC) showed identical T_g values for the monomers A-*exo*-MI and A-*endo*-MI at −42 °C, and no evidence for crystallinity was observed for either isomer. FT-IR spectroscopy showed characteristic peaks at 1740 and 1717 cm^{-1} corresponding to the acyl and methacrylate esters, respectively, and the C=C bond stretch of the methacrylate group was apparent at 1637 cm^{-1} (Figure 2.2). Other than subtle differences at low wavenumbers, no significant difference was observed in the FT-IR spectra for A-*exo*-MI and A-*endo*-MI. ^{1}H NMR spectra differed significantly between A-*exo*-MI and A-*endo*-MI due to the different arrangement of substituents about the isosorbide core (Figures 2.3 and 2.4). Of particular note is the difference in chemical shift observed for the vinyl protons *cis* to the carbonyl oxygen (Figure 2.5). Additional structural confirmation was provided by high resolution mass spectroscopy of the 4:1 mixture of A-*exo*-MI : A-*endo*-MI (expected: 256.2518; found: 279.0839 ($M + Na^+$); error 4.63 ppm). Overall, AMI was readily prepared as a mixture of isomers in two steps from isosorbide on a ~20 g scale with a final (unoptimized) overall yield of 44%. The use of low catalyst loadings, mild reaction conditions, and inexpensive commercially available reagents make this synthetic pathway appealing for potential large scale production of this new monomer.

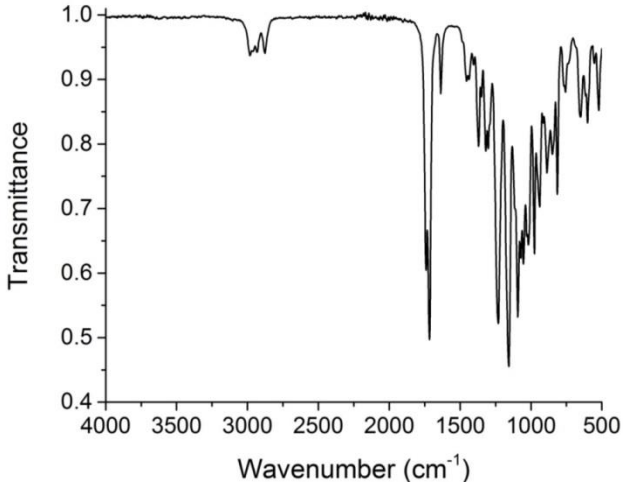

Figure 2.2. ATR-FTIR of neat A-*exo*-MI.

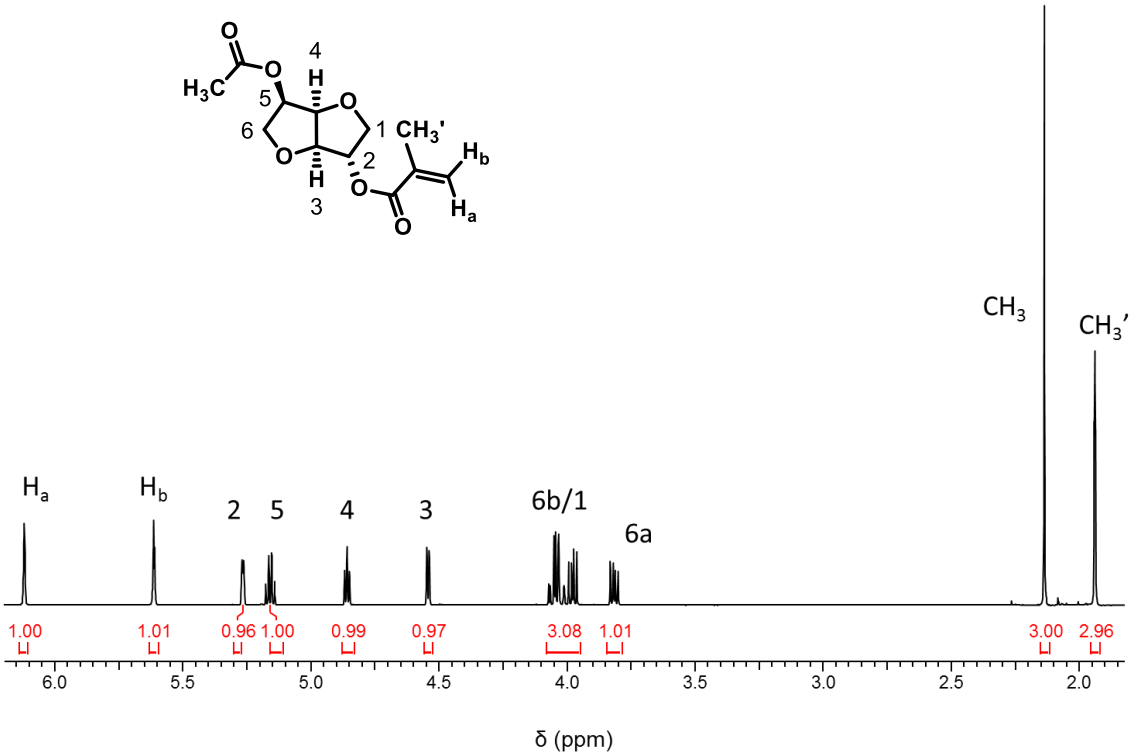

Figure 2.3. ^{1}H NMR spectrum of A-*exo*-MI in $CDCl_3$.

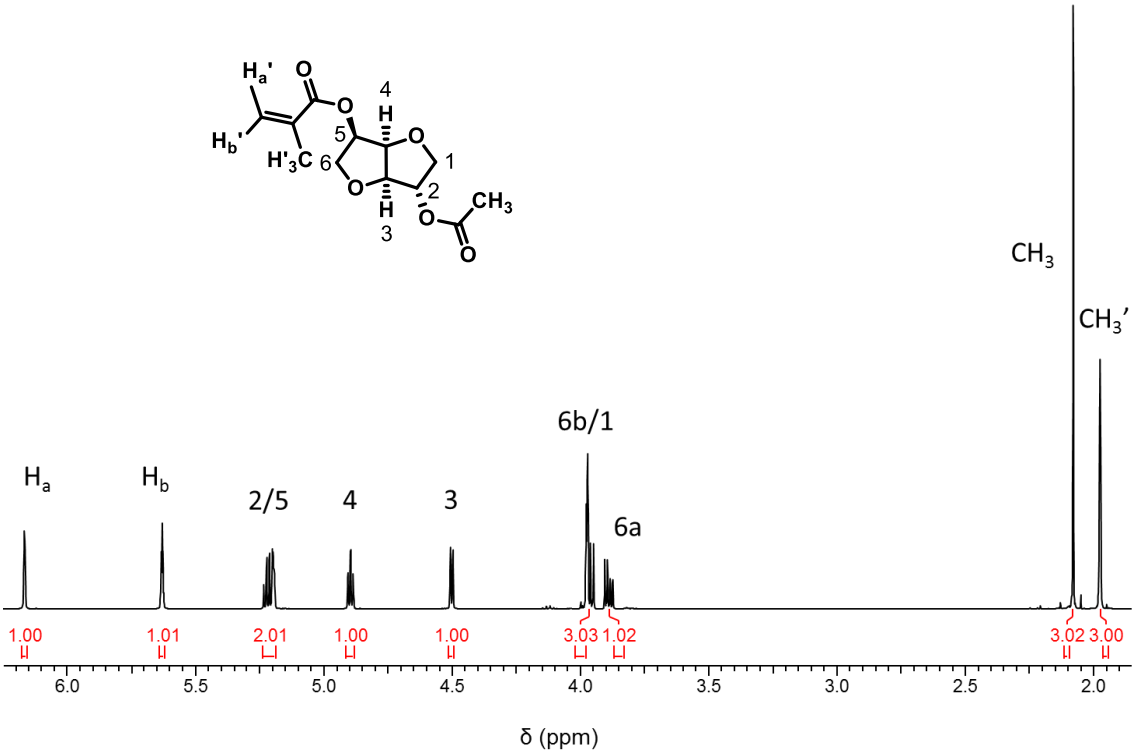

Figure 2.4. ^{1}H NMR spectrum of A-*endo*-MI in $CDCl_3$.

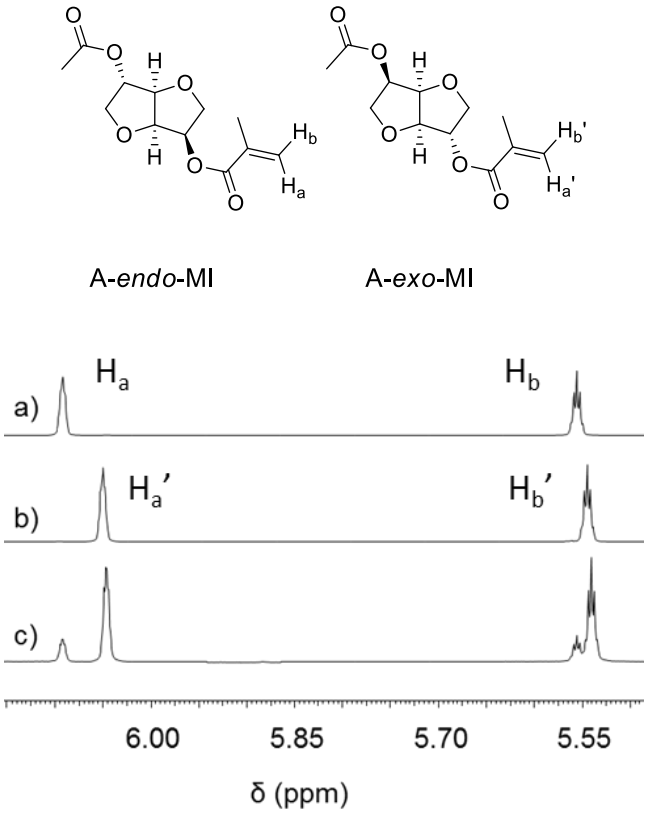

Figure 2.5. ^{1}H NMR spectra in $CDCl_3$ of the vinyl region for a) A-*endo*-MI, b) A-*exo*-MI, and c) 4:1 mixture of A-*exo*-MI : A-*endo*-MI.

2.2.2 Free radical polymerization of AMI

Thermally initiated free radical polymerization of AMI (4:1 A-*exo*-MI:A-*endo*-MI) was carried out in the presence of azobisisobutyronitrile (AIBN) at 70 °C in $CHCl_3$. Aliquots taken during the polymerization were analyzed by ^{1}H NMR spectroscopy to determine conversion as a function of time (Figure 2.6). ^{1}H NMR analysis indicated 83% monomer conversion after 4 h. Monitoring the relative integrations of resonances corresponding to H_a and H_a' (Figure 2.5) indicated no significant difference in reactivity between A-*endo*-MI and A-*exo*-MI. After precipitation and drying, this sample of PAMI was soluble at 10 wt% in acetone, EtOAc, CH_2Cl_2, $CHCl_3$, THF, and DMF but was insoluble in water, MeOH, iPrOH, and toluene. The number average molar mass (M_n) of

this sample by size exclusion chromatography in THF with multiangle laser light scattering detection (SEC-MALLS) was 88.9 kg mol^{-1} with $Đ$ = 1.80. Thermogravimetric analysis (TGA) showed a T_d (5% weight loss) of 251 °C and 217 °C under N_2 and air, respectively. Similar values of T_d (~230 °C) under inert atmosphere have been reported previously for poly(methyl methacrylate) (PMMA) prepared by free radical polymerization.[30] Under air this sample of PAMI was stable for ~20 minutes at 180 °C (<1% weight loss, Figure 2.7). The sample exhibited a remarkably high T_g of 130 °C by DSC (Figure 2.8). Since the T_g of PMMA is ~110 °C,[31] the relatively high T_g of PAMI is attributed to reduced polymer flexibility caused by additional steric bulk of the pendant isosorbide acetate groups.

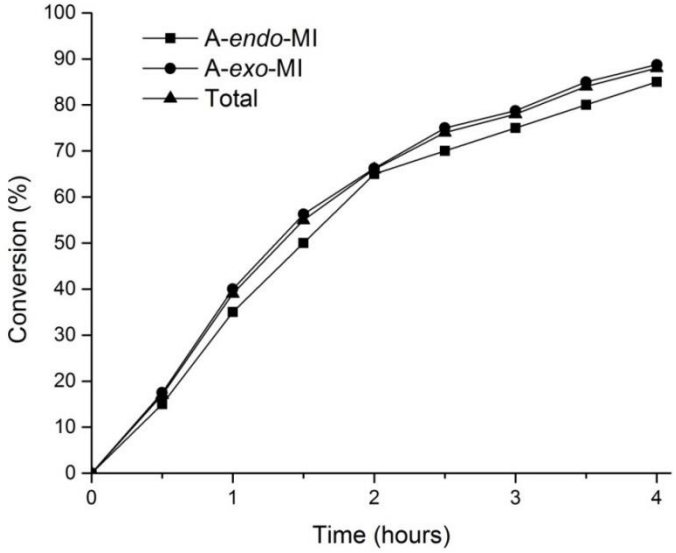

Figure 2.6. Conversion vs time for the free radical polymerization of AMI in $CHCl_3$. Conditions: $[AMI]_0$ = 1 M, 1 mol % AIBN, 70 °C.

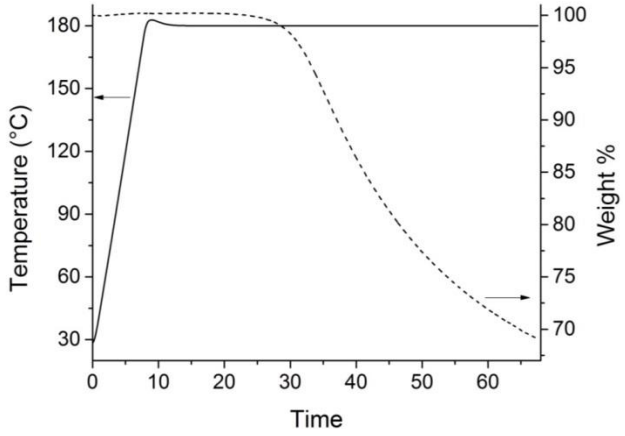

Figure 2.7. TGA in air at 180 °C of PAMI (M_n = 88.9 kg mol^{-1}) prepared by free radical polymerization.

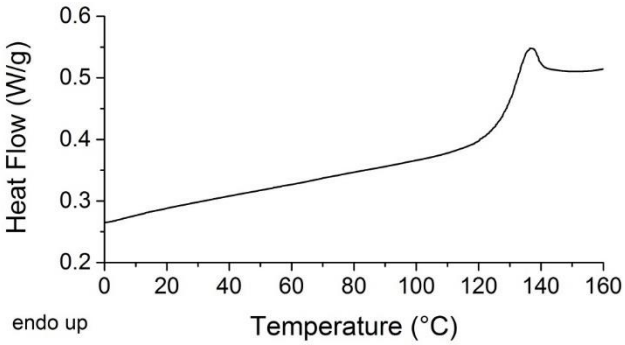

Figure 2.8. DSC of PAMI (M_n = 88.9 kg mol^{-1}) in N_2. Second heating, heating rate = 10 °C min^{-1}.

To determine the effect of stereochemistry on polymer thermal properties, an isomerically pure sample of PAMI was prepared from A-*endo*-MI under the same conditions described above. Similarly, after 4 h at 70 °C the polymerization of A-*endo*-MI reached 84% conversion as determined by ^{1}H NMR spectroscopy. M_n and $Đ$ of PA-*endo*-MI by SEC-MALLS analysis were 105 kg mol^{-1} and 1.48, respectively. TGA and DSC revealed no significant difference in T_d or T_g between PAMI and PA-*endo*-MI, indicating that the regiochemistry of substituents on isosorbide does not alter the thermal properties of PAMI (Table 2.1). Based on these results, AMI and PAMI can be prepared without the

need for careful consideration of isomer composition in the final product. By contrast, Beghdadi *et al*. reported that regiochemistry had a significant impact on the T_g of poly(VDT)s.[12] A key difference between the reported poly(VDT)s and PAMI is the absence of hydroxyl groups in the latter, suggesting that these groups, if left unprotected, play an important role in determining polymer properties.

Table 2.1. Comparison of molar mass and thermal properties of PAMI vs PA-*endo*-MI.

Sample	AMI composition[a]	M_n (kg mol^{-1})[b]	$Đ$[b]	T_d (N_2, air, °C)[c]	T_g (°C)[d]
PAMI	4.0 : 1	88.9	1.80	251, 217	130
PA-*endo*-MI	0 : 1	105	1.48	250, 221	123

[a]Monomer feed ratio. [b]Determined by SEC-MALLS in THF. [c]From TGA. [d]From DSC.

2.2.3 PAMI-CTA via RAFT polymerization

Controlled radical polymerization allows for the synthesis of macromolecules with well-defined architectures.[32–35] Block copolymers, which find use in many applications such as thermoplastic elastomers, pressure sensitive adhesives, and toughening agents,[36] are readily prepared by controlled radical polymerization methods. The thermal stability and high T_g of PAMI make it a promising sustainable candidate for a hard component of a block copolymer system.[37] To demonstrate the ability to incorporate PAMI into a block copolymer, AMI was polymerized via RAFT to give PAMI-CTA (Scheme 2.2). An initial screening showed that dithiobenzoates were the most suitable class of chain transfer agent (CTA) for RAFT polymerization of AMI, while trithiocarbonates did not result in well controlled polymerizations (Table 2.2). The CTA that afforded the highest monomer conversion while maintaining low $Đ$ of the resultant polymer was 4-cyano-4-

(phenylcarbonothioylthio)pentanoate (HO-CPAD). This new CTA, a structural analogue of the previously reported CTA 4-cyano-1-hydroxypent-4-yl dithiobenzoate,[38] was synthesized by Steglich esterification of the commercially available 4-cyano-4-(phenylcarbonothioylthio)pentanoic acid with excess ethylene glycol (Scheme 2.3). After purification by column chromatography, HO-CPAD was isolated in a 67% yield. Use of HO-CPAD as a RAFT CTA results in functional polymers with a hydroxyl end group (Scheme 2.2), a particularly useful structural motif given the synthetic versatility of a hydroxyl group (*e.g.*, in the preparation of block copolymers containing mechanistically differentiated components). A linear increase in M_n with conversion and narrow molecular weight distribution indicated the RAFT polymerization of AMI with HO-CPAD was well controlled (Figure 2.9). However, the linear fit to the M_n vs. conversion data has a non-zero intercept. This phenomenon can be attributed to non-RAFT propagation events occurring at low conversion before the main RAFT equilibrium has been established.[39]

Table 2.2. RAFT polymerization of AMI with different CTAs.

CTA	Conversion [a] (%)	M_n [b] (kg/mol)	$Đ$ [b]
HO-CPAD	92	30.9	1.08
1	57	20.7	1.08
2	61	30.0	1.11
3	69	20.2	1.10
4	77	46.4	1.80
5	22	n.d.	n.d.

[AMI]:[CTA]:[AIBN]=100:1:0.1, 70 °C, DMF, 18 h. [a]From ^{1}H NMR spectroscopy; [b]Determined by SEC-MALLS in THF. n.d. = not determined.

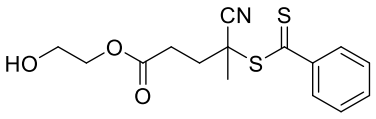

HO-CPAD

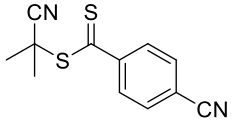

1

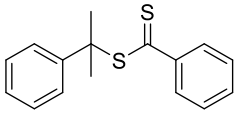

2

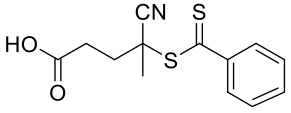

3

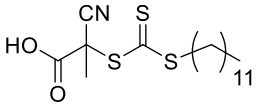

4

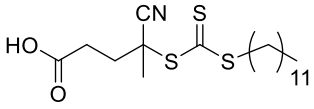

5

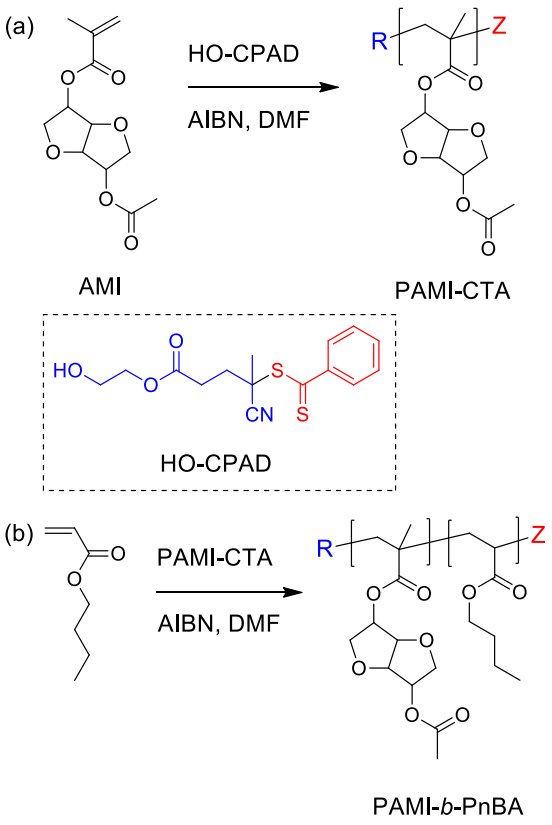

Scheme 2.2. Synthesis of (a) PAMI-CTA, [HO-CPAD]:[AIBN] = 10:1, 70 °C, 18 h; (b) PAMI-*b*-PnBA, [*n*-butyl acrylate]:[PAMI-CTA]:[AIBN] = 870:1:0.1, 70 °C, 20 h. Z and R correspond to the dithiobenzoate and free radical leaving group fragments, respectively, of HO-CPAD.

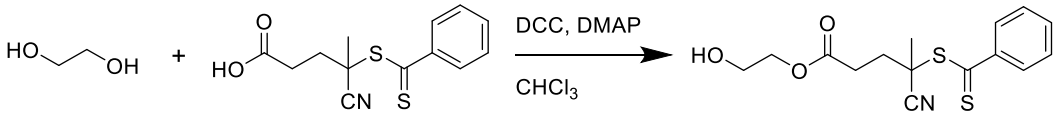

Scheme 2.3. Synthesis of HO-CPAD.

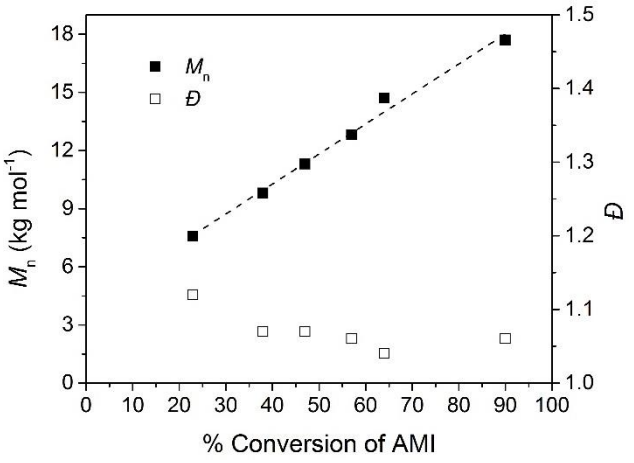

Figure 2.9. M_n and $Đ$ as a function of conversion for RAFT polymerization of AMI. [AMI]:[HO-CPAD]:[AIBN] = 60:1:0.1. Conversion determined by ^{1}H NMR spectroscopy, M_n and $Đ$ determined by SEC-MALLS in THF. Dashed line indicates a linear regression, $R^2 = 0.99$.

Since a key advantage of controlled radical polymerization is the ability to synthesize materials with targeted molar masses and narrow distributions, AMI was polymerized by RAFT employing different ratios of $[AMI]_0$:$[HO\text{-}CPAD]_0$ (Table 2.3). In all cases the polymerization proceeded to > 92% conversion after 18 h and $Đ < 1.09$ was achieved for all samples. Analysis of PAMI-CTA (14) by ^{1}H NMR spectroscopy confirmed the presence of the expected end groups (Figure 4.10). Resonances between 7.36 and 7.89 ppm correspond to the aromatic protons of the dithiobenzoate group, while a peak at 4.23 ppm corresponds to the protons α to the alcohol of the free radical leaving group fragment. Further proof of a terminal hydroxyl group was demonstrated by reacting PAMI-CTA (14) with a tenfold excess of methacrylic anhydride in the presence of $Sc(OTf)_3$ (14 mol% relative to polymer) to give ene-PAMI-CTA (14) (Scheme 2.4). Again, $Sc(OTf)_3$ was found to be an efficacious esterification catalyst. After 1 h of reaction at room temperature followed by repeated precipitation into MeOH and drying under vacuum, ene-PAMI-CTA

(14) was isolated as a pink powder. The disappearance of the peak at 4.23 ppm along with the appearance of a new peak at 4.36 ppm confirmed the terminal hydroxyl group was fully functionalized, while resonances corresponding to the methacrylic protons were observed in the vinyl region at 5.62 and 6.14 ppm (Figure 4.11).

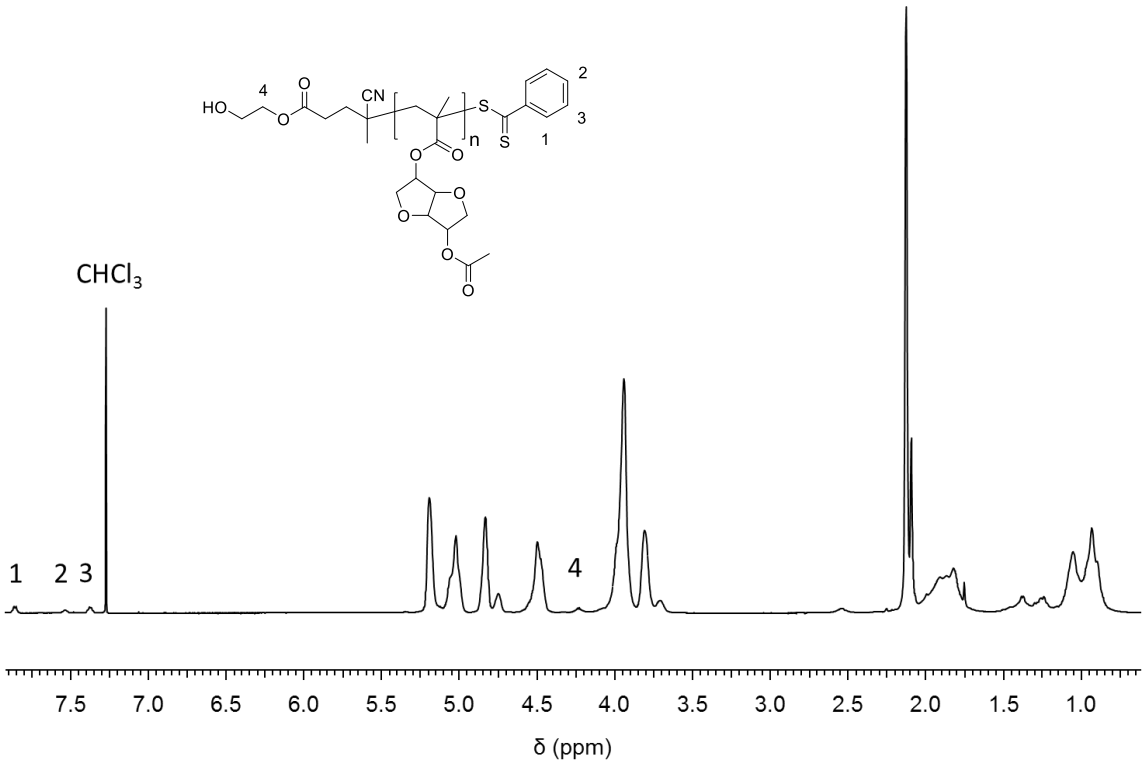

Figure 2.10. ^{1}H NMR spectrum of PAMI-CTA (14) in $CDCl_3$.

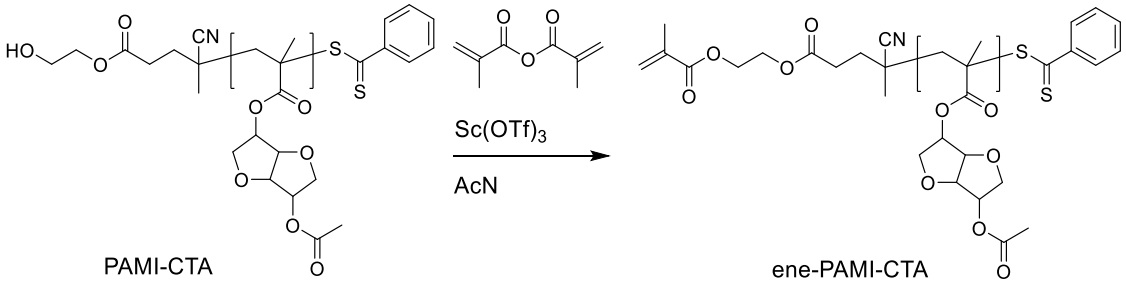

Scheme 2.4. Synthesis of ene-PAMI-CTA. [PAMI-CTA]:[anhydride]:[$Sc(OTf)_3$] = 1:10:0.14.

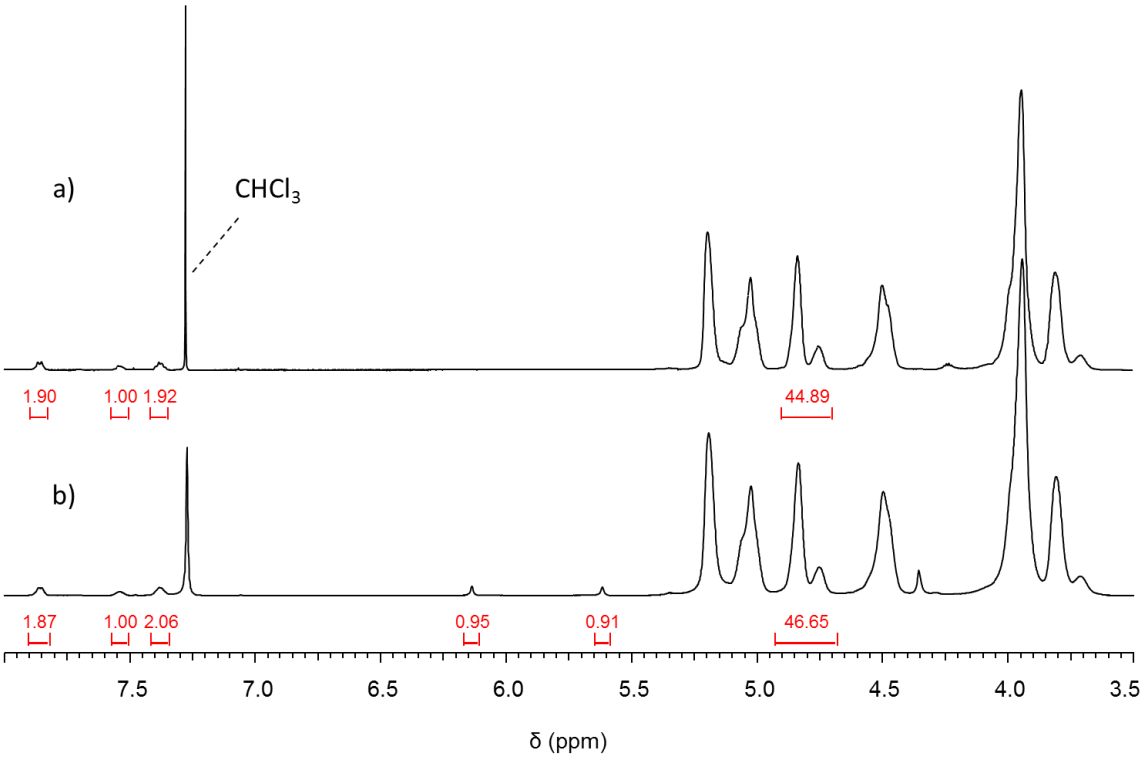

Figure 2.11. ^{1}H NMR spectrum of a) PAMI-CTA (14) and b) ene-PAMI-CTA (14) in $CHCl_3$. Molar ratio based on integrations of end group$_{CTA}$:end group$_{ene}$ for ene-PAMI-CTA (14) = 1:0.94. Integration ratio of aromatic protons of PAMI-CTA:ene-PAMI-CTA = 1:0.98 (standardized to repeat unit integration).

Values of M_n as determined by ^{1}H NMR end group analysis (assuming one CTA fragment per chain) and SEC-MALLS were in reasonably good agreement, although the values determined by SEC-MALLS were consistently higher (see Table 2.3). Values of M_n (calc.)/M_n (SEC) was < 1 for all trials, indicating a deviation from the ideal one CTA per chain model (i.e CTA efficiency factor < 1).[40] For comparison, the M_n (calc.)/M_n (NMR) values were consistently closer to 1. Since conversion and M_n (calc.)/M_n (SEC) and M_n (calc.)/M_n (NMR) were consistent across all trials, PAMI-CTA of a targeted M_n can be reliably synthesized by RAFT using HO-CPAD.

Table 2.3. PAMI-CTA and PAMI-*b*-PnBA sample information.

Sample	$[M]_0/[CTA]_0$	Conv. (%)[a]	M_n (NMR) (kg mol^{-1})[b]	M_n (SEC) (kg mol^{-1})[c]	M_n (calc.) (kg mol^{-1})[d]	M_n (calc.)/ M_n (SEC)	M_n (calc.)/ M_n (NMR)	$Đ$[c]
PAMI-CTA (14)	40	95	11.8	13.8	10.1	0.73	0.86	1.07
PAMI-CTA (17)	50	95	15.0	16.7	12.5	0.75	0.83	1.06
PAMI-CTA (19)	60	95	16.9	18.7	14.9	0.80	0.88	1.09
PAMI-CTA (24)	80	92	21.7	24.2	19.2	0.79	0.88	1.07
PAMI-CTA (31)	100	92	28.1	30.9	23.9	0.77	0.85	1.08
PAMI-*b*-PnBA (14-69)	870	64	82.7	88.3	85.1	0.96	1.03	1.12
PAMI-*b*-PnBA (17-55)	870	51	71.8	70.7	73.5	1.04	1.02	1.12
PAMI-*b*-PnBA (19-60)	870	56	78.6	85.7	81.1	0.95	1.03	1.19
PAMI-*b*-PnBA (24-54)	870	50	80.3	78.7	79.9	1.01	1.00	1.14
PAMI-*b*-PnBA (31-56)	870	52	87.1	102	88.8	0.87	1.02	1.24

[a]Of monomer, determined by ^{1}H NMR spectroscopy; [b]From end group analysis; [c]Determined by SEC-MALLS in THF. [d] Assuming each CTA generates 1 polymer chain (See SI).

PAMI-CTA (14) exhibited similar thermal stability under N_2 and air (T_d = 255 and 252 °C, respectively.) T_g values of PAMI-CTA ranged from 91–108 °C depending on M_n of the sample (Figure 2.12). From the linear regression of T_g vs. $1/M_n$ data based on the Flory-Fox equation, T_g becomes essentially constant at 130 °C for PAMI at molar masses > 55 kg mol^{-1} (Figure 2.13). These predicted values are in good agreement with the T_g values observed for PAMI and PA-*endo*-MI prepared by conventional free radical polymerization.

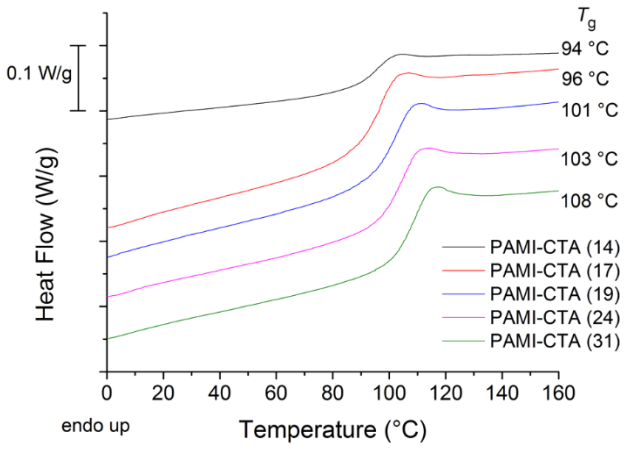

Figure 2.12. DSC of PAMI-CTA. Second heating, heating rate = 10 °C min^{-1}.

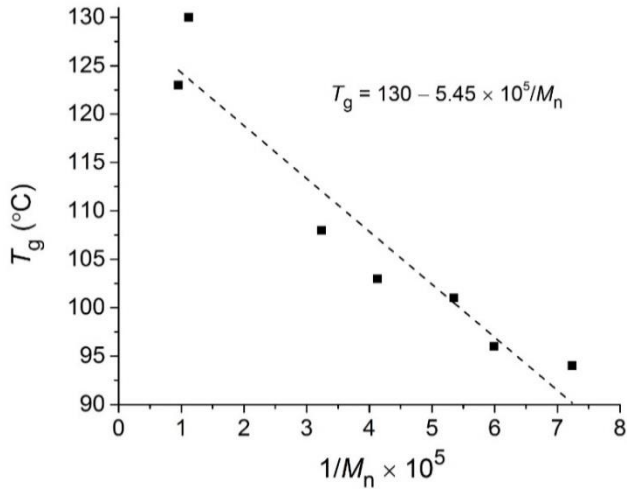

Figure 2.13. Plot of T_g vs. $1/M_n$ for PAMI-CTA, PAMI, and PA-*endo*-MI. Dashed line is a linear regression of the form $T_g(M_n) = T_g(M_n \to \infty) - A/M_n$, where A is an empirical parameter. $R^2 = 0.90$.

2.2.4 PAMI-*b*-PnBA

Chain extension of PAMI-CTA with *n*-butyl acrylate afforded the block copolymer samples PAMI-*b*-PnBA (Scheme 2.2b, Table 2.3). PnBA is an appealing option for a rubbery counterpart to PAMI due to its low T_g (~−50 °C)[31] and recent developments towards the commercial production of biobased acrylates.[41] In all cases the PAMI-*b*-PnBA samples had a broader molar distribution relative to that of PAMI-CTA. Inspection of the

SEC traces showed a slight high molar mass shoulder, likely due to termination by combination of propagating radicals (Figures 2.14). Termination events are deviations from ideal behavior for controlled radical polymerizations and result in broadened molar mass distributions. TGA of PAMI-*b*-PnBA showed marked increase in T_d compared to PAMI-CTA (14) homopolymer (T_d, 5% weight loss; N_2 = 316 °C, air = 296 °C). The higher T_d of PAMI-*b*-PnBA compared to PAMI is due to the differences in thermal stability and decomposition mechanisms between poly(acrylate)s and poly(methacrylate)s. Poly(acrylate)s undergo thermal decomposition by a random-chain scission mechanism with a T_d ~310 °C,[42] while poly(methacrylate)s decompose by an end-chain mechanism at relatively lower temperatures.[43] For PAMI-CTA, methacrylic chain ends are likely generated by *in situ* thermolysis of the CTA end group during TGA.[44] Therefore, the relatively higher thermal stability of PAMI-*b*-PnBA is attributed to the absence of methacrylic chain ends. All samples of PAMI-*b*-PnBA exhibited two well-separated T_g values at approximately −45 and 120 °C (Figure 2.15). The presence of both T_gs near that of the respective homopolymers suggests the PAMI and PnBA domains are microphase separated, an essential feature for thermoplastic elastomer applications.

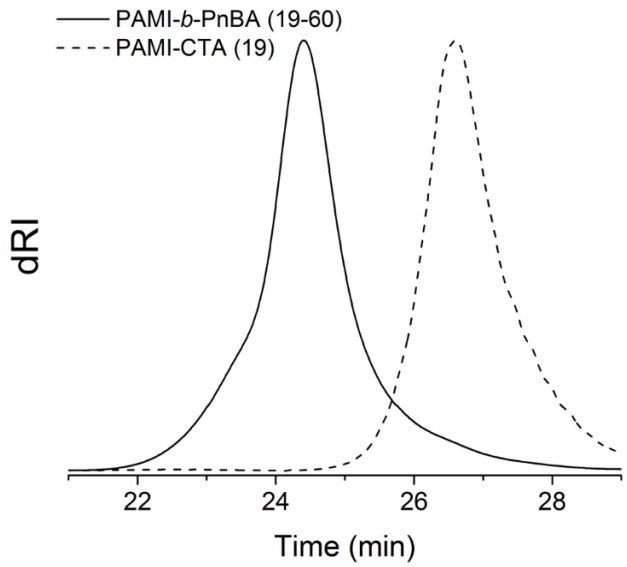

Figure 2.14. THF-SEC of PAMI-*b*-PnBA (19-60) and PAMI-CTA (19) prepared by RAFT polymerization.

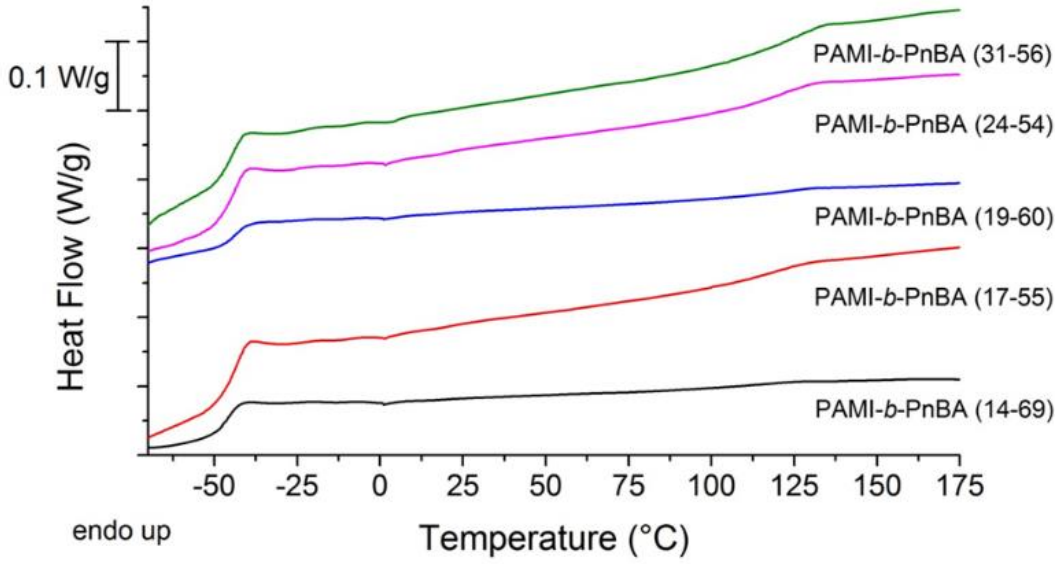

Figure 2.15. DSC of PAMI-*b*-PnBA in N_2. Second heating, heating rate = 10 °C min^{-1}.

2.3 Conclusion

In summary, we have reported the synthesis of a new isosorbide derived monomer AMI in two steps from commercially available starting materials. $Sc(OTf)_3$ was employed in both steps as a highly active Lewis acid catalyst for the esterification of isosorbide with anhydrides. PAMI prepared by free radical polymerization was found to have a high T_g and similar thermal stability relative to PMMA. Comparison of PAMI and PA-*endo*-MI demonstrated that the regiochemistry of AMI was not a determining factor for polymer thermal properties. AMI was successfully polymerized via RAFT using the novel CTA HO-CPAD to afford PAMI-CTA with good control of M_n and narrow $Đ$. Esterification of the hydroxyl end group of PAMI-CTA with methacrylic anhydride yielded ene-PAMI-CTA, further demonstrating the utility of $Sc(OTf)_3$ as a Lewis acid catalyst. PAMI-CTA was subsequently chain extended with *n*-butyl acrylate to give the block copolymer PAMI-*b*-PnBA. Combined, these advances have tremendous potential for the valorization of the biobased and low cost isosorbide. Additional research focusing on thermoplastic elastomer applications for PAMI containing block copolymers is ongoing.

2.4 Experimental

All chemicals were purchased from Aldrich and used without further purification unless otherwise noted. Methacrylic anhydride was passed over basic alumina to remove inhibitor prior to use. *N*-butyl acrylate was purified by vacuum distillation.

Characterization ^{1}H NMR and ^{13}C NMR spectroscopy experiments were performed on a Bruker Avance III HD 500 spectrometer at 500 MHz and 125 MHz, respectively, equipped

with a 5mm Prodigy TCI cryoprobe and referenced to TMS. FT-IR was performed using a Bruker Alpha Platinum ATR spectrometer. High resolution mass spec was performed using a Bruker Bio-TOF II in positive mode ESI. SEC was carried out in THF using three Phenomenex Phenogel-5 columns connected in series at a flow rate of 1 ml min^{-1} at 25 °C. Chromatograms were collected using a Wyatt Technology DAWN DSP MALLS detector and a Wyatt optilab EX RI detector. PAMI dn/dc was calculated from the RI signal using a known sample concentration and assuming 100% mass recovery from the column. Copolymer dn/dc was calculated using a weighted average of homopolymer dn/dc values. TGA was performed on a TA Instruments Q500 at a heating rate of 10 °C min^{-1}. DSC measurements were carried out using a TA Instruments Discovery DSC under N_2. T_g values were determined on the second heating at a heating rate of 10 °C min^{-1}. Monomer conversion during polymerization was monitored by ^{1}H NMR spectroscopy by removing aliquots from the reaction via syringe under inert atmosphere and diluting with $CDCl_3$. Conversion values were calculated by comparing the integrations of vinyl protons to protons of the isosorbide core. M_n (calc.) was calculated according to the formula $M_n\,(\text{calc.}) = \text{MW}_{\text{CTA}} + [\text{M}]_0 \times \text{MW}_\text{M} \times \text{conversion}/[\text{CTA}]_0$, where $[\text{M}]_0$ and $[\text{CTA}]_0$ are the initial concentrations of monomer and CTA, respectively, and MW_M and MW_{CTA} are the molar masses of monomer and CTA, respectively.

Isosorbide monoacetate. *Caution: This reaction is both exothermic and rapid. While no runaway reactions were observed under the conditions reported below, appropriate preventative engineering measures should be carefully considered if performing this reaction on a larger scale.* Isosorbide (20.0 g, 137 mmol) and acetic anhydride (12.9 ml,

137 mmol) were dissolved in 200 ml acetonitrile with stirring. $Sc(OTf)_3$ (34 mg, 0.069 mmol) was added and within 1 min a slight exotherm was observed. After 10 min, the reaction was concentrated by rotary evaporation. Removal of acetic acid was facilitated by dissolving the concentrate in 20 ml toluene and removing the volatiles by rotary evaporation. The monoacetylated products were isolated from the crude mixture by column chromatography on silica gel (CH_2Cl_2 → 1:1 CH_2Cl_2:EtOAc) to give a mixture of isosorbide *endo*- and *exo*- acetate as a clear viscous liquid (13.9 g, 54.0%). ^{1}H NMR ($CDCl_3$, 500 MHz): δ_{ppm}: isosorbide *endo*-acetate: 5.16 (q, *J* = 5.5 Hz, 1H), 4.86 (t, *J* = 5.0 Hz, 1H), 4.42 (d, *J* = 4.4 Hz, 1H), 4.36 (bs, 1H), 3.93 (m, 3H), 3.77 (dd, *J* = 9.6, 5.3 Hz, 1H), 2.13 (s, 3H), 1.81 (d, *J* = 4.9 Hz, 1H). isosorbide *exo*-acetate: 5.23 (d, *J* = 3.1, 1H), 4.65 (t, *J* = 4.9, 1H), 4.49 (d, *J* = 4.3, 1H), 4.04 (m, 2H), 3.91 (dd, *J* = 9.6, 6, 1H), 3.59 (dd, *J* = 9.5, 5.8, 1H), 2.57 (d, *J* = 7.3, 1H), 2.10 (s, 3H). ^{13}C NMR ($CDCl_3$, 125 MHz): δ_{ppm}: isosorbide *endo*-acetate: 170.49, 88.16, 80.29, 76.19, 75.54, 74.08, 70.12, 20.66. isosorbide *exo*-acetate: 169.92, 85.56, 81.93, 78.35, 73.58, 73.50, 72.26, 20.88.

Acetylated methacrylic isosorbide (AMI). Isosorbide monoacetate (mixture of isomers) (5.00 g, 26.6 mmol), methacrylic anhydride (3.97 g, 25.8 mmol), and $Sc(OTf)_3$ (131 mg, 0.266 mmol) in 3 ml acetonitrile were added to a screw capped vial and stirred vigorously. After 4 h, the reaction was taken up in 300 ml EtOAc and rinsed once with 300 ml DI H_2O and 3x300 ml sat. $NaHCO_3$. After drying over $MgSO_4$ the solvent was removed under reduced pressure to give AMI as a clear viscous liquid (5.40 g, 81.8% yield). ^{1}H NMR ($CDCl_3$, 500 MHz): δ_{ppm}: *endo*-acetyl-*exo*-methacryl-isosorbide: 6.12 (s, 1H), 5.62 (t, *J* = 1.53 Hz, 1H), 5.27 (d, *J* = 3.66 Hz, 1H), 5.16 (q, *J* = 5.70 Hz, 1H), 4.86 (t, *J* = 4.88 Hz,

1H), 4.54 (d, *J* = 4.58 Hz, 1H), 4.02 (m, 3H), 3.82 (dd, *J* = 9.61, 5.65 Hz, 1H), 2.14 (s, 3H), 1.94 (t, *J* = 1.37 Hz, 3H). *exo*-acetyl-*endo*-methacryl-isosorbide: 6.17 (s, 1H), 5.63 (t, *J* = 1.53 Hz, 1H), 5.21 (m, 2H), 4.90 (t, *J* = 5.19 Hz, 1H), 4.50 (d, *J* = 4.88 Hz, 1H), 3.97 (m, 3H), 3.89 (dd, *J* = 10.05, 4.90, 1H), 2.08 (s, 3 H), 1.97 (t, *J* = 1.50 Hz, 3H). ^{13}C NMR ($CDCl_3$, 125 MHz): δ_{ppm}: *endo*-acetyl-*exo*-methacryl-isosorbide: 170.37, 166.32, 135.68, 126.53, 85.89, 80.71, 78.24, 74.00, 73.48, 70.11, 20.66, 18.17. *exo*-acetyl-*endo*-methacryl-isosorbide: 170.06, 166.63, 135.65, 126.32, 85.99, 80.89, 78.07, 74.06, 73.36, 70.67, 20.91, 18.29. ATR-FTIR (neat): $\upsilon_{cm^{-1}}$: 2931 (C-H), 1740 (C=O), 1717 (C=O), 1637 (C=C), 1230 (C-O), 1157 (C-O), 1093 (C-O). MS (ESI-TOF, *m/z*) Calcd. for $C_{12}H_{16}O_6$: 256.2518; found: 279.0839 ($M + Na^+$); error 4.63 ppm.

Hydroxyethyl 4-cyano-4-(phenylcarbonothioylthio)pentanoate (HO-CPAD). 4-cyano-1-hydroxypent-4-yl dithiobenzoate (1.00 g, 3.58 mmol), ethylene glycol (2 ml, 17.9 mmol), and 4-dimethylaminopyridine (43.7 mg, 0.358 mmol) were dissolved in 20 ml CH_2Cl_2 in a flame dried 100 ml round bottom flask and cooled in an ice bath. N,N'-dicyclohexylcarbodiimide (886 mg, 4.30 mmol) in 7 ml CH_2Cl_2 was added dropwise via addition funnel. The reaction was allowed to reach room temperature and stirred for a total of 18 h. The precipitate was then removed by vacuum filtration and washed with CH_2Cl_2 until colorless. The filtrate was diluted to 100 ml with CH_2Cl_2 and washed with 3x50 ml DI H_2O and 1x50 ml brine. The organic layer was dried over $MgSO_4$ and concentrated. Residual urea was removed by addition of Et_2O, filtering off the precipitate, and concentrating. The crude product was purified by column chromatography on silica gel (1:9 → 1:1 CH_2Cl_2:EtOAc) to give HO-CPAD as a deep red syrup (743 mg, 67% yield).

^{1}H NMR ($CDCl_3$, 500 MHz): δ_{ppm}: 7.92 (m, 2H), 7.58 (m, 1H), 7.41 (m, 2H), 4.27 (m, 2H), 3.87 (m, 2H), 2.75 (m, 2H), 2.65 (m, 1H), 2.46 (m, 1H), 1.96 (s, 3H), 1.91 (t, J = 6.0 Hz, 1H). ^{13}C NMR ($CDCl_3$, 500 MHz): δ_{ppm}: 222.2, 171.8, 144.5, 133.0, 128.6, 126.7, 118.5, 66.6, 61.0, 45.7, 33.4, 29.8, 24.2. MS (ESI-TOF, *m/z*) Calcd. for $C_{15}H_{17}NO_3S_2$: 323.4304; found: 346.0542 ($M + Na^+$); error 0.54 ppm.

Polymerization of AMI (PAMI). AMI (4.62 g, 18.0 mmol), azobisisobutyronitrile (AIBN) (1 mol%) and $CHCl_3$ were added to a 50 ml Schlenk flask. The solution was degassed by consecutive freeze pump thaw cycles and heated to 70 °C for 4 h. The solution was then cooled to room temperature and an aliquot was taken to determine % conversion of AMI. The polymer was isolated by precipitation into MeOH and further purified by precipitation from CH_2Cl_2 into MeOH. After drying under vacuum, PAMI was isolated as a white powder (83% conversion by ^{1}H NMR spectroscopy; 3.33 g, 72% yield). SEC-MALLS analysis: M_n = 88.9 kg mol^{-1}. $Đ$ = 1.80. dn/dc = 0.0925 ml g^{-1}. T_d (5 wt%); N_2 = 251 °C, air = 217. T_g = 130 °C.

RAFT polymerization of AMI (PAMI-CTA). An illustrative example is provided: AMI (5.49 g, 21.4 mmol), OH-CPAD, (173 mg, 0.535 mmol), and AIBN (8.79 mg, 0.0535 mmol) were dissolved in 21 ml DMF in a 100 ml round bottom flask sealed with a septum. After sparging with argon for 20 min, the reaction was heated to 70 °C and stirred for 18 h. The reaction was then cooled to room temperature and an aliquot was taken to determine % conversion of AMI. After precipitation into MeOH, the polymer was collected by filtration and reprecipitated from CH_2Cl_2 into MeOH. After drying under vacuum PAMI-CTA (14) was isolated as a pink powder (95% conversion by ^{1}H NMR spectroscopy; 4.44

g, 81% yield). SEC-MALLS analysis: M_n = 13.8 kg mol^{-1}, $Đ$ = 1.07. T_d (5 wt%); N_2 = 255 °C, air = 252 °C. T_g = 94 °C.

Ene-PAMI-CTA. PAMI-CTA (14) (200 mg, 14.5 μmol) and methacrylic anhydride (20 μl, 145 μmol) and $Sc(OTf)_3$ (1 mg, 2 μmol) were dissolved in 0.5 ml acetonitrile with stirring. After 1 h the reaction mixture was precipitated into MeOH and the precipitate was collected by filtration. After reprecipitating from CH_2Cl_2 into MeOH, collecting by filtration, and drying under vacuum ene-PAMI-CTA was isolated as a pink powder.

PAMI-*b*-PnBA. An illustrative example is provided: PAMI-CTA (13.8 kg mol^{-1}, 240 mg) was dissolved in DMF (0.020 mmol/ml) followed by addition of *n*-butyl acrylate and AIBN ([*n*-butyl acrylate]:[CTA]:[AIBN] = 870:1:0.1) in a round bottom flask and sealed with a septum. After sparging with argon for 20 min the reaction was heated to 70 °C and stirred for 20 hr. After cooling to room temperature, CH_2Cl_2 was added (4:1 CH_2Cl_2:DMF by volume) and the mixture was precipitated into MeOH. The polymer was removed and purified by precipitation from CH_2Cl_2 into MeOH and dried under vacuum to give PAMI-PnBA (14-69) as a pink rubbery solid (64% conversion by ^{1}H NMR spectroscopy). SEC-MALLS analysis: M_n = 88.3 kg mol^{-1}, $Đ$ = 1.12. T_d (5 wt%); N_2 = 316 °C, air = 296 °C. T_g = −46, 121 °C.

2.5 References

(1) Zhang, J.; Li, J.; Wu, S.-B.; Liu, Y. *Ind. Eng. Chem. Res.* **2013**, *52* (34), 11799–11815.

(2) Scott, A. *C&EN* **2014**, *90* (27), 16–17.

(3) Fenouillot, F.; Rousseau, A.; Colomines, G.; Saint-Loup, R.; Pascault, J. P. *Prog.*

Polym. Sci. **2010**, *35* (5), 578–622.

(4) Rose, M.; Palkovits, R. *ChemSusChem* **2012**, *5* (1), 167–176.

(5) Besset, C.; Pascault, J.-P.; Fleury, E.; Drockenmuller, E.; Bernard, J. *Biomacromolecules* **2010**, *11* (10), 2797–2803.

(6) Shin, S.; Kim, B.-C. C.; Chang, E.; Cho, J. K.; Suh, D. H. *RSC Adv.* **2014**, *4* (12), 6226.

(7) Sadler, J. M.; Nguyen, A. P. T.; Toulan, F. R.; Szabo, J. P.; Palmese, G. R.; Scheck, C.; Lutgen, S.; La Scala, J. J. *J. Mater. Chem. A* **2013**, *1* (40), 12579–12586.

(8) Ge, J.; Trujillo, M.; Stansbury, J. *Dent. Mater.* **2005**, *21* (12), 1163–1169.

(9) Pion, F.; Reano, A. F.; Ducrot, P.-H.; Allais, F. *RSC Adv.* **2013**, *3* (23), 8988–8997.

(10) Feng, X.; East, A. J.; Hammond, W. B.; Zhang, Y.; Jaffe, M. *Polym. Adv. Technol.* **2011**, *22* (1), 139–150.

(11) Besset, C.; Bernard, J.; Fleury, E.; Pascault, J. P.; Cassagnau, P.; Drockenmuller, E.; Williams, R. J. J. *Macromolecules* **2010**, *43*, 5672–5678.

(12) Beghdadi, S.; Miladi, I. A.; Ben Romdhane, H.; Bernard, J.; Drockenmuller, E. *Biomacromolecules* **2012**, *13* (12), 4138–4145.

(13) Mansoori, Y.; Hemmati, S.; Eghbali, P.; Zamanloo, M. R.; Imanzadeh, G. *Polym. Int.* **2013**, *62* (2), 280–288.

(14) Koyama, H.; Tsutsumi, K. Polymerizable monomer polymeric compound resin compositions for photoresist and method for producing semiconductor. wo 2004113404, 2004.

(15) Sato, K.; Kodama, K. Positive-working far-UV photoresists. JP 2004341062, 2004.

(16) Cekovic, Z.; Tokic, Z. *Synthesis* **1989**, 610–612.

(17) Shaikh, A. L.; Kale, A. S.; Shaikh, M. A.; Puranik, V. G.; Deshmukh, A. R. A. S. *Tetrahedron* **2007**, *63* (16), 3380–3388.

(18) Stoss, P.; Merrath, P.; Schlüter, G. *Synthesis* **1987**, *1987* (2), 174–176.

(19) Berini, C.; Lavergne, A.; Molinier, V.; Capet, F.; Deniau, E.; Aubry, J.-M. *European J. Org. Chem.* **2013**, *2013* (10), 1937–1949.

(20) Abenhaïm, D.; Loupy, A.; Munnier, L.; Tamion, R.; Marsais, F.; Quéguiner, G. *Carbohydr. Res.* **1994**, *261* (2), 255–266.

(21) Van Buu, O. N.; Aupoix, A.; Hong, N. D. T.; Vo-Thanh, G. *New J. Chem.* **2009**, *33* (10), 2060–2072.

(22) Lemieux, R.; McInnes, A. *Can. J. Chem.* **1960**, *38* (1), 136–140.

(23) Xu, M.; Wang, W.; Xia, L.; Lin, G. *J. Org. Chem.* **2001**, *66* (11), 3953–3962.

(24) Kobayashi, S.; Sugiura, M. *Chem. Rev.* **2002**, *102* (6), 2227–2302.

(25) Kobayashi, S. *European J. Org. Chem.* **1999**, No. 1992, 15–27.

(26) Ishihara, K.; Kubota, M.; Kurihara, H.; Yamamoto, H. *J. Am. Chem. Soc.* **1995**, *117* (15), 4413–4414.

(27) Ishihara, K.; Kubota, M. *J. Org. Chem.* **1996**, *3263* (12), 4560–4567.

(28) Barrett, A.; Braddock, D. C. *Chem. Commun.* **1997**, *10*, 351–352.

(29) Howard, S.; Hagberg, E.; Rockafellow, E. Method for quantitative analysis of sugars, sugar alcohols and related dehydration products. US 20130337570.

(30) Ferriol, M.; Gentilhomme, A.; Cochez, M.; Oget, N.; Mieloszynski, J. L. *Polym. Degrad. Stab.* **2003**, *79* (2), 271–281.

(31) Brandrup, J.; Immergut, E.; Grulke, E.; Abe, A.; Bloch, D. *Polymer handbook*, 4th ed.; 1999; Vol. 49.

(32) Gregory, A.; Stenzel, M. H. *Prog. Polym. Sci.* **2012**, *37* (1), 38–105.

(33) Boyer, C.; Stenzel, M.; Davis, T. *J. Polym. Sci. Part A Polym. Chem.* **2011**, *49*, 551–595.

(34) Moad, G.; Rizzardo, E.; Thang, S. H. *Aust. J. Chem.* **2012**, *65* (8), 985.

(35) Matyjaszewski, K. *Macromolecules* **2012**, *45* (10), 4015–4039.

(36) Bates, F. S.; Fredrickson, G. H. *Phys. Today* **1999**, *52* (2), 32–38.

(37) Holmberg, A. L.; Reno, K. H.; Wool, R. P.; Epps Iii, T. H. *Soft Matter* **2014**, *10* (38), 7405–7424.

(38) Chong, Y.; Krstina, J.; Le, T.; Moad, G. *Macromolecules* **2003**, *60*, 2256–2272.

(39) Favier, A.; Charreyre, M.; Chaumont, P.; Pichot, C. *Macromolecules* **2002**, *35* (22), 8271–8280.

(40) Favier, A.; Charreyre, M.-T. *Macromol. Rapid Commun.* **2006**, *27* (9), 653–692.

(41) Tullo, A. H. *Chem. Eng. News* **2013**, *91* (46), 18–19.

(42) Liufu, S.-C.; Xiao, H.-N.; Li, Y.-P. *Polym. Degrad. Stab.* **2005**, *87* (1), 103–110.

(43) Beyler, C. L.; Hirschler, M. M. In *SFPE Handbook of Fire Protection Engineering*; DiNenno, P. J., Ed.; 2001; pp 110–131.

(44) Willcock, H.; O'Reilly, R. K. *Polym. Chem.* **2010**, *1* (2), 149–157.

Chapter 3: Acrylic triblock copolymers incorporating isosorbide for pressure sensitive adhesives[*]

[*] Reproduced in part with permission from Gallagher, J. J.; Hillmyer, M. A.; Reineke, T. M. *ACS Sustainable Chem. Eng.* **2016**, J*ust accepted*. DOI: 10.1021/acssuschemeng.6b00455

3.1 Introduction

Polymers derived from renewable resources have recently experienced a remarkable resurgence due to long-term environmental and availability concerns associated with petroleum derivatives.[1–4] The bicyclic sugar derivative isosorbide has garnered much attention as a bio-based feedstock for polymer applications and has become available on the commercial scale as a result of improvements in production technology.[5] For example, the French agricultural company Roquette recently completed the world's largest isosorbide production plant capable of producing 20,000 tons annually of high purity polymer grade isosorbide.[6] Incorporating isosorbide into a polymer imparts desirable qualities such as high glass transition temperature (T_g) and thermal stability (as characterized by the temperature at 5% mass loss, T_d). The diol functionality of isosorbide naturally lends itself to use in step growth polymers such as polyesters, polyurethanes, and polycarbonates. The application of isosorbide and the related dianhydrohexitols isomannide and isoidide in this area has been extensively studied.[7–9] An example of a commercial isosorbide based polymer is Mitsubishi's poly(isosorbide carbonate) product Durabio™, which finds use in automotive and electronic display applications due to its superior durability and optical clarity.[10,11]

A distinct advantage of controlled chain growth polymerization over step growth polymerizations is the ability to achieve narrow molar mass distributions and well-defined polymer architectures. However, only a few reports have focused on using isosorbide in chain growth polymerizations.[12–16] We previously described the preparation of a new monofunctional methacrylic isosorbide monomer (AMI) and its incorporation into block

copolymers by Reversible Addition Fragmentation chain Transfer (RAFT) polymerization.[12] Preparation of PAMI samples from different monomer regioisomer composition showed that regiochemistry did not have a significant impact on polymer properties. Macro chain transfer agents of PAMI were prepared with a narrow molar mass distribution ($Đ$) and controlled number average molar mass (M_n). Subsequent chain extension with *n*-butyl acrylate afforded a series of well-defined PAMI-PnBA diblock copolymers. Likewise, the synthesis of vinyl triazole monomers derived from isosorbide, isomannide, and isoidide and the polymerization thereof using RAFT polymerization has also been reported.[13] It was shown that the regiochemistry of poly vinyl triazoles from isosorbide had a significant impact on T_g and water solubility.

The ability to incorporate isosorbide into block polymers is appealing because it expands the scope of potential applications for this bio-based feedstock. Block copolymers find use as toughening agents, thermoplastic elastomers, and pressure sensitive adhesives (PSAs).[17] When the traditional poly(styrene)-poly(isoprene)-poly(styrene) block polymers are used as PSAs, it is necessary to compound them with midblock miscible tackifiers.[18] Tackifiers effectively increase the entanglement molecular weight (M_e) of the midblock and thus lower the storage modulus of the elastomer, which would otherwise be too high to allow intimate contact with a substrate to form an adhesive bond.[18] Acrylic block copolymers have been investigated as an alternative to styrenic block copolymers for various applications.[19–24] The most prominent example of an acrylic block copolymer is poly(methyl methacrylate)-poly(*n*-butyl acrylate)-poly(methyl methacrylate) (PMMA-PnBA-PMMA).[20,24] The commercial grade version of this triblock copolymer is produced

by Kuraray Co., Ltd for use in PSA applications as Kurarity LA2140e. Unlike styrenic block copolymers, PMMA-PnBA-PMMA can be used with or without tackifier for PSA applications.[23] The M_e of PnBA is ~5–10 times higher than poly(butadiene) or poly(isoprene), resulting in a storage modulus that is inherently low enough to form an adhesive bond. Moreover, acrylic block copolymers have certain advantages over styrenic block copolymers such as UV and oxidation resistance. Acrylics also have more functional versatility due to the ability to vary the pendant ester group without significantly altering the reactivity of the acrylate moiety. As a result polyacrylates can occupy an exceptionally broad range of polarity and T_g.[25]

Supplementing petroleum derived feedstocks with bio-based resources is a vital aspect to improving the sustainability of PSAs.[26] Previous reports describing sustainable triblock copolymers for PSA applications focused on the ring opening polymerization of bio-based lactones to afford the corresponding polyesters.[27–30] Similar to the styrenic block copolymers, PSA formulations featuring the triblock copolyesters required addition of tackifier due to the relatively low M_e of the, for example, poly(menthide) and poly(ε-caprolactone) midblocks. Results from adhesion testing of the triblock copolyester and tackifier formulations demonstrated performance similar to commercial PSAs. Renewably sourced acrylates have also been reported for use in PSA applications.[26] For example, Severtson and coworkers described a platform based on acrylic functionalized poly(lactide-*co*-caprolactone) and random copolymers thereof with various (meth)acrylic comonomers.[31–33] An example of a PSA system incorporating isosorbide was recently described by Vandamme and Eevers.[34] The PSAs were prepared by polycondensation

between isosorbide and a dimerized fatty acid followed by thermal curing of the resultant polyester with epoxidized plant oils. The researchers reported an increase in T_g and peel force for the PSAs incorporating isosorbide over those derived from dimerized fatty alcohols.

In this work we endeavored to expand the utility of isosorbide by incorporating it into an all acrylic triblock copolymer via a controlled chain growth polymerization. To this end, we detail (i) synthesis of a new monomer acetylated acrylic isosorbide (AAI) in two steps from common reagents without the need for chromatographic separations; (ii) free radical polymerization of AAI to afford a thermally stable and high T_g thermoplastic PAAI; (iii) incorporation of PAAI into well-defined triblock copolymers with low T_g acrylic midblocks via RAFT polymerization; and (iv) evaluation of PSA performance as a function of PAAI content and midblock structure.

3.2 Results and Discussion

3.2.1 Synthesis of AAI

AAI was prepared in two steps according to Scheme 3.1. In the first step, the monoacetate was prepared by esterification of isosorbide with acetic acid, followed by a tandem transesterification-distillation step to afford isosorbide *exo* acetate in a crude yield of 69%. After recrystallization from methyl ethyl ketone, the purified product was obtained in a 38% yield. While the yield on a per distillation basis was modest in our hands, the yield can be increased by resubjecting the mother liquor to the reactive distillation process. Additional improvements in the yield could be achieved by using a distillation column with more theoretical plates. This method for preparing isosorbide *exo* acetate was first reported

by Stoss[35,36] and is remarkable for its ability to provide an isosorbide monoacetate in good yield and high purity. Furthermore, this route utilizes common reagents and minimal solvent making it particularly appealing for scalable production. The acrylate moiety was then installed by esterifying the pure monoacetate with acryloyl chloride to afford AAI as a crystalline solid.

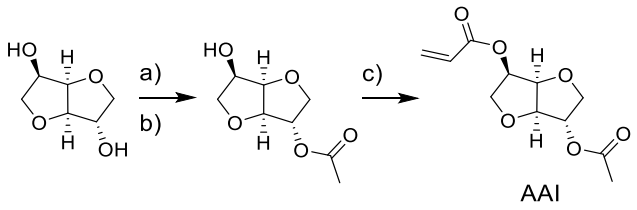

Scheme 3.1. Synthesis of AAI. a) 1.3 mol eq. acetic acid, 1 wt% *p*-toluenesulfonic acid, refluxed toluene, Dean Stark trap; b) 2 wt% KOH, 200 mTorr, reactive distillation; c) 1.05 mol eq. acryloyl chloride, 1.1 mol eq. triethylamine, 0 °C to r.t., 18 h, DCM.

The structure of AAI was confirmed by NMR and IR spectroscopy. The acrylic protons are clearly visible in the ^{1}H NMR spectrum between 6.47 and 5.81 ppm (Figure 3.1) and the vinyl carbons appear in the ^{13}C NMR spectrum at 132 and 128 ppm (Figure 3.2). The presence of only one set of resonances in the NMR spectra indicates that only the *exo*-acyl-*endo*-acryloyl-isosorbide isomer is present in the product. The acrylic moiety is also indicated by the vibrations at 1726 cm^{-1} (C=O) and 1637 cm^{-1} (C=C) in the IR spectrum (Figure 3.3). Further structural confirmation was provided by high-resolution mass spectrometry ([M + Na^{+}] expected = 265.0688; found: 265.0684; error 1.51 ppm).

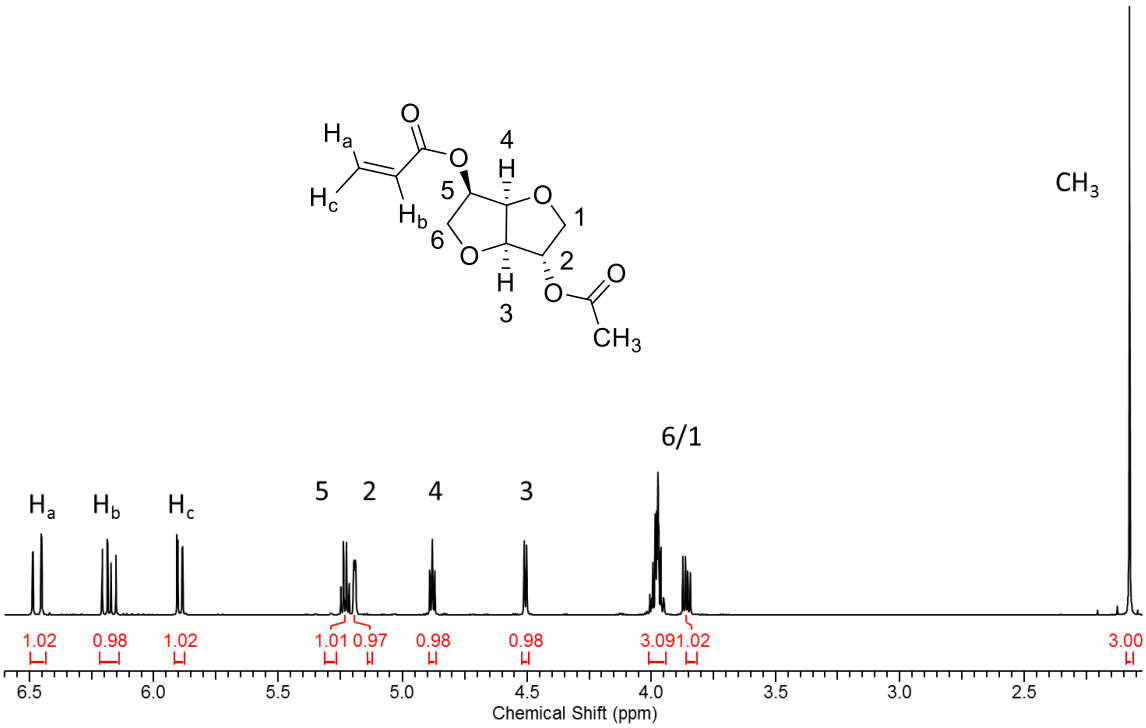

Figure 3.1. ^{1}H NMR of AAI in $CDCl_3$.

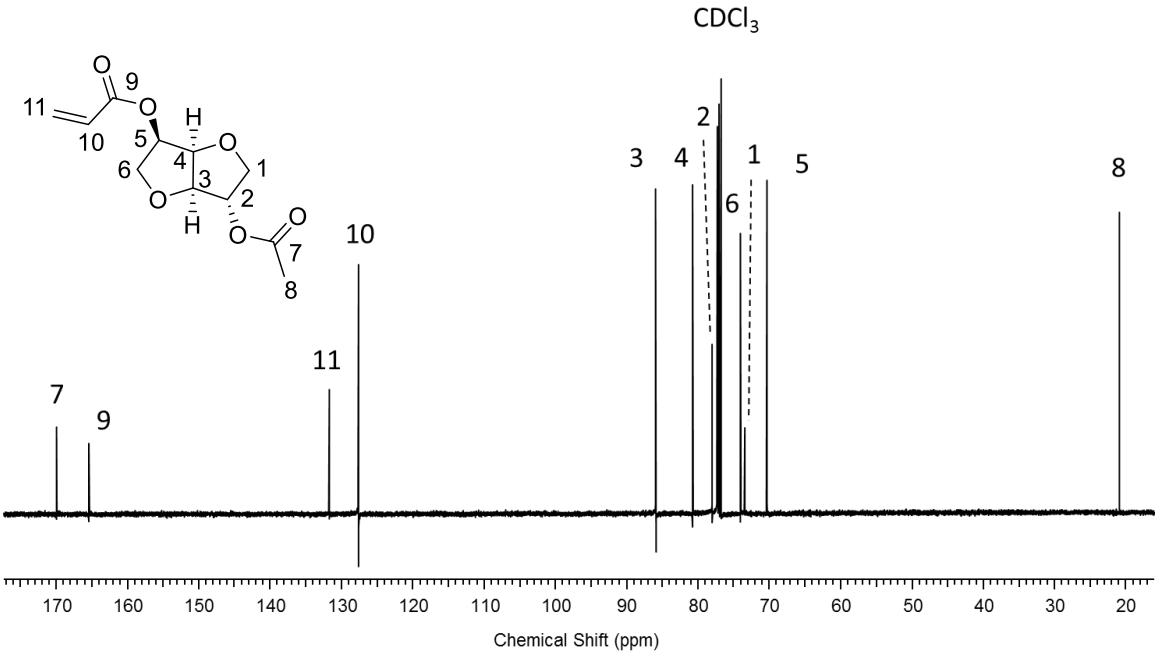

Figure 3.2. ^{13}C NMR of AAI in $CDCl_3$.

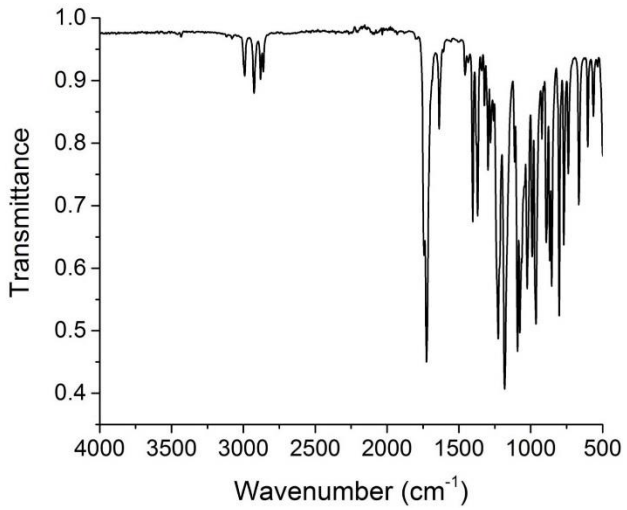

Figure 3.3. ATR FTIR of AAI.

The thermal properties of AAI were investigated using thermogravimetric analysis (TGA) and differential scanning calorimetry (DSC). Two mass loss events were observed by TGA of AAI in N_2 and air (Figure 3.4). The onset of the first mass loss occurred at a higher temperature (152 °C) under air and constituted a smaller mass loss (6 wt%) than the result in N_2 (148 °C and 21 wt%) likely due to the *in situ* polymerization of AAI during TGA in the presence of oxygen. This hypothesis is supported by the TGA result in the presence of the free radical inhibitor butylated hydroxytoluene where 95 % of the mass loss occurs during the first mass loss event, indicating that polymerization was suppressed. DSC of AAI was used to determine a melting point and T_g of 38 and –36 °C, respectively (Figure 3.5). A difference of ~100 °C between the melting point and onset of degradation of AAI indicates this monomer can be processed in the liquid state without incurring degradation.

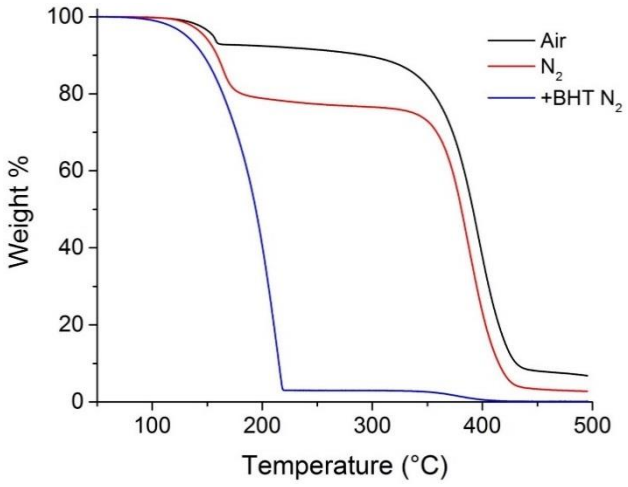

Figure 3.4. TGA of AAI. Heating rate = 10 °C min^{-1}.

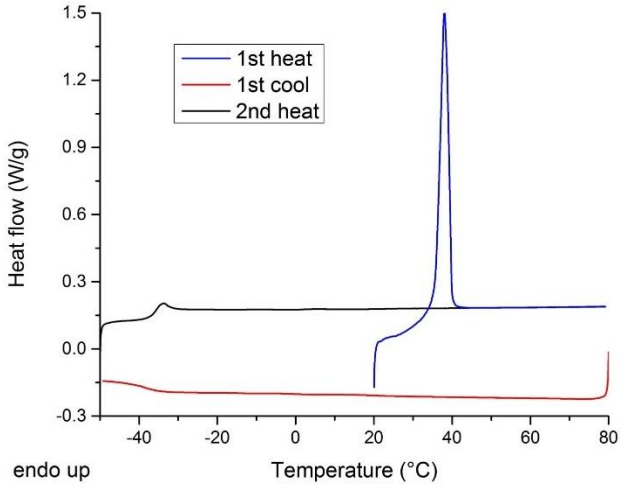

Figure 3.5. DSC of AAI. Heating and cooling rate = 10 °C min^{-1}.

3.2.2 Free radical polymerization of AAI

A sample of PAAI prepared by normal free radical polymerization (Scheme 3.2) was soluble at 10 wt% in THF, ethyl acetate, CH_2Cl_2, $CHCl_3$, acetone, and DMF but was insoluble in water, MeOH, ether, and hexanes. Size exclusion chromatography with multiangle laser light scattering detection (SEC-MALLS) in THF was used to determine a number average molar mass (M_n) = 120 kg mol^{-1} and a molar mass distribution ($Đ$) = 4.00.

Thermal degradation temperatures (T_d, 5% wt loss) of PAAI under N_2 and air were determined by TGA to be 337 °C and 291 °C, respectively, while DSC analysis showed a T_g = 95 °C (Figure 3.7). The thermal stability of PAAI is significantly higher than that reported for PAMI prepared by free radical polymerization (T_d, 5% wt loss; N_2 = 251 °C, air = 217 °C). The higher T_d of PAAI supports our previous hypothesis that the onset of thermal degradation of PAMI was due to the instability of the methacrylic backbone rather than that of the pendant isosorbide groups.[12] Polymethacrylates undergo thermal decomposition at ~200–250 °C due the favorable depolymerization of the polymer backbone, while polyacrylates typically degrade at ~300–350 °C via a random chain scission mechanism.[37,38] The similar T_d of PAAI to other polyacrylates exemplifies the desirable thermal stability of isosorbide. The T_g of PAAI is lower than what was previously reported for PAMI (T_g = 130 °C) due to the increased flexibility of the polyacrylic backbone relative to the polymethacrylic backbone. Nevertheless, the steric bulk of the pendant isosorbide acetate groups of PAAI impart enough rigidity to afford a T_g within the realm of typical glassy polymers such as PMMA and poly(styrene) (T_g ~110 and 100 °C, respectively).

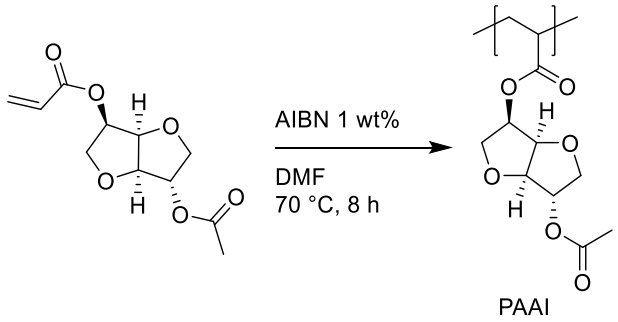

Scheme 3.2. Free radical polymerization of AAI.

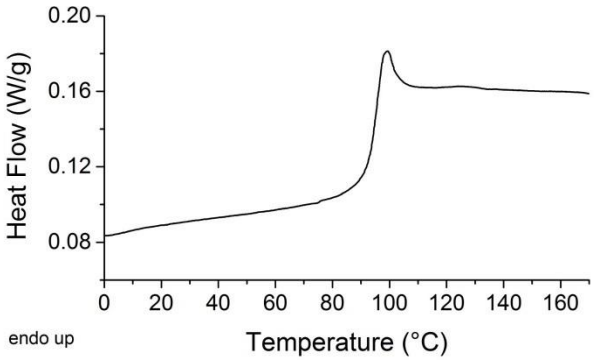

Figure 3.7. DSC of PAAI prepared by free radical polymerization. Ramp rate = 10 °C min^{-1}. Second heat.

3.2.3 PAAI-PnBA-PAAI and PAAI-PEHA-PAAI via RAFT polymerization

RAFT polymerization was selected as a means to prepare the desired triblock copolymers.[39,40] To determine the appropriate RAFT agent for controlled polymerization of AAI, a series of RAFT chain transfer agents (CTAs) were screened (Table 3.1, Figure 3.8). Trithiocarbonates afforded PAAI with $Đ \leq 1.20$ and a M_n (SEC) within 5% error of M_n (calc), while no significant polymerization of AAI was observed with dithiobenzoates after 18 h. Dithiobenzoates have been reported to inhibit polymerization of acrylates due to their low rate of fragmentation.[41] Therefore the commercially available CTA 3,5-Bis(2-dodecylthiocarbonothioylthio-1-oxopropoxy)benzoic acid (BTCBA) was selected to construct the desired library of triblock copolymers. While there are no reports of BTCBA being used in the open literature the butyl trithiocarbonate analogue has been reported to successfully control the polymerization of nBA.[41] A distinct advantage of BTCBA over other monofunctional RAFT CTAs is the ability to construct the desired ABA triblock in only two consecutive polymerization steps.

Table 3.1. Screening RAFT agents for PAAI polymerization

CTA	% conv.[a]	M_n (calc)[b] (kg mol^{-1})	$M_{n,}$ (SEC) [c] (kg mol^{-1})	$Đ$[c]
1	<5	-	-	-
2	<5	-	-	-
3	77	18.6	18.5	1.20
4	56	13.6	13.0	1.15

[a]From ^{1}H NMR; [b]Assuming 1 CTA per chain; [c]SEC-MALLS in THF.

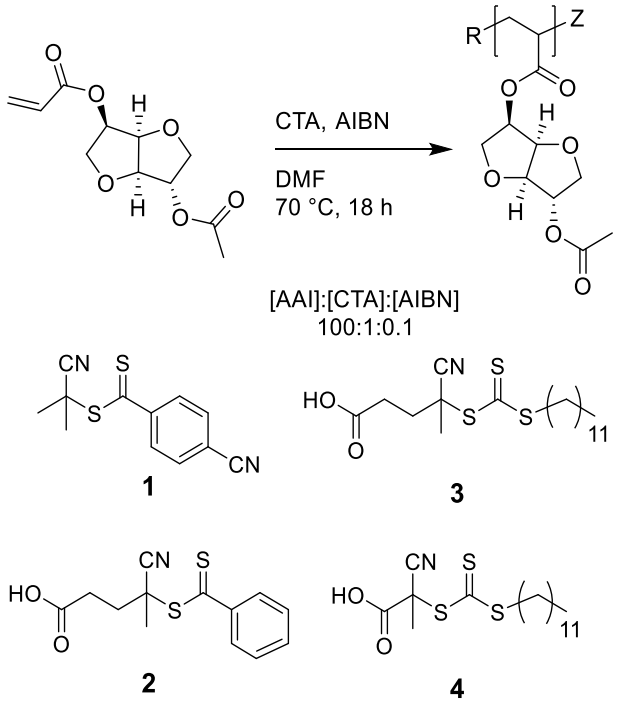

Figure 3.8. RAFT polymerization of AAI.

2-ethylhexyl acrylate (EHA) and nBA were selected to construct the midblock portion of the triblock copolymers. Both monomers are commercially available, inexpensive, and find extensive use as low T_g components in polyacrylates.[43] Acrylics are

particularly attractive from a sustainability point of view as the development of bio-based acrylic acid has been actively pursued recently.[44] The monomer nBA is also appealing due to the potential for bio-sourced *n*-butanol.[26] Furthermore, PEHA is known to have good film formation properties.[45] PnBA and PEHA have distinct M_e values (28 and 59 kg mol^{-1}, respectively) allowing us to determine the effect of midblock structure on the adhesive performance of the materials. nBA and EHA were polymerized neat in the presence of BTCBA and AIBN at 70 °C to afford the corresponding macro-CTAs (Scheme 3.3, Table 3.2). ^{1}H NMR analysis confirmed the presence of the expected mid and end groups (Figures 3.9 and 3.10). Resonances at 7.68 and 7.13 ppm correspond to the aryl mid group protons, the tertiary proton of the terminal repeat unit appears at 4.82 ppm, and the α methylene protons of the trithiocarbonate are visible at 3.33 ppm. No significant difference was observed for the mid and end group resonances between PnBA and PEHA. The observed resonances were in excellent agreement with those reported previously for the butyl trithiocarbonate analogue.[42] M_n (NMR) and M_n (SEC) were also in good agreement (Table 3.2) and $Đ < 1.06$ was achieved for all three macro-CTAs indicating good control of the RAFT polymerization.

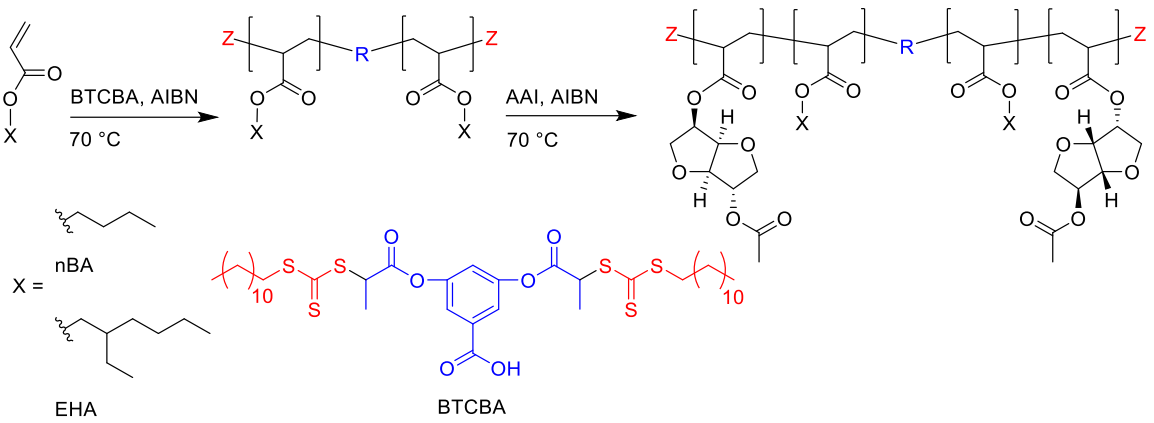

Scheme 3.3. Synthesis of PAAI-PnBA-PAAI and PAAI-PEHA-PAAI by RAFT polymerization.

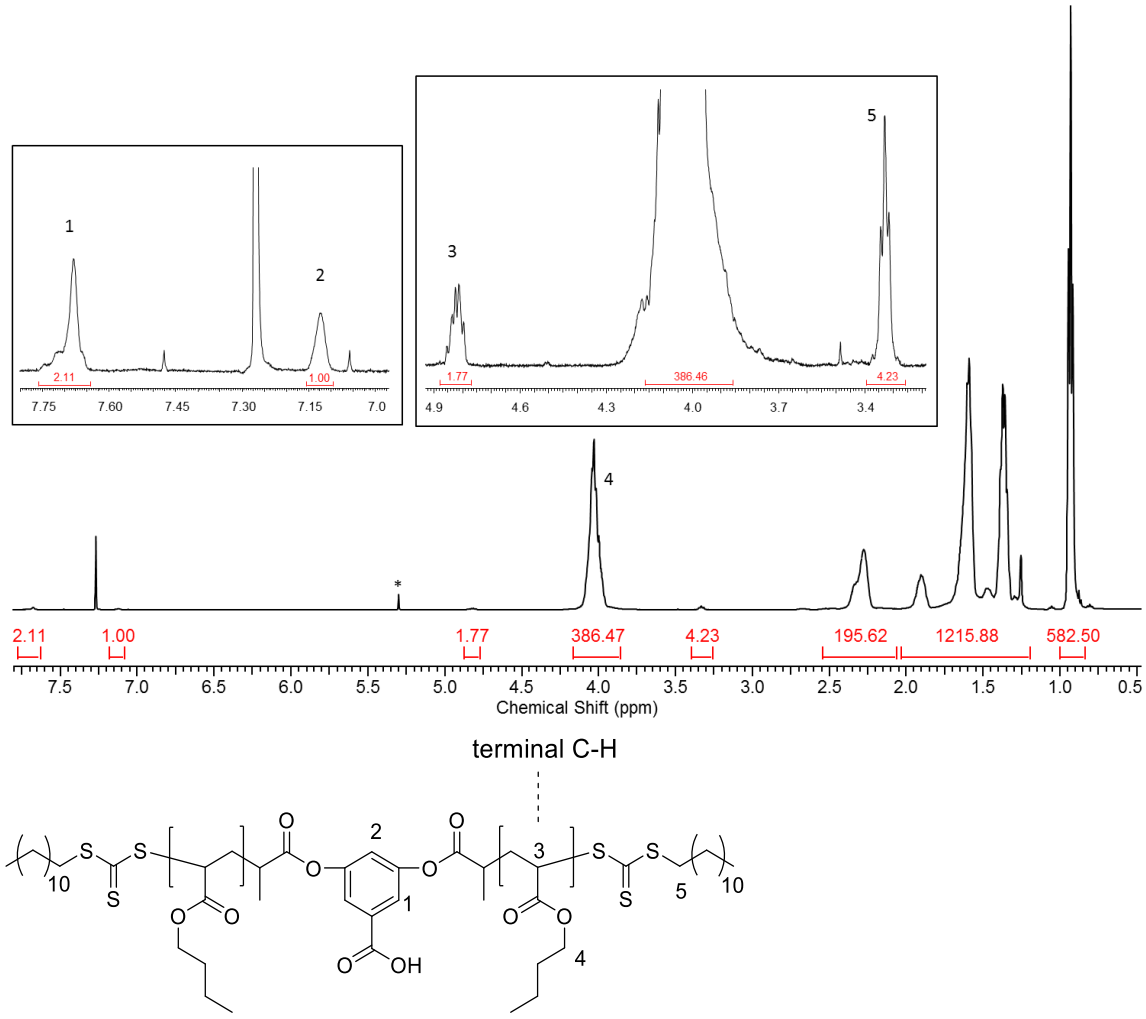

Figure 3.9. ^{1}H NMR of PnBA 27k in $CDCl_3$. End group resonances in insert. * = residual CH_2Cl_2.

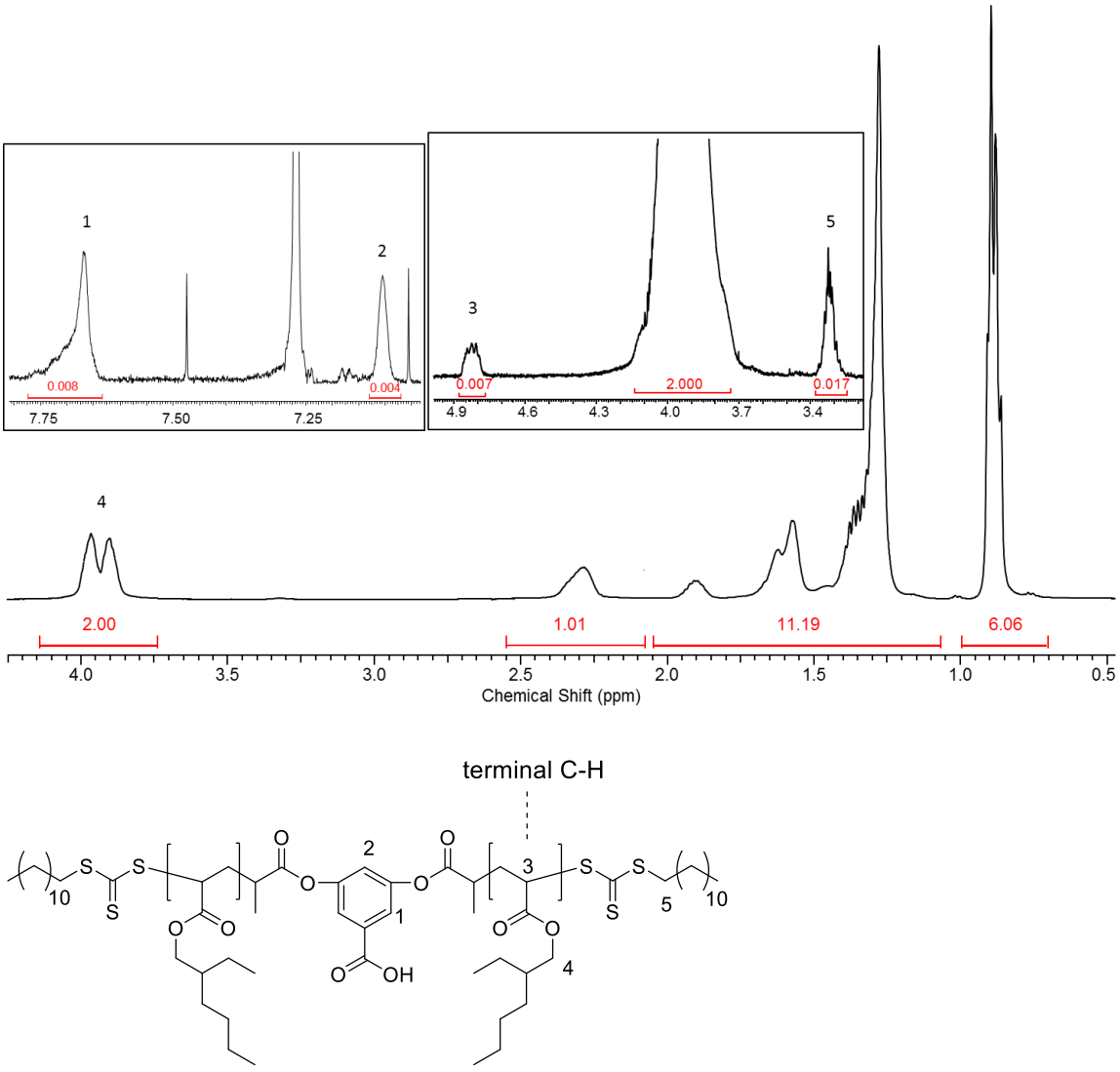

Figure 3.10. ^{1}H NMR of PEHA 45k in $CDCl_3$. End group resonances in insert.

Table 3.2. PAAI-PnBA-PAAI and PAAI-PEHA-PAAI molar mass data.

Polymer	[M]/[CTA][a]	time (h)	conv (%)	M_n (calc)[b] (kg mol^{-1})	M_n (SEC)[c] (kg mol^{-1})	M_n (NMR)[d] (kg mol^{-1})	$Đ$[c]	PAAI[e] (wt%)
PnBA 27k	100	2	86	22.0	27.4	25.8	1.06	0
PAAI-PnBA-PAAI (63k, 54%)	94	2	68	58.4	63.2	52.1	1.19	54
PnBA 45k	250	2	69	44.2	45.3	44.4	1.03	0
PAAI-PnBA-PAAI (53k, 12%)	39	1.5	34	51.7	53.3	49.8	1.09	12
PAAI-PnBA-PAAI (60k, 17%)	39	2	57	56.1	60.2	65.6	1.12	17
PAAI-PnBA-PAAI (70k, 21%)	55	2.5	48	59.5	69.2	67.5	1.15	21
PEHA 45k	115	1	90	38.1	44.7	43.4	1.06	0
PAAI-PEHA-PAAI (51k, 8%)	14	2	58	58.5	51.3	51.3	1.18	7.9
PAAI-PEHA-PAAI (54k, 14%)	22	2	70	52.2	54.2	52.3	1.2	14
PAAI-PnBA-PAAI (64k, 24%)	36	2	79	48.6	63.5	60.9	1.25	24

[a]CTA defined as trithiocarbonate moiety (i.e. 2 CTA per BTCBA), [CTA]:[AIBN] = 10:1. [b]Assuming 1 BTCBA molecule per polymer chain (see SI); [c]From SEC-MALLS in THF; [d]Determined relative to aromatic mid group; [e]From ^{1}H NMR spectroscopy.

Chain extension of the PnBA and PEHA macro-CTAs with AAI afforded the triblocks PAAI-PnBA-PAAI and PAAI-PEHA-PAAI, respectively. An advantage of AAI over AMI is that acrylic monomers can be used for controlled chain extension via RAFT from an acrylic macro-CTA while methacrylic monomers can not.[40] To first demonstrate the ability to affect a controlled chain extension reaction, PnBA 27k was used as a macro-CTA to prepare a sample of PAAI-PnBA-PAAI with 54 wt% PAAI. A clear shift to lower

elution volume in the SEC trace indicated successful chain extension (Figure 3.11). A high molar mass shoulder was present in the SEC trace of the triblock likely due to termination by combination, however the molar mass distribution was relatively narrow ($Đ$ = 1.19) suggesting that the chain extension reaction was well controlled. M_n (SEC) was 63.2 kg mol^{-1} in good agreement with the theoretical M_n (calc) (58.4 kg mol^{-1}). The aromatic mid group and α methylene protons of the trithiocarbonate end group were visible in the ^{1}H NMR spectrum at the same chemical shifts as for PnBA 27k (Figure 3.12). The terminal repeat unit tertiary proton was no longer visible as it was obscured by the PAAI repeat unit resonances. Two series of triblock copolymers to be evaluated as pressure sensitive adhesives were then prepared by chain extension of PnBA 45k and PEHA 45k. Different lengths of the PAAI end block were prepared by varying the ratio of CTA to AAI during the polymerization. The M_n (SEC) in kg mol^{-1} and wt% of PAAI as determine by NMR are indicated for each sample (Table 3.2). Again, a shift in the peak in the SEC trace to lower elution times (Figure 3.13) and $Đ$ < 1.25 was maintained for all triblock copolymers indicating successful chain extension. The wt% of PAAI ranged from 8–24 consistent with typical hard block composition for triblock copolymers in PSA applications.[23,27–29]

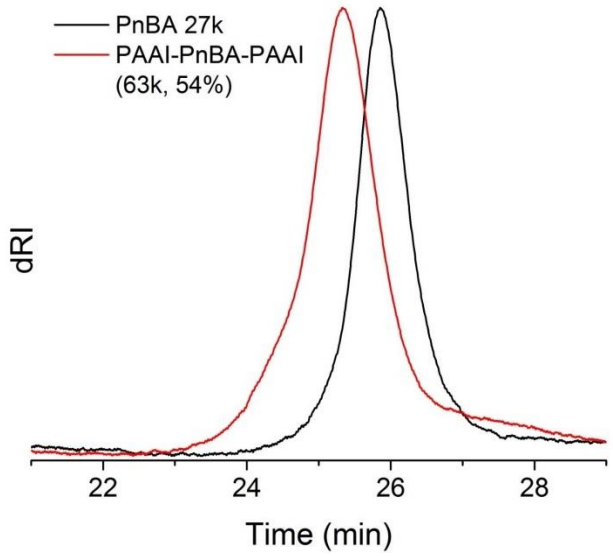

Figure 3.11. THF SEC of PnBA 27k macro-CTA and PAAI-PnBA-PAAI (63k, 54%).

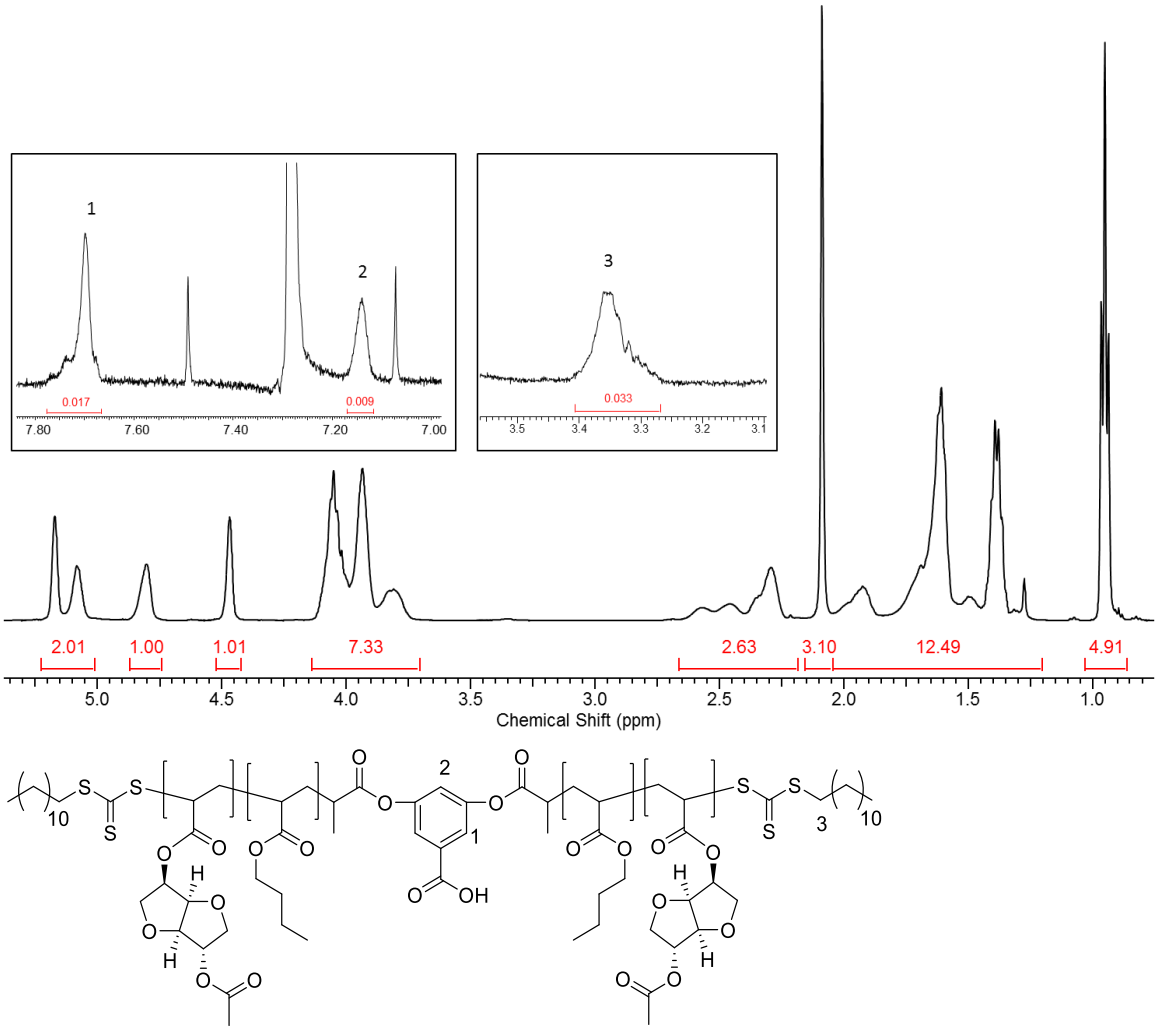

Figure 3.12. ^{1}H NMR of PAAI-PnBA-PAAI (63k, 54%) in $CDCl_3$. End group resonances in insert.

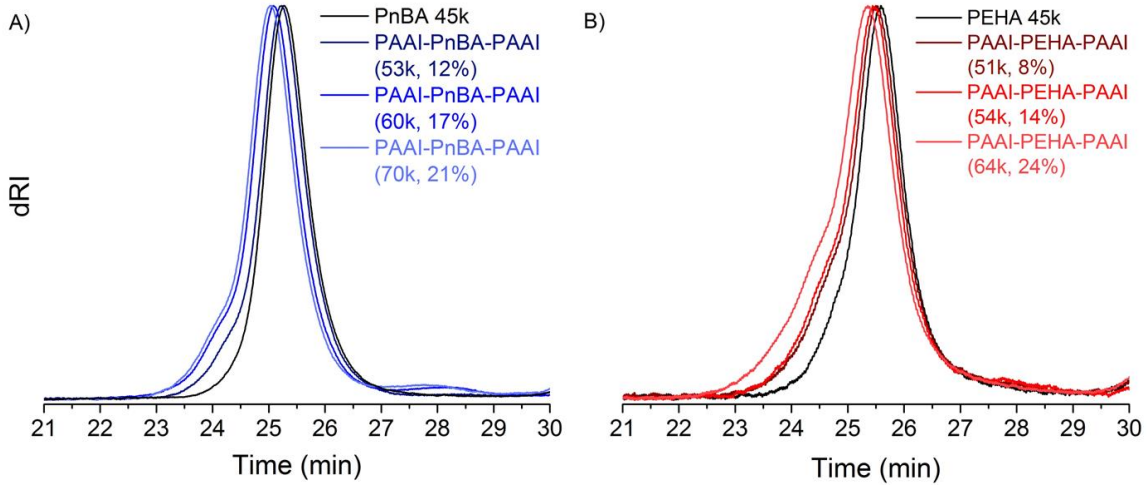

Figure 3.13. THF SEC with differential refractive index (dRI) detector of A) PAAI-PnBA-PAAI and B) PAAI-PEHA-PAAI triblock copolymers used for adhesion testing.

Alcoholysis was performed on a sample of triblock in order to confirm symmetric growth from the central initiating fragment. PAAI-PnBA-PAAI (60k, 17%) was heated to 130 °C in the presence of *p*-toluenesulfonic acid and excess *n*-butanol for 48 h (Scheme 3.4). ^{1}H NMR analysis after purification by precipitation and drying showed no aromatic resonances corresponding to the mid group, indicating full alcoholysis of the benzylic esters (Figure 3.14). Trace amounts of broad resonances between 3.75 and 5.25 ppm suggest some residual pendant isosorbide groups. The chemical shifts do not match that of PAAI and likely correspond to a deacetylated isosorbide group. Based on peak integration relative to PnBA the residual isosorbide pendant groups are estimated to be present at < 5 wt%. The SEC trace of PAAI-PnBA-PAAI (60k, 17%) after alcoholysis was monomodal with M_n = 35.4 kg mol^{-1}, near the expected value of 30.1 kg mol^{-1} (Figure 3.15). Thus, we conclude that RAFT polymerization allowed preparation of two series of triblock copolymers in two steps with good control over molar mass composition and a symmetric polymer architecture.

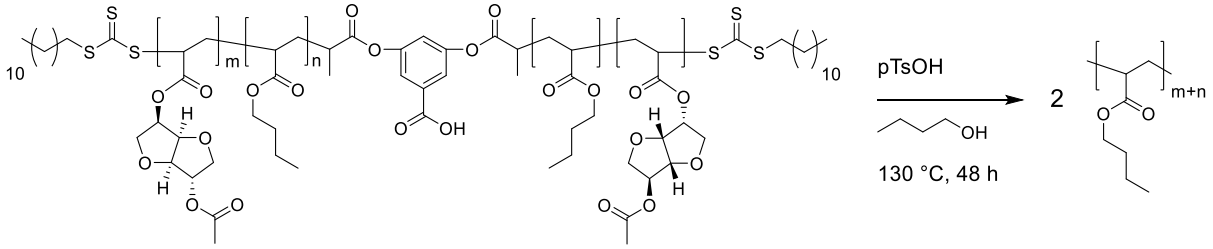

Scheme 3.4. Alcoholysis of PAAI-PnBA-PAAI (60k, 17%).

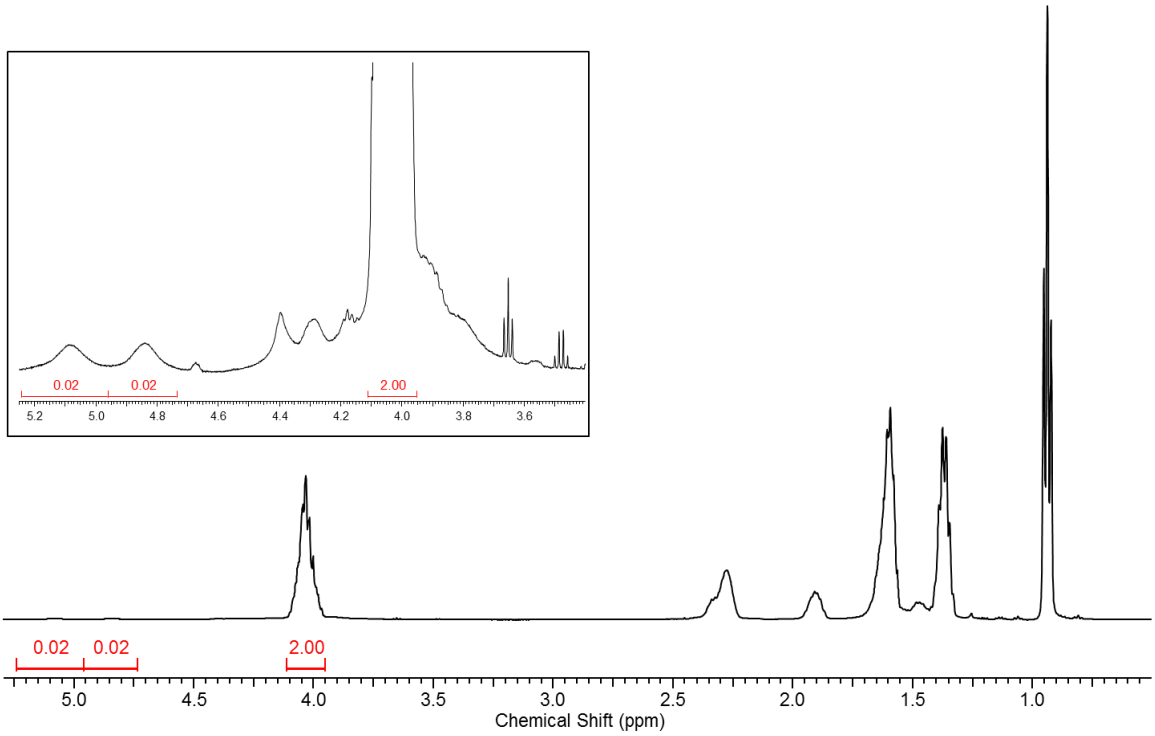

Figure 3.14. ^{1}H NMR in $CDCl_3$ of PAAI-PnBA-PAAI (60k, 17%) after alcoholysis.

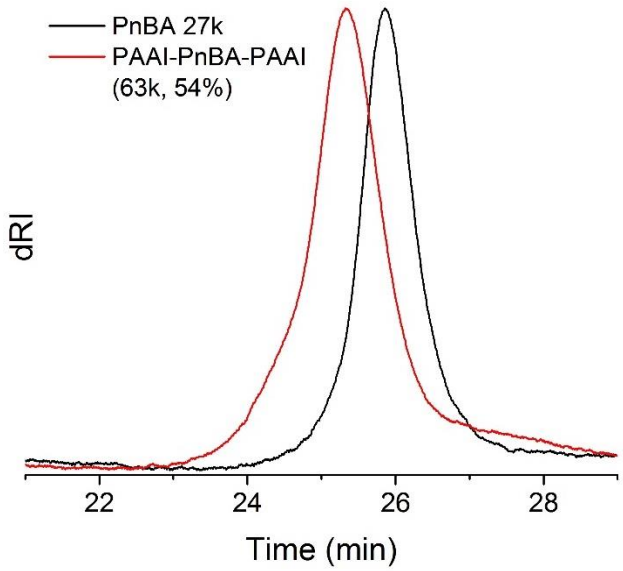

Figure 3.15. THF SEC of PAAI-PnBA-PAAI (60k, 17%) before and after alcoholysis.

3.2.4 Thermal, morphological, and mechanical characterization of triblock copolymers.

PAAI-PnBA-PAAI (60k, 17%) and PAAI-PEHA-PAAI (54k, 14%) exhibited similar thermal stability under N_2 (T_d = 334 and 338 °C, respectively) (Figures 3.16 and 3.17). Thermal stability in the presence of oxygen however differed significantly between the two samples. PAAI-PnBA-PAAI (60k, 17%) had a higher thermal stability in air (T_d = 304 °C) than PAAI-PEHA-PAAI (54k, 14%) (T_d = 264 °C). The onset of degradation for PAAI-PEHA-PAAI (54k, 14%) at lower temperature may be due to the tertiary carbons present in the PEHA pendant groups, which are prone toward oxidative degradation. DSC analysis of the triblocks showed T_g values corresponding to PnBA and PEHA midblocks at ~ −45 and −60 °C, respectively (Figure 3.18). With the exception of PAAI-PnBA-PAAI (63k, 54%) which exhibited two T_g values at −45 and 80 °C, no clear transition could be assigned to the T_g of the PAAI end blocks in the other block copolymer samples. A potential explanation is that the DSC is not sensitive enough to determine the T_g of the end

blocks due to their relatively small M_n and low wt% present in each sample. The presence of midblock T_g near that of the homopolymer and independent of wt% PAAI suggests that the two polymer components are not mixed. For example, based on homopolymer T_g of −65 and 95 °C and assuming the two components are mixed, the Fox equation predicts T_g for PAAI-PEHA-PAAI (51k, 8%) = −57 °C and PAAI-PEHA-PAAI (64k, 24%) = −41°C.

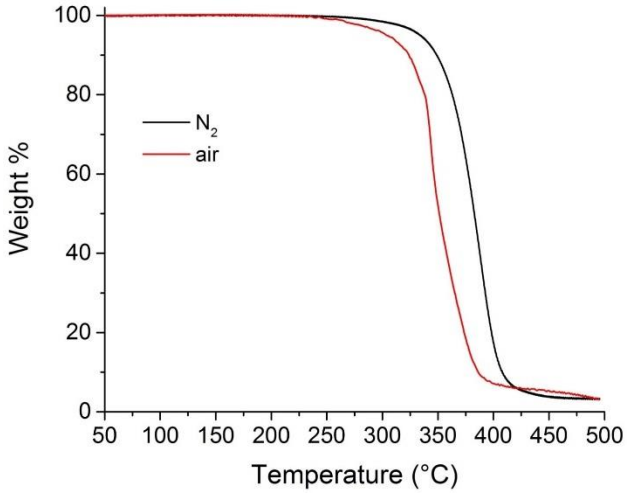

Figure 3.16. TGA of PAAI-PnBA-PAAI (60k, 17%). Heating rate = 10 °C min^{-1}.

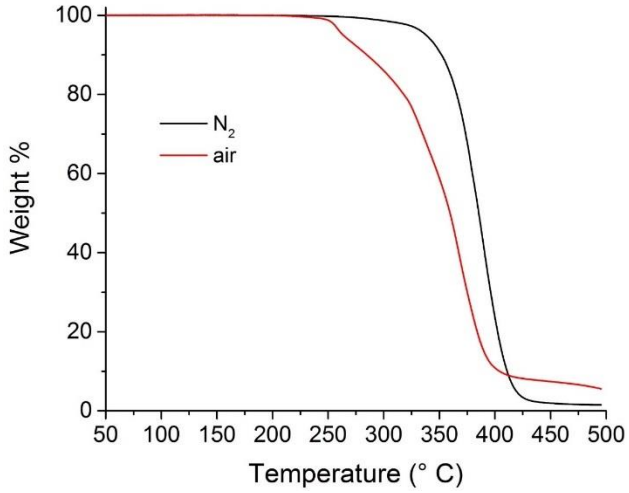

Figure 3.17. TGA of PAAI-PEHA-PAAI (54k, 14%). Heating rate = 10 °C min^{-1}.

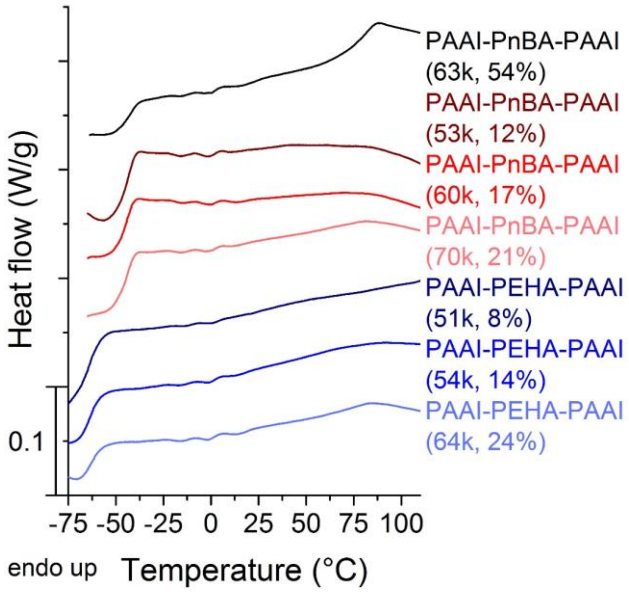

Figure 3.18. DSC of PAAI-PnBA-PAAI and PAAI-PEHA-PAAI triblock copolymers. Heating rate = 10 °C min^{-1}, 2nd heating. Data are shifted vertically for clarity.

Small angle X-ray scattering (SAXS) was used to probe the phase separation of the triblock copolymers. The scattering profile of PAAI-PnBA-PAAI (63k, 54%) confirmed the expected lamellar morphology of this sample with peaks distinctly visible at integer multiples of the principle scattering peak (q^*) (Figure 3.18). The scattering profiles of triblocks with lower PAAI content exhibited a q^* as well as broad higher order reflections (Figure 3.19). The broad nature of the higher order peaks precludes the definitive assignment of the morphology of these samples, however other reports of similar scattering patterns from triblocks with low end block content have been claimed to indicate a spherical morphology with limited long range order.[29,30] The principle domain spacing ($D^* = 2\pi/q^*$) of the triblock copolymer samples ranged from 16.3–20.8 nm and the sphere radii were estimated to be between 4.5–7.9 nm based on fitting a spherical form factor to the SAXS scattering profiles (Table S2).

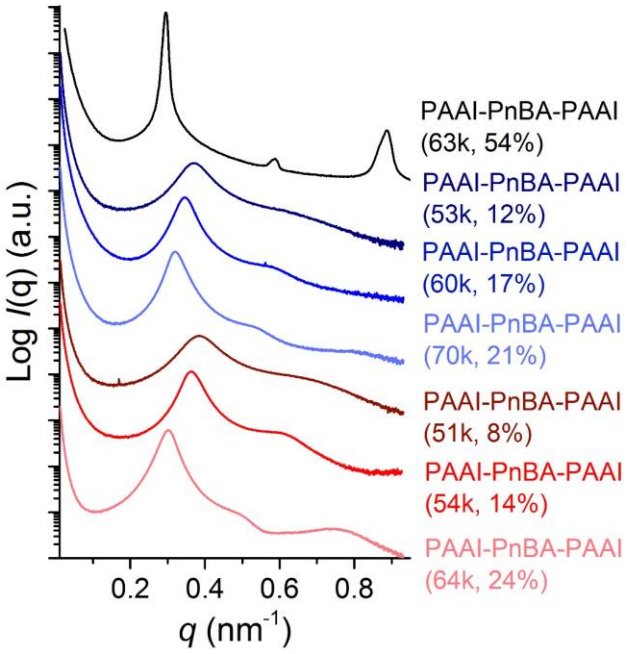

Figure 3.19 SAXS patterns for PAAI-PnBA-PAAI and PAAI-PEHA-PAAI triblock copolymers. Data are shifted vertically for clarity.

The mechanical properties of an elastomer play an important role in PSA performance. Elastomers that exhibit low toughness tend to fail within the elastomer layer and leave residue on the adherend (cohesive failure), while tougher elastomers tend to fail at the interface between adherend and elastomer without leaving residual material on the adherend (adhesive failure). Adhesive failure is required for removable PSAs such as masking tape, whereas cohesive failure is desirable for permanent PSA applications such as labels and packaging. To this end, the mechanical properties of PAAI-PnBA-PAAI (60k, 17%) and PAAI-PEHA-PAAI (54k, 14%) were evaluated using tensile testing (Figure 3.20). Significant differences were observed in the stress vs strain curves between the two triblocks. Young's moduli (*E*) of PAAI-PnBA-PAAI (60k, 17%) and PAAI-PEHA-PAAI (54k, 14%) were 106 ± 12 and 85 ± 8 kPa, respectively. PAAI-PnBA-PAAI (60k, 17%) also displayed higher elongation at break, stress at break, and toughness than PAAI-PEHA-

PAAI (54k, 14%). All samples tore at the grips of the tensile tester rather than in the gauge region, therefore preventing the quantitative description of the ultimate tensile behavior of these samples. However, because the samples were all tested under the same conditions, the qualitative difference between the two polymer samples is worth noting. Higher values of E and toughness for PAAI-PnBA-PAAI (60k, 17%) are a result of the lower M_e of PnBA relative to PEHA. At a midblock length of 45 kg mol^{-1} PnBA is expected to be moderately entangled, while PEHA should be completely unentangled. The lack of entanglements to dissipate the applied tensile stress results in relatively poor mechanical properties. Commercial PSA grade PMMA-PnBA-PMMA triblock copolymer with 23 wt% PMMA was reported to have E = 1.00 MPa and tensile strength = 6.24 MPa,[27] however the unknown molar mass of the commercial sample precludes any useful comparison to the properties reported above for PAAI-PEHA-PAAI (54k, 14%) and PAAI-PnBA-PAAI (60k, 17%). The polyester triblocks previously reported for use as PSAs showed even higher values of E and tensile strength (up to 5.97 and 13.6 MPa, respectively) due to the high molar mass and low midblock M_e.[27–29]

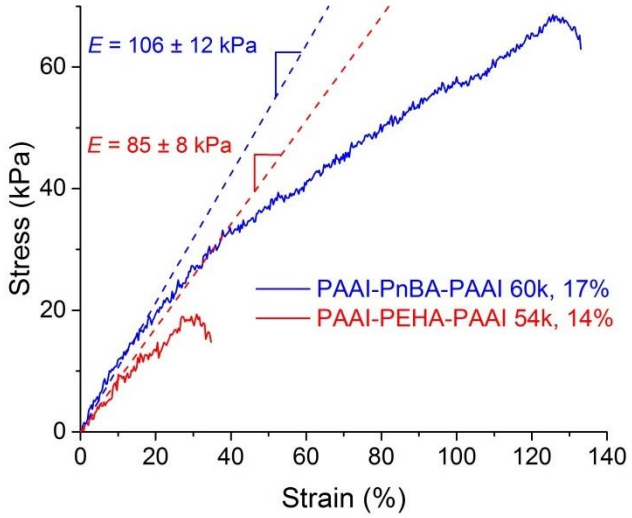

Figure 3.20. Representative stress vs. strain curves for PAAI-PnBA-PAAI (60k, 17%) and PAAI-PEHA-PAAI (54k, 14%). Moduli are averages of five samples, see Figures S28 and S29.

3.2.5 Adhesive performance of triblock copolymers

The adhesives were prepared by dissolving the polymer in ethyl acetate and solution coating onto a sheet of poly(ethylene terephthalate) using a wound wire rod. The films were then left to dry under ambient conditions for 24 h before testing. The adhesive performance of the triblock copolymers was evaluated by 180° peel, loop tack, and static shear tests (Figure 3.21). A significant difference was observed in the 180° peel test results between the PAAI-PnBA-PAAI and PAAI-PEHA-PAAI series of polymers. The PAAI-PEHA-PAAI series exhibited average peel forces in the range of 0.13 to 0.24 N cm^{-1}, with no significant differences observed between samples with 8, 14, and 24 wt% PAAI. Cohesive failure was observed for PAAI-PEHA-PAAI (51k, 8%) and (54k, 14%) as expected due to its rather low toughness. Similar values of peel adhesion are reported for excellent removable types of adhesives, however the cohesive mode of failure is unacceptable for removable PSAs. By contrast, average values of peel adhesion for the

PAAI-PnBA-PAAI series of polymers ranged from 2.5 to 2.9 N cm^{-1}. Similar peel force values of ~1−3 N cm^{-1} for commercially available PMMA-PnBA-PMMA triblock copolymers have been previously reported.[23,44] Other than the cohesive failure observed for PAAI-PnBA-PAAI (53k, 12%) no significant difference was observed across the range of different wt% of PAAI. Loop tack testing also produced significantly different results between the two sets of polymers. PAAI-PEHA-PAAI (51k, 8wt%) was the only sample among the PAAI-PEHA-PAAI series that was able to form a bond to the stainless steel substrate during testing. The other samples formed no interaction with the substrate and did not register a force during loop tack testing. All samples in the PAAI-PnBA-PAAI series registered an average tack force between 1.8 and 3.2 N cm^{-1}. The shear test results indicated that the PAAI-PnBA-PAAI series showed good resistance to shear failure, particularly the samples with 17 and 21 wt% PAAI which showed no failure after 10,000 min. PAAI-PEHA-PAAI (51k, 8wt%) and (54k, 14%) showed poor shear resistance with failure occurring in less than 200 min. Results from the shear test of PAAI-PEHA-PAAI (64k, 24%) were inconsistent across the three samples tested, with one failure occurring at 230 min and no failure observed after 10,000 min for the other two.

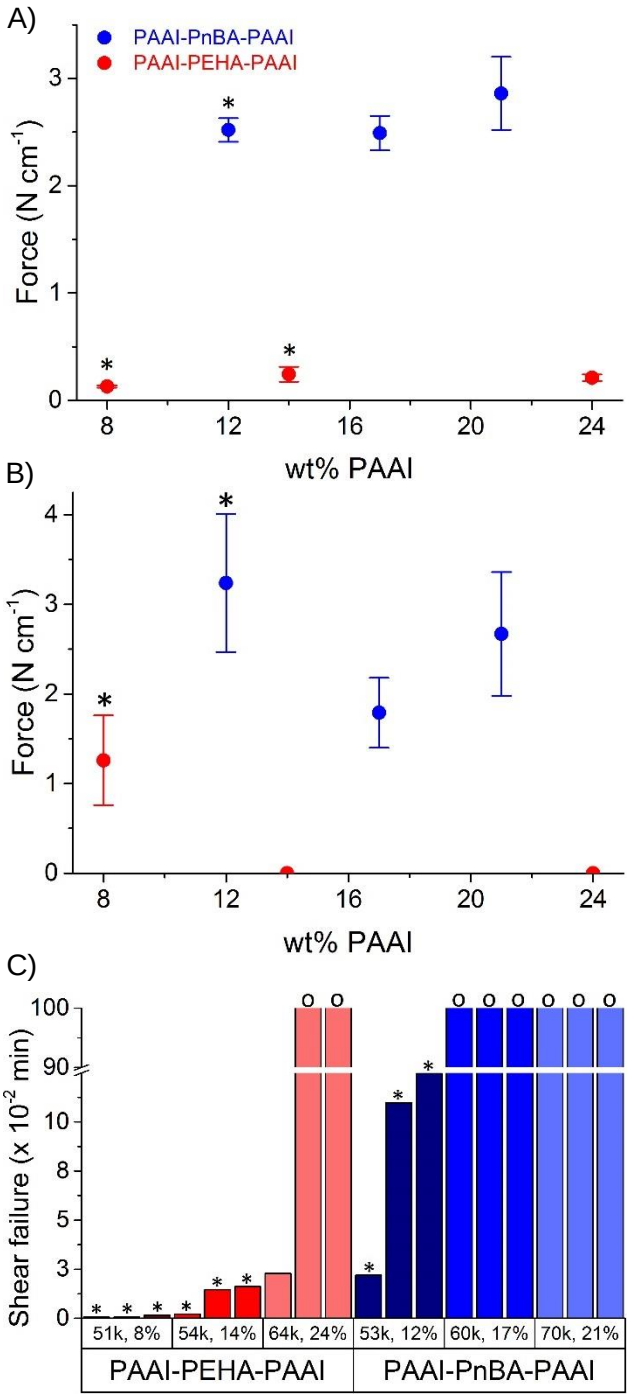

Figure 3.21. Adhesive performance of PAAI-PnBA-PAAI and PAAI-PEHA-PAAI triblock copolymers. A) 180° peel test; B) loop tack test; C) shear test, each bar represents one sample. * = cohesive failure, o = no failure after 10,000 min.

Polymers for adhesive applications are typically blended with additives such as tackifiers and plasticizers to tune adhesive properties and processability. For example, addition of a tackifier can impact adhesive performance by increasing T_g and dissipative qualities.[47] To improve the tack and peel forces of PEHA based series of polymers, PAAI-PEHA-PAAI (54k, 14%) was blended with 25 and 50 wt% of a rosin ester tackifier. Rosin esters are commonly used as tackifiers for adhesives and have the added benefit of being renewably derived.[46] After solvent casting and drying under ambient conditions for 24 h, the resulting polymer films appeared homogeneous and clear, indicating good compatibility between the tackifier and polymer. DSC showed an increase in T_g from −63 to −21 °C with increasing wt% of the tackifier (Figure 3.22). Both tack and peel forces increased significantly with increasing tackifier content (Figure 3.23). Cohesive failure was observed in both the loop tack and 180° peel experiments due to the poor toughness of the base elastomer. With a peel force > 4 N cm^{-1} and cohesive mechanism of failure, PAAI-PEHA-PAAI (54k, 14%) with 50 wt% tackifier fits the definition of a permanent PSA.[49]

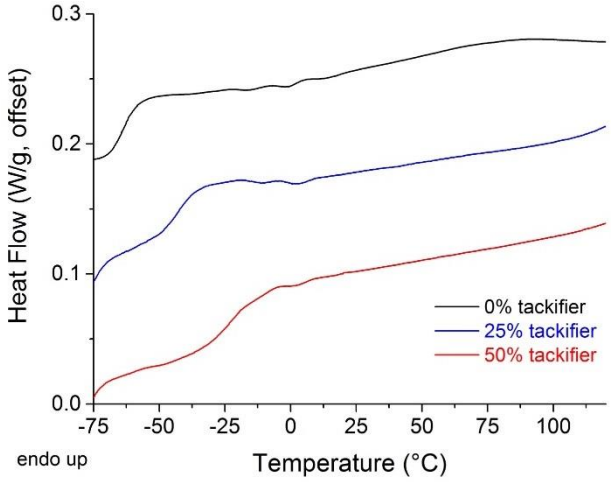

Figure 3.22. DSC of PAAI-PEHA-PAAI (54k, 14%) with rosin ester tackifier. Ramp rate = 10 °C min^{-1}. Second heat.

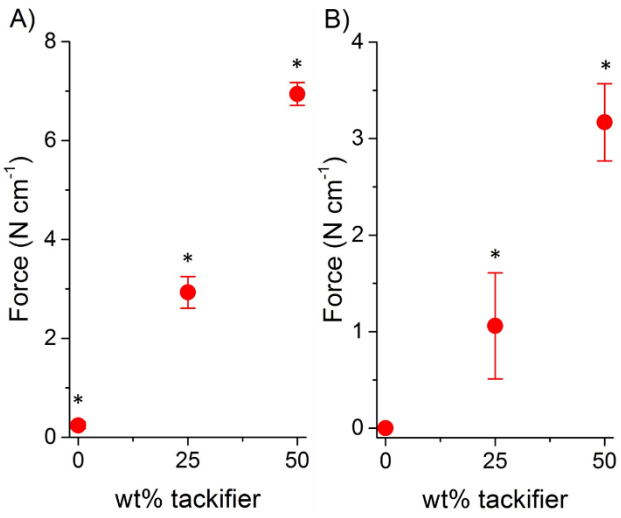

Figure 3.23. Adhesion testing of PAAI-PEHA-PAAI (54k, 14%) plus rosin ester tackifier. A) loop tack test; B) 180° peel test. * = cohesive failure.

3.2.6 Dynamic mechanical analysis

To gain insight into the cause for the dramatic differences in adhesive qualities between PAAI-PEHA-PAAI and PAAI-PnBA-PAAI we turned to dynamic mechanical analysis (DMA). Researchers Chang and Yang demonstrated the ability to directly

correlate the behavior of an adhesive during tack and peel testing to the response observed during DMA at bonding and debonding frequencies, respectively.[45] Specifically, the response of the material during a bonding event correlates to a frequency of ~1 rad s^{-1}, while debonding under standard 180° peel testing conditions roughly corresponds to higher frequencies of ~435 rad s^{-1}. Characterizing the elastic and viscous response of the material (G' and G", respectively) at the bonding and debonding frequencies therefore allows one to connect the observed behavior during adhesion testing to fundamental viscoelastic properties.

While a frequency of 1 rad s^{-1} is well within the typical operating range of rheometers, accessing a frequency of 435 rad s^{-1} requires employing the time temperature superposition principle (TTS). Dynamic frequency sweeps between 100 and 0.1 s^{-1} at temperatures from 20 to −20 °C were performed for PAAI-PnBA-PAAI (60k, 17%) and PAAI-PEHA-PAAI (54k, 14%). Shift factors (a_T) were then applied to generate master curves for each polymer with 20 °C as the reference temperature (Figures 3.24 and 3.25). In both cases the Williams–Landel–Ferrey model was successfully fit to the plot of $a_{T,20\,°C}$ vs temperature. It should be noted that attempts to generate a full master curve for the triblock copolymers by including dynamic frequency sweeps measured at higher temperatures were unsuccessful (Figures 3.26 and 3.27). At temperatures above 30 °C TTS could not be applied successfully, potentially due to the difference in relaxation times of the different blocks or the presence of a transition such as T_g or mixing of the PAAI and midblock components.[50]

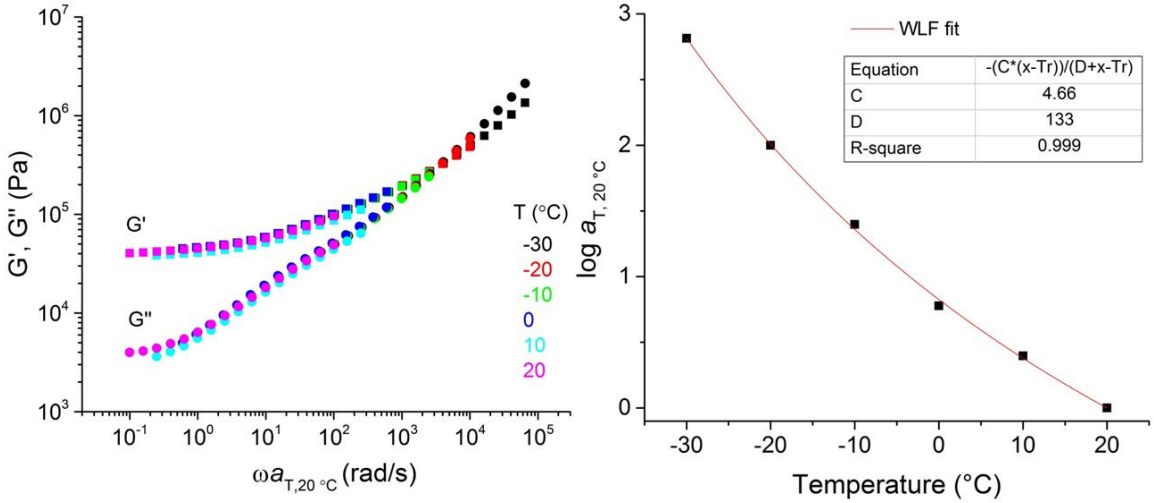

Figure 3.24. Time temperature superposition and William–Landel–Ferrey fit for DMA of PAAI-PEHA-PAAI (54k, 14%).

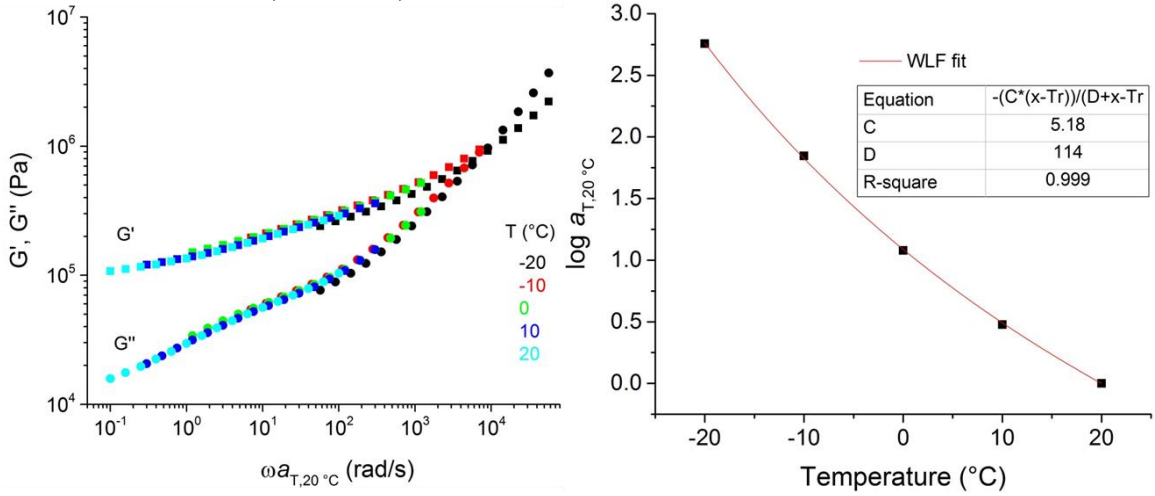

Figure 3.25. Time temperature superposition and William–Landel–Ferrey fit for DMA of PAAI-PnBA-PAAI (60k, 17%).

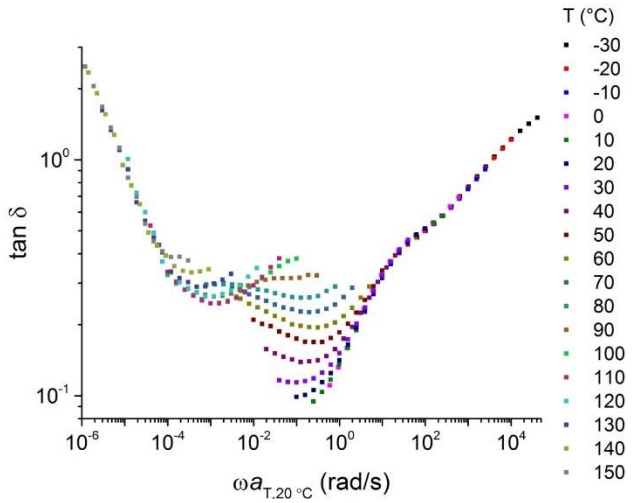

Figure 3.26. Attempted time temperature superposition for DMA of PAAI-PEHA-PAAI (54k, 14%).

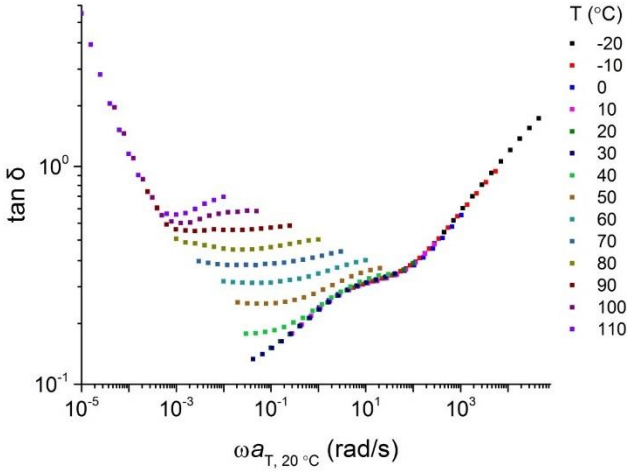

Figure 3.27. Attempted time temperature superposition for DMA of PAAI-PnBA-PAAI (60k, 17%).

The resulting plots of moduli vs frequency from DMA of PAAI-PnBA-PAAI (60k, 17%) and PAAI-PEHA-PAAI (54k, 14%) are shown in Figure 3.28. At the bonding and debonding frequencies, both G' and G" for PAAI-PnBA-PAAI (60k, 17%) are higher than for PAAI-PEHA-PAAI (54k, 14%). This observation is in good agreement with the results from tensile testing where PAAI-PnBA-PAAI exhibited higher *E* than PAAI-PEHA-PAAI. Both polymer samples satisfy the Dahlquist criterion, which states that for measurable tack to occur G' should be $< 3x10^5$ Pa in the bonding region. However this criterion clearly does

not predict the behavior of PAAI-PEHA-PAAI (54k, 14%) as this sample registered no measurable force during loop tack testing.

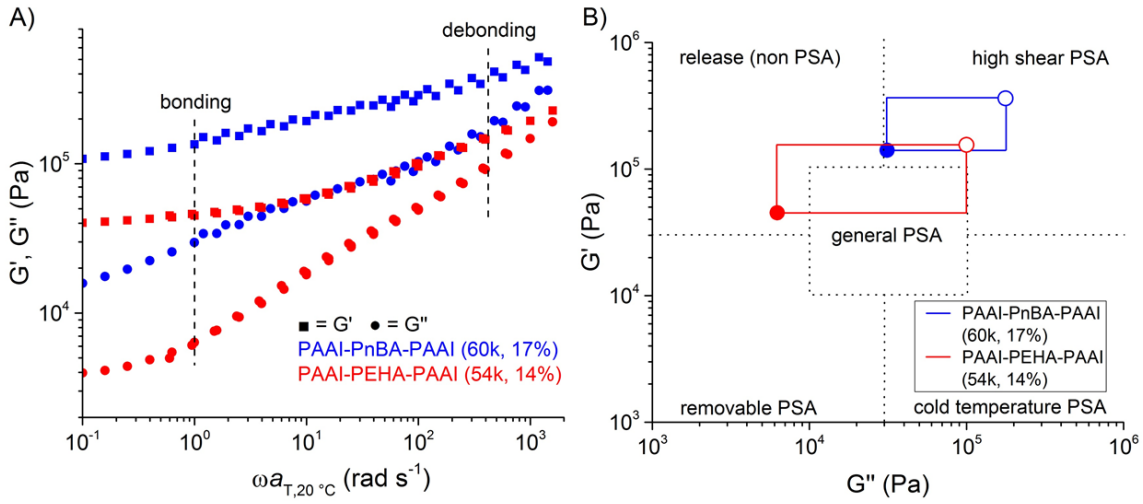

Figure 3.28. A) DMA of PAAI-PnBA-PAAI (60k, 17%) and PAAI-PEHA-PAAI (54k, 14%). Bonding and debonding frequencies correspond to 1 and 435 rad s^{-1}, respectively; B) viscoelastic windows for PAAI-PnBA-PAAI (60k, 17%) and PAAI-PEHA-PAAI (54k, 14%) constructed from bonding (•) and debonding (o) frequencies.

Appling the viscoelastic window concept as outlined by Yang and Chang[45] allowed for a better understanding of how the viscoelastic behavior at bonding and debonding frequencies can be used to understand the difference in adhesive qualities. The viscoelastic window is constructed by plotting G' and G" at bonding and debonding frequencies on a plot of G' vs G". The region in which the viscoelastic window lies can then be used to qualitatively assess the behavior of the PSA and its area of application. For PAAI-PnBA-PAAI (60k, 17%) the window lies within the high shear region. PSAs with windows in this region are described as having moderate peel forces and high resistance to shear, which is in good agreement with the results from 180° peel and shear testing. By contrast, a high ratio of G' to G" in the bonding region of PAAI-PEHA-PAAI (54k, 14%) results in a viscoelastic window that partially lies within the non- PSA region. If the ratio of G' to G"

is too high, the polymer lacks the liquid like quality needed to form intimate contact with the substrate. In other words, dissipation is low. As a result the polymer does not register a tack force during loop tack testing.

3.3 Conclusion

In summary, we have reported the synthesis of a new isosorbide derived monomer AAI in two steps using common reagents. PAAI had a T_g near that of commercially relevant glassy polymers such as poly(styrene) and PMMA and demonstrated good thermal stability. RAFT polymerization was used to prepare two series of triblock copolymers PAAI-PnBA-PAAI and PAAI-PEHA-PAAI with varying wt% PAAI. The adhesive qualities of the triblock copolymers were evaluated by 180° peel, loop tack, and shear testing. Results for the PAAI-PnBA-PAAI series were promising and comparable to previously reported results for PMMA-PnBA-PMMA, while rather poor adhesive qualities were observed for the PAAI-PEHA-PAAI series. DMA provided insight into the cause for the observed differences in adhesive performance, suggesting that a high ratio of G' to G" in the bonding regime of PAAI-PEHA-PAAI limits adhesion to the substrate. Together the above results demonstrate the utility of isosorbide in thermoplastic elastomer applications and provide a robust approach to incorporating this low cost bio-based feedstock into new polymer materials.

3.4 Experimental

All chemicals were purchased from Aldrich and used without further purification unless otherwise noted. Acryloyl chloride was purified by distillation prior to use. *N*-butyl

acrylate (nBA) and 2-ethylhexyl acrylate (EHA) were purified by passing through a column of basic alumina. The rosin ester tackifier Sylvalite 2E 80HP was provided by Arizona Chemical.

Characterization ^{1}H NMR and ^{13}C NMR spectroscopy experiments were performed on a Bruker Avance III HD 500 spectrometer at 500 MHz and 125 MHz, respectively, equipped with a 5mm Prodigy TCI cryoprobe and referenced to tetramethylsilane. FT-IR was performed using a Bruker Alpha Platinum ATR spectrometer. High-resolution mass spectrometry was performed using a Bruker Bio-TOF II in positive mode ESI. Size exclusion chromatography (SEC) was carried out in THF using three Phenomenex Phenogel-5 columns connected in series at a flow rate of 1 ml min^{-1} at 25 °C. Chromatograms were collected using a Wyatt Technology DAWN DSP MALLS detector and a Wyatt optilab EX RI detector. PAAI dn/dc was calculated from the RI signal using a known sample concentration and assuming 100% mass recovery from the column. Copolymer dn/dc was calculated using a weighted average of homopolymer dn/dc values. Thermogravimetric analysis (TGA) was performed on a TA Instruments Q500 at a heating rate of 10 °C min^{-1}. Differential scanning calorimetry (DSC) measurements were carried out using a TA Instruments Discovery DSC under N_2. T_g values were determined on the second heating at a heating rate of 10 °C min^{-1}. Small angle X-ray scattering (SAXS) was performed at the Advanced Photon Source at Argonne National Labratories on the Sector 5-ID-D beamline maintained by DuPont-Northwestern-Dow Collaborative Access Team. Dynamic mechanical analysis (DMA) was performed on a TA Instruments ARES rheometer under N_2. Dynamic frequency sweeps were performed from 100 to 0.1 rad s^{-1} at

1% strain. Monomer conversion values were calculated by comparing the integrations of vinyl protons to protons of the isosorbide core. M_n (calc) was calculated according to the formula $M_n\ (\text{calc}) = \text{MW}_{\text{CTA}} + [\text{M}]_0 \times \text{MW}_{\text{M}} \times \text{conversion}/[\text{CTA}]_0$, where $[\text{M}]_0$ and $[\text{CTA}]_0$ are the initial concentrations of monomer and CTA, respectively, and MW_{M} and MW_{CTA} are the molar masses of monomer and CTA, respectively.

***exo*-acetyl isosorbide (AI).** AI was prepared according to the literature.[34,35] Briefly, isosorbide (146 g, 1.00 mol), acetic acid (78.0 ml, 1.35 mol), *p*-toluenesulfonic acid monohydrate (1.00 g, 5.26 mmol), and toluene (150 ml) were added to a 500 ml round bottom flask equipped with a Dean-Stark trap. The reaction was heated to reflux until removal of H_2O was complete. Toluene was removed under reduced pressure and KOH (3.00 g) was added. The mixture was distilled with heating through a Vigreux column at 200 mTorr. The distillate was purified by recrystallization from methyl ethyl ketone to afford AI as a white crystalline solid (71.1g, 38% yield).

***exo*-acetyl-*endo*-acryl-isosorbide (AAI).** AI (30.3 g, 0.161 mol), triethylamine (24.6 ml, 0.177 mol) and 300 ml DCM were added to a 1 L round bottom flask. The flask was immersed in an ice water bath and acryloyl chloride (13.7 ml, 0.169 mol) was added dropwise with stirring. The reaction was allowed to reach room temperature and after 18 h the triethylamine salts were filtered off. The filtrate was passed through a plug of silica (~200 g) and eluted with diethyl ether. The solvent was removed by rotary evaporation and the concentrate was passed through a plug of basic alumina (~200 g) eluting with diethyl ether. The eluent was concentrated to ~100 ml and crystallization was aided by addition of pentane to afford AAI as a clear crystalline solid after filtration and drying (22.5 g, 58%

yield). ^{1}H NMR (500 MHz, $CDCl_3$) δ ppm: 6.47 (dd, *J* = 17.40, 1.53 Hz, 1 H) 6.18 (dd, *J* = 17.39, 10.38 Hz, 1 H) 5.89 (dd, *J* = 10.38, 1.53 Hz, 1 H) 5.23 (q, *J* = 5.49 Hz, 1 H) 5.19 (d, *J* = 3.05 Hz, 1 H) 4.88 (t, *J* = 5.04 Hz, 1 H) 4.51 (d, *J* = 4.88 Hz, 1 H) 3.94 - 4.01 (m, 3 H) 3.86 (dd, *J*=9.77, 5.19 Hz, 1 H) 2.08 (s, 3 H). ^{13}C NMR (125 MHz, $CDCl_3$) δ ppm: 170.01, 165.36, 131.77, 127.58, 85.90, 80.80, 78.00, 74.00, 73.44, 70.32, 20.88. ATR FT-IR (neat) $\upsilon_{cm^{-1}}$: 2926 (C–H), 1743 (C=O), 1726 (C=O), 1637 (C=C), 1228 (C–O), 1180(C–O), 1092 (C–O), 1076 (C–O). m.p. = 38 °C. T_g = -36 °C. MS (ESI-TOF, *m/z*) Calcd. for $C_{11}H_{14}O_6$: 242.0790; found: 265.0684 ($M + Na^+$); error 1.51 ppm.

Polymerization of AAI (PAAI). AAI (1.03 g, 4.27 mmol), AIBN (10.3 mg 0.0628 mmol), DMF (4 ml), and a stir bar were added to a 25 ml round bottom flask and sparged with Ar for 30 min. The reaction was then heated to 70 °C with stirring for 8 h. The reaction was then cooled to room temperature and exposed to air. An aliquot was taken to determine conversion by ^{1}H NMR. The polymer was isolated by precipitation into cold MeOH and dried in a vacuum oven at 60 °C for 24 h to give PAAI as a white solid (91% conversion by ^{1}H NMR spectroscopy). SEC-MALLS analysis: M_n = 120 kg mol^{-1}. $Đ$ = 4.00. dn/dc = 0.0959 ml g^{-1}. T_d (5 wt%); N_2 = 337 °C, air =291 °C. T_g = 95 °C.

RAFT polymerization of nBA with BTCBA (CTA-PnBA-CTA). The following is an illustrative example: nBA (10.0 g, 11.2 ml, 78.1 mmol), BTCBA (128 mg, 0.156 mmol), and AIBN (5.12 mg, 0.0312 mmol) and a stir bar were added to a 50 ml round bottom flask and sealed with a septum. After sparging with Ar for 30 min, the reaction was stirred and heated to 70 °C under positive Ar pressure. After 2 h, the reaction was immersed in an ice bath, exposed to air, and 20 ml DCM was added. An aliquot was taken to determine

conversion by ^{1}H NMR. The polymer was isolated by precipitation into cold MeOH, pouring off the supernatant, and drying the polymer at 70 °C in a vacuum oven for 24 h to give CTA-PnBA-CTA as a yellow viscous liquid (63% conversion by ^{1}H NMR spectroscopy, 5.71 g, 91% yield). SEC-MALLS analysis: M_n = 45.3 kg mol^{-1}, $Đ$ = 1.03.

RAFT polymerization of EHA with BTCBA (CTA-EHA-CTA). EHA (9.87 g, 53.6 mmol), BTCBA (191 mg, 0.233 mmol), and AIBN (7.65 mg, 0.0223 mmol) were added to a 50 ml round bottom flask, sparged with Ar for 30 min, and heated to 70 °C with stirring for 1 h. The reaction was then immersed in an ice bath, exposed to air, and 20 ml of toluene was added. An aliquot was take to determine conversion by ^{1}H NMR. The polymer was then isolated by precipitation into cold MeOH, pouring off the supernatant and drying at 70 °C in a vacuum oven for 24 h to give CTA-EHA-CTA as a yellow viscous liquid (90% conversion by ^{1}H NMR, 6.02 g, 68% yield). SEC-MALLS analysis: M_n = 44.7 kg mol^{-1} $Đ$ = 1.06.

Chain extension of CTA-PnBA-CTA with AAI (PAAI-PnBA-PAAI). The following is an illustrative example: CTA-PnBA-CTA (3.94 g, 0.348 mmol), AAI (1.64 g, 6.78 mmol), AIBN (2.8 mg, 0.017 mmol), DMF (17 ml), and a stir bar were added to a 50 ml round bottom flask. After sparging with Ar for 30 min, the reaction was heated to 70 °C with stirring under positive Ar pressure. After 2 h, the reaction was immersed in an ice bath and exposed to air. An aliquot was taken to determine conversion by ^{1}H NMR. The polymer was isolated by precipitating into cold MeOH, pouring off the supernatant, and drying the polymer at 70 °C in a vacuum oven for 24 h to give PAAI-PnBA-PAAI as a yellow rubbery solid (57% conversion by ^{1}H NMR spectroscopy, 4.43 g, 91% yield). SEC-MALLS

analysis: M_n = 60.2 kg mol^{-1}, $Đ$ = 1.12). T_d (5 wt%); N_2 = 334 °C, air = 304 °C. T_g = −45 °C.

Chain extension of CTA-EHA-CTA with AAI (PAAI-EHA-PAAI). The following is an illustrative example: CTA-EHA-CTA (1.50 g, 0.0664 mmol), AAI (354 mg, 1.46 mmol), AIBN (1.09 mg, 6.64 µmol), toluene (4.5 ml), and a stir bar were added to a 20 ml septa capped vial. The solution was sparged with Ar for 30 min then heated to 70 °C with stirring under positive Ar pressure. After 2 h, the reaction was immersed in an ice bath and exposed to air. An aliquot was taken to determine conversion by NMR. The polymer was isolated by precipitating into cold MeOH followed by drying at 70 °C in a vacuum oven for 24 h to give PAAI-PEHA-PAAI as a yellow rubbery solid (70% conversion by ^{1}H NMR, 1.41 g, 81% yield). SEC-MALLS analysis: M_n = 54.2 kg mol^{-1}, $Đ$ = 1.20). T_d (5 wt%); N_2 = 338 °C, air = 264 °C. T_g = −63 °C.

Alcoholysis of PAAI-PnBA-PAAI. PAAI-PnBA-PAAI (360 mg) and *p*-toluenesulfonic acid monohydrate (36 mg) were added to n-butanol (5 ml) in a 15 ml pressure vessel with a stir bar. The vessel was sealed and heated to 130 °C with stirring for 48 h. The vessel was then placed in a freezer for 24 h. The supernatant was poured off and the residual polymer was dried in a vacuum oven for 24 h at 80 °C to give the product as a colorless viscous liquid.

Adhesive testing. Samples for adhesion testing were prepared by dissolving 100 mg of polymer and tackifier in 266 µl ethyl acetate (i.e. total solids content = 100 mg) to give a solution with 30 wt% solids. The solution was then solvent cast onto a 50 µm thick sheet of PETE using a wire wound rod and the films were then left to dry under ambient

conditions for 24 h before adhesion testing. The targeted dry film thickness was ~20 µm. PSTC-grade polished stainless steel plates were used as the adherend during testing.

180°peel test. A 1.27 cm wide strip of the polymer coated PETE film was adhered to the stainless steel plate using a 500 g roller. The sample was then tested using a Shimadzu ASG-X tensile tester at a peel rate of 305 mm min^{-1}. The peel force was recorded as the maximum measure force and averaged across at least three samples.

Loop tack test. A 1.27 cm wide strip of the polymer coated PETE film was formed into a teardrop shaped loop and mounted to the upper grip of the tensile tester. The loop was then lowered onto the stainless steel plate mounted to the lower grip of the tensile tester to a total contact area of 1.27 cm x 2.54 cm. The tack force was then measured as the maximum force observed while raising the upper grip at a rate of 305 mm min^{-1}. The average of at least 3 samples is reported.

Shear test. A strip of the polymer coated PETE film was adhered to the stainless steel plate to give a contact area of 1.27 x 1.27 cm^{-1} and rolled five times with a 500 g roller. A 500 g weight was then suspended from the sample and the time to failure was recorded for 3 samples.

3.5 References

References

(1) Gandini, A. The irruption of polymers from renewable resources on the scene of macromolecular science and technology. *Green Chem.* **2011**, *13*, 1061–1083.

(2) Delidovich, I.; Hausoul, P. J. C.; Deng, L.; Pfützenreuter, R.; Rose, M.; Palkovits, R. Alternative Monomers Based on Lignocellulose and Their Use for Polymer Production. *Chem. Rev.* **2016**, *116*, 1540–1599.

(3) Isikgor, F. H.; C. Remzi Becer. Lignocellulosic Biomass: a sustainable platform for production of bio-based chemicals and polymers. *Polym. Chem.* **2015**, *6*, 4497–4559.

(4) Holmberg, A. L.; Reno, K. H.; Wool, R. P.; Epps, T. H. I. Biobased building blocks for the rational design of renewable block polymers. *Soft Matter* **2014**, *10*, 7405–7424.

(5) Scott, A. Roquette embraces biobased materials. *C&EN* **2014**, *90*, 16–17.

(6) Roquette. *ROQUETTE reinforces its position as world leader in ISOSORBIDE for the performance plastics and chemistry markets ROQUETTE*; 2015.

(7) Fenouillot, F.; Rousseau, A.; Colomines, G.; Saint-Loup, R.; Pascault, J. P. Polymers from renewable 1,4:3,6-dianhydrohexitols (isosorbide, isomannide and isoidide): A review. *Prog. Polym. Sci.* **2010**, *35*, 578–622.

(8) Rose, M.; Palkovits, R. Isosorbide as a renewable platform chemical for versatile applications–quo vadis? *ChemSusChem* **2012**, *5*, 167–176.

(9) Galbis, J. A.; García-Martín, M. G. Synthetic polymers from readily available monosaccharides. In *Topics in Current Chemistry*; 2010; Vol. 295, pp. 147–176.

(10) Mitsubishi Chemical. World-First — DURABIO^{TM}, Bio-based Engineering Plastic from Mitsubishi Chemical, Used on the Front Panel of Sharp's New AQUOS CRYSTAL 2 Smartphone http://www.m-kagaku.co.jp/english/newsreleases/00258.html (accessed Mar 23, 2016).

(11) Mitsubishi Chemical. New biobased engineering plastic "DURABIO" http://www.m-kagaku.co.jp/english/products/business/polymer/sustainable/details/1194667_3255.html (accessed Mar 23, 2016).

(12) Gallagher, J. J.; Hillmyer, M. A.; Reineke, T. M. Isosorbide-based Polymethacrylates. *ACS Sustainable Chem. Eng.* **2015**, *3*, 662–667.

(13) Beghdadi, S.; Miladi, I. A.; Ben Romdhane, H.; Bernard, J.; Drockenmuller, E. RAFT polymerization of bio-based 1-vinyl-4-dianhydrohexitol-1,2,3-triazole stereoisomers obtained via click chemistry. *Biomacromolecules* **2012**, *13*, 4138–4145.

(14) Sato, K.; Kodama, K. Positive-working far-UV photoresists. JP 2004341062, 2004.

(15) Koyama, H.; Tsutsumi, K. Polymerizable monomer polymeric compound resin compositions for photoresist and method for producing semiconductor. wo 2004113404, 2004.

(16) Mansoori, Y.; Hemmati, S.; Eghbali, P.; Zamanloo, M. R.; Imanzadeh, G. Nanocomposite materials based on isosorbide methacrylate/Cloisite 20A. *Polym. Int.* **2013**, *62*, 280–288.

(17) Bates, F. S.; Fredrickson, G. H. Block Copolymers—Designer Soft Materials. *Phys. Today* **1999**, *52*, 32–38.

(18) Creton, C. Pressure-Sensitive Adhesives: An Introductory Course. *MRS Bull.* **2003**, *28*, 434–439.

(19) Moineau, C.; Minet, M.; Teyssié, P.; Jérôme, R. Synthesis and Characterization of Poly(methyl methacrylate)-block-poly(n-butyl acrylate)-block-poly(methyl methacrylate) Copolymers by Two-Step Controlled Radical Polymerization (ATRP) Catalyzed by NiBr2 (PPh3)2, 1†. *Macromolecules* **1999**, *32*, 8277–8282.

(20) Tong, J. D.; Jerôme, R. Synthesis of poly(methyl methacrylate)-b-poly(n-butyl acrylate)-b-poly(methyl methacrylate) triblocks and their potential as thermoplastic elastomers. *Polymer* **2000**, *41*, 2499–2510.

(21) Haloi, D. J.; Ata, S.; Singha, N. K.; Jehnichen, D.; Voit, B. Acrylic AB and ABA block copolymers based on poly(2-ethylhexyl acrylate) (PEHA) and poly(methyl methacrylate) (PMMA) via ATRP. *ACS Appl. Mater. Interfaces* **2012**, *4*, 4200–4207.

(22) Dufour, B.; Koynov, K.; Pakula, T.; Matyjaszewski, K. PBA–PMMA 3-Arm Star Block Copolymer Thermoplastic Elastomers. *Macromol. Chem. Phys.* **2008**, *209*, 1686–1693.

(23) Oshita, S.; Chapman, B. K.; Hirata, K. Acrylic Block Copolymer for Adhesive Application. In *PSTC Tape Summit 2012*; Boston, 2012.

(24) Hamada, K.; Ishiura, K.; Takahashi, T.; Yaginuma, S.; Akai, M.; Ono, T.; Shachi, K. Process for polymerizing a methacrylic ester or an acrylic ester. US 6,767,976 B2, 2004.

(25) Brandrup, J.; Immergut, E.; Grulke, E.; Abe, A.; Bloch, D. *Polymer handbook*; 4th ed.; 1999; Vol. 49.

(26) Vendamme, R.; Schüwer, N.; Eevers, W. Recent synthetic approaches and emerging bio-inspired strategies for the development of sustainable pressure-

sensitive adhesives derived from renewable building blocks. *J. Appl. Polym. Sci.* **2014**, *131*, 8379–8394.

(27) Lee, S.; Lee, K.; Kim, Y.-W.; Shin, J. Preparation and Characterization of a Renewable Pressure-Sensitive Adhesive System Derived from ε-Decalactone, L-Lactide, Epoxidized Soybean Oil, and Rosin Ester. *ACS Sustainable Chem. Eng.* **2015**, *3*, 2309–2320.

(28) Ding, K.; John, A.; Shin, J.; Lee, Y.; Quinn, T.; Tolman, W. B.; Hillmyer, M. A. High-Performance Pressure-Sensitive Adhesives from Renewable Triblock Copolymers. *Biomacromolecules* **2015**, *16*, 2537–2539.

(29) Shin, J.; Martello, M. T.; Shrestha, M.; Wissinger, J. E.; Tolman, W. B.; Hillmyer, M. A. Pressure-Sensitive Adhesives from Renewable Triblock Copolymers. *Macromolecules* **2011**, *44*, 87–94.

(30) Shin, J.; Lee, Y.; Tolman, W. B.; Hillmyer, M. A. Thermoplastic elastomers derived from menthide and tulipalin A. *Biomacromolecules* **2012**, *13*, 3833–3840.

(31) Gu, C.; Dubay, M. R.; Severtson, S. J.; Gwin, L. E. Hot-Melt Pressure-Sensitive Adhesives Containing High Biomass Contents. *Ind. Eng. Chem. Res.* **2014**, *53*, 11000–11006.

(32) Pu, G.; Hauge, D. A.; Gu, C.; Zhang, J.; Severtson, S. J.; Wang, W.; Houtman, C. J. Influence of Acrylated Lactide-Caprolactone Macromonomers on the Performance of High Biomass Content Pressure-Sensitive Adhesives. *Macromol. React. Eng.* **2013**, *7*, 515–526.

(33) Pu, G.; Dubay, M. R.; Zhang, J.; Severtson, S. J.; Houtman, C. J. Polyacrylates with high biomass contents for pressure-sensitive adhesives prepared via mini-emulsion polymerization. *Ind. Eng. Chem. Res.* **2012**, *51*, 12145–12149.

(34) Vendamme, R.; Eevers, W. Sweet Solution for Sticky Problems: Chemoreological Design of Self-Adhesive Gel Materials Derived From Lipid Biofeedstocks and Adhesion Tailoring via Incorporation of Isosorbide. *Macromolecules* **2013**, *46*, 3395–3405.

(35) Stoss, P.; Merrath, P.; Schlüter, G. Regioselektive Acylierung von 1,4:3,6-Dianhydro-D-glucit. *Synthesis* **1987**, 174–176.

(36) Stoss, P. Process for the production of isosorbide-5-nitrate. US 4,371,703, 1983.

(37) Beyler, C. L.; Hirschler, M. M. Thermal Decomposition of Polymers. In *SFPE Handbook of Fire Protection Engineering*; DiNenno, P. J., Ed.; 2001; pp. 110–131.

(38) Mahalik, J. P.; Madras, G. Effect of the Alkyl Group Substituents on the Thermal and Enzymatic Degradation of Poly(n-alkyl acrylates). *Ind. Eng. Chem. Res.* **2005**, *44*, 4171–4177.

(39) Moad, G.; Rizzardo, E.; Thang, S. H. Living Radical Polymerization by the RAFT Process - A Third Update. *Aust. J. Chem.* **2012**, *65*, 985–1076.

(40) Keddie, D. J. A guide to the synthesis of block copolymers using reversible-addition fragmentation chain transfer (RAFT) polymerization. *Chem. Soc. Rev.* **2014**, *43*, 496–505.

(41) Perrier, S.; Barner-Kowollik, C.; Quinn, J. F.; Vana, P.; Davis, T. P. Origin of Inhibition Effects in the Reversible Addition Fragmentation Chain Transfer (RAFT) Polymerization of Methyl Acrylate. *Macromolecules* **2002**, *35*, 8300–8306.

(42) Malic, N.; Evans, R. A. Synthesis of Carboxylic Acid and Ester Mid-Functionalized Polymers using RAFT Polymerization and ATRP. *Aust. J. Chem.* **2006**, *59*, 763–771.

(43) Ohara, T.; Sato, T.; Shimizu, N.; Prescher, G.; Schwind, H.; Weiberg, O.; Marten, K.; Greim, H. Acrylic Acid and Derivatives. In *Ullmann's Encyclopedia of Industrial Chemistry*; Wiley-VCH Verlag GmbH & Co. KGaA: Weinheim, Germany, 2000; Vol. 60, pp. 1–18.

(44) Tullo, A. H. Hunting For Biobased Acrylic Acid. *Chem. Eng. News* **2013**, *91*, 18–19.

(45) Kavitha, A. A.; Singha, N. K. Smart "all acrylate" ABA triblock copolymer bearing reactive functionality via atom transfer radical polymerization (ATRP): Demonstration of a "click reaction" in thermoreversible property. *Macromolecules* **2010**, *43*, 3193–3205.

(46) Nakamura, Y.; Adachi, M.; Tachibana, Y.; Sakai, Y.; Nakano, S.; Fujii, S.; Sasaki, M.; Urahama, Y. Tack and viscoelastic properties of an acrylic block copolymer/tackifier system. *Int. J. Adhes. Adhes.* **2009**, *29*, 806–811.

(47) Yang, H. W. H.; Chang, E.-P. The role of viscoelastic properties in the design of pressure-sensitive adhesives. *Trends Polym. Sci.* **1997**, *5*, 380–384.

(48) Fiebach, K.; Grimm, D. Resins, Natural. In *Ullmann's Encyclopedia of Industrial Chemistry*; Wiley-VCH Verlag GmbH & Co. KGaA: Weinheim, Germany, 2000; Vol. 9, pp. 245–260.

(49) Benedek, I. *Pressure-Sensitive Adhesives and Applications*; CRC Press, 2004.

(50) Hiemenz, P. C.; Lodge, T. P. *Polymer Chemistry, Second Edition*; Taylor & Francis, 2007.

Chapter 4: Degradable Thermosets from Sugar-Derived Dilactones[*]

[*] Reproduced in part with permission from Gallagher, J. J.; Hillmyer, M. A.; Reineke, T. M. *Macromolecules* **2014**, *47* (2), 498–505. © American Chemical Society 2014.

4.1 Introduction

The increased demand and limited supply of petroleum-based chemical feedstocks have spurred a large research push in the area of renewably-sourced polymers. Bio-based feedstocks such as carbohydrates offer great promise for materials development due to their rich functionality (high heteroatom content and stereochemistry) and renewable production on an impressive scale (~10^{14} kg/yr).[1] Sugars currently comprise a large sector of the chemical industry, with annual production on the order of ~10^{11} kg.[1] Some sugar derivatives are already being touted as viable substitutes for petroleum-based chemicals in polymer applications. For example, isosorbide has been extensively studied in the realm of polymer chemistry[2] and is currently marketed as an alternative to bisphenol A (BPA).[3] Thus, sugars and derivatives thereof are a rich resource for the development of new bio-sourced polymers.[4,5]

Excellent examples of the unique functionality provided by sugar derivatives are the dilactones glucarodilactone (GDL) and mannarodilactone (MDL) (Scheme 1). These molecules, derived from glucose and mannose respectively, are lactone analogues of the dianhydrohexitols isosorbide and isomannide and have been under-utilized in materials development. The presence of both diol and dilactone functionality affords two routes for polymer design from GDL and MDL. As dilactones, they have been used in conjunction with various diamines to produce a class of polymers known as polyhydroxy polyamides via opening of the lactone ring.[6–10] In contrast to typical aliphatic polyamides that are stable towards hydrolysis, polyhydroxy polyamides have been shown to degrade under mild aqueous conditions.[11] Alternatively, the dilactones can be polymerized through the

secondary alcohols. For example, Hashimoto and coworkers synthesized polyurethanes by coupling GDL and MDL with isocyanates in the presence of dibutyltin dioxide (DBTDL).[12–14] To date, these structures have been the only example that contain the dilactone structure intact within a polymer backbone. In that study, they revealed that although polyurethanes typically resist hydrolysis, the polyurethanes prepared with GDL or MDL degraded readily in phosphate buffered solutions (pH 4–8). They proposed a degradation mechanism consisting of hydrolytic ring opening of the dilactone, followed by scission of the urethane bond.[14]

Dimethacrylate monomers are ubiquitous and utilized in coatings, structural materials, adhesives, chromatography packing, and biomaterials (i.e. dental composites).[15–17] Bulk polymerization of dimethacrylates results in highly crosslinked thermoset polymer networks, which yields highly stable structures. Due to the high degree of crosslinking, dimethacrylate polymerizations exhibit a number of phenomena such as autoacceleration and gel point at low conversion, incomplete conversion of methacrylate groups, and exceptionally long macromolecular radical lifetimes.[15,17–23] The final conversion value is an important parameter for the mechanical properties of poly(dimethacrylates), which also highly depends on the reaction conditions and, particularly, the chemical structure of monomer.[17,21] Renewable monomer sources for these materials and products could offer environmentally benign properties such as degradability and low toxicity, which can further increase applicability. Examples of degradable dimethacrylate chemistries previously utilized include acetals and anhydrides that undergo hydrolysis, and tertiary esters that degrade by thermolysis.[24–27] Poly(dimethacrylates) from these monomer types

have been evaluated for controlled drug release, nanoimprint lithography, and reworkable electronic components.[26,28,29]

Derivatives of sugars are renewably sourced, offer interesting functionality, and have rigid ring structures, thus having potential to replace BPA and related petroleum-derived structures in thermoset plastics. Indeed, GDL and MDL offer excellent platforms for materials synthesis. These sugar-derived dilactones contain both diol groups to install polymerizable vinyl moieties (i.e. methacrylates) and a unique heteroatom ring system susceptible to further functionalization or degradation (Scheme 4.1). Herein, we present the synthesis of two new dimethacrylate feedstocks, glucarodilactone methacrylate (GDMA) and mannarodilactone methacrylate (MDMA), that contain rigid core structures derived from glucose and mannose. Thermal initiated free radical polymerization of these substrates formed highly crosslinked thermoset materials with mechanical properties comparable to those reported for commercially available stiff poly(dimethacrylates). We show that materials derived from these structures, while stable in aqueous neutral and acidic conditions, rapidly degrade in aqueous basic conditions, offering a potential triggered degradation pathway. Further studies exploring the utility of these monomers in clear film and monodisperse microgel particle formation are reported and support the utility of this sugar dilactone feedstock platform for a variety of sustainable applications.

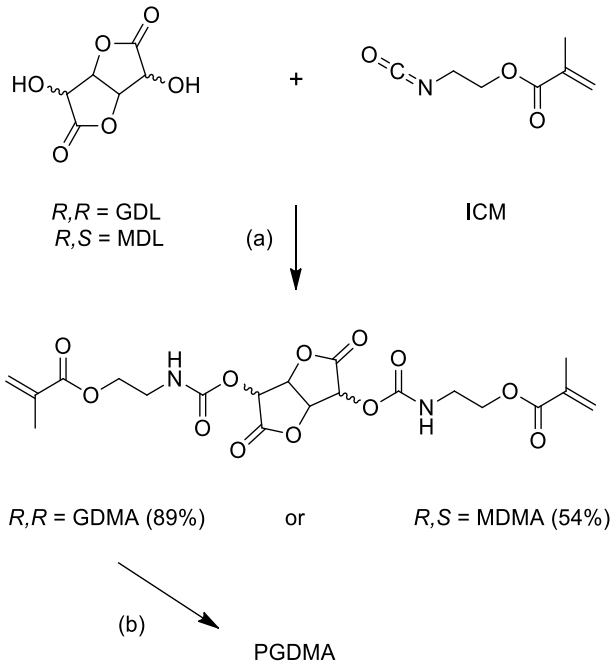

Scheme 4.1. GDMA, MDMA, and PGDMA syntheses. Conditions: (a) Dibutyltin dilaurate (1:500), THF or THF/DMF (1:1 v/v), r.t. (b) Dicumyl peroxide (1.5 wt%), 135 °C, 30 min.

4.2 Results and Discussion

4.2.1 Synthesis of GDMA and MDMA

The monomers glucaro-dimethacrylate and mannaro-dimethacrylate (GDMA and MDMA, respectively) were readily synthesized in two steps from commercially available sources (Scheme 4.1). The dilactone syntheses were accomplished using previously published procedures in the literature. The synthesis of GDL proceeded in ~62% yield, produces only benign byproducts, and is easily scalable.[30] On the other hand, the synthesis of MDL proceeded in ~18% yield and is accompanied by the evolution of NO_2, rendering scale up in a laboratory setting more challenging.[7,9,10] The introduction of a methacrylate moiety was achieved using a DBTDL catalyzed alcohol isocyanate coupling reaction between GDL or MDL and isocyanatoethyl methacrylate (ICM). This approach is

analogous to that used by Hashimoto and co-workers to form polyurethanes.[14] GDMA was synthesized in ~89% yield in 4 hours with only a slight excess of ICM. However, even with a large excess of ICM and a longer reaction time, the synthesis of MDMA offered only ~54% yield. The dilactone structures adopt puckered conformations and as a result, hydroxyl groups in the *endo* position are located above the lactone ring. MDL has both hydroxyls in *endo* positions, while GDL has one hydroxyl in the *endo* position and one in the *exo* position. When one of the hydroxyls of MDL is functionalized with a rather bulky carbamate ethylene methacrylate group, the steric crowding on the *endo* face of the dilactone ring is exacerbated and the other hydroxyl group is therefore much harder to functionalize. By contrast, the hydroxyls of GDL are on opposite sides of the dilactone ring and thus their respective steric environments are independent of each other. Because of the facile reaction and high yields, we have focused mostly on utilizing GDMA in thermoset synthesis.

4.2.2 Bulk polymerization of GDMA

GDMA was selected for initial studies of polymers from dimethacrylates with a dilactone core. Polymerization in the bulk required a temperature that was between the melting point (m.p.) and the onset of decomposition (T_d) of GDMA. The m.p. of GDMA was determined to be 118 °C and TGA revealed that the T_d was 166 °C (Figure 4.1). Thus, a temperature of 135 °C was selected for the bulk polymerization of GDMA. Using 1.5 wt% of the radical initiator, dicumyl peroxide (DCP), PGDMA samples were formed by compression molding in a stainless steel tensile bar mold with Teflon inserts. Curing at 135 °C for 30 minutes afforded PGDMA as opaque, off yellow samples.

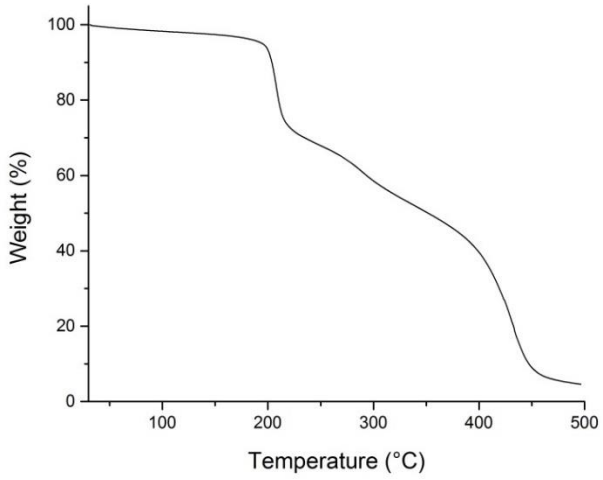

Figure 4.1. TGA data for GDMA (heating rate = 10 °C/min).

The fractional conversion (p) of methacrylate groups was determined by FT-IR (Figure 4.2). Quantifying the conversion of methacrylate groups by this technique required standardizing the area under the absorbance peak corresponding to the methacrylate C=C stretch (1635 cm^{-1}) between the GDMA and PGDMA spectra relative to an internal standard. For poly(dimethacrylates), an IR-active functional group unaffected during polymerization serves as the internal standard.[20] In this particular case, the carbonyl stretch and N-H bend were used as internal standards. The values of p obtained using each internal standard were in good agreement with each other, with an average value of p = 0.64. The inability to obtain full conversion was due to unreacted methacrylate groups becoming physically entrapped as the reaction mixture undergoes vitrification during polymerization. The gel fraction of PGDMA was determined to be 97.8 wt% by soxhlet extraction with CH_2Cl_2. The masses of PGDMA before and after extraction, along with the value of p determined by FT-IR (Figure 4.2), were used to calculate values for crosslink density (i.e., the mole fraction of repeat units that are crosslinks, a) and molar mass between crosslinks ($\overline{M_c}$) of 0.46 and 1.1 kg/mol, respectively (Eqs. 1 and 2). The values of p, a, and $\overline{M_c}$ for

PGDMA are comparable to those previously reported for commercially available dimethacrylate thermosets (example reported values for P(UDMA) as shown in Figure 2: p = 0.70; a = 0.57; ($\overline{M_c}$) = 822 g/mol).[20,22,31]

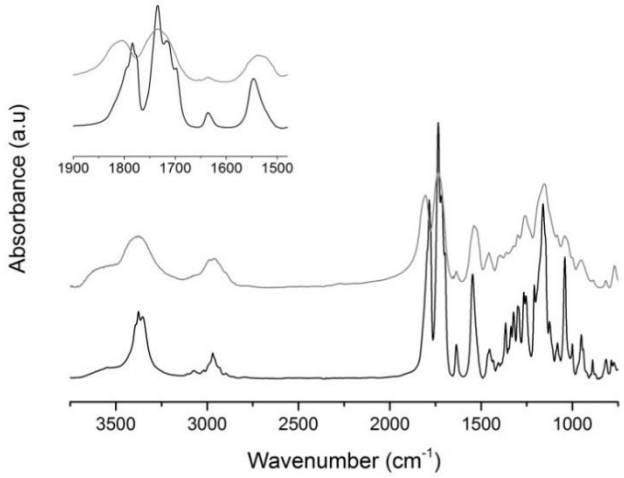

Figure 4.2. FT-IR spectra of GDMA (—) and PGDMA (—). Inset is region used for determining fractional conversion of methacrylate groups.

Tensile testing was performed to investigate the mechanical properties of PGDMA (Figure 4.3). Values for Young's modulus, ultimate tensile stress, and elongation at break were 1.4 ± 0.2 GPa, 51 ± 13 MPa, and 3.7 ± 0.7 %, respectively. The low elongation at break and high modulus, indicative of a stiff and brittle material, are a result of the densely crosslinked network. The modulus of PGDMA is comparable to previously reported values for the moduli of thermosets from the related, rigid, and commercially available bis-GMA and UDMA monomers (Figure 4.4) (Moduli for the related P(bis-GMA) and P(UDMA) as shown in Figure 4.4 are also ~ 1.4 GPa).[22] GMDA falls into the stiff dimethacrylate category and this can be attributed to the fused dilactone ring structure, as well as hydrogen bonding between urethane groups.

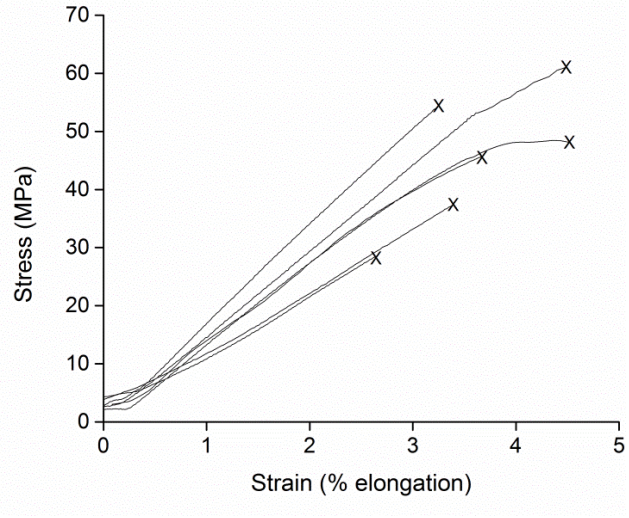

Figure 4.3. Tensile testing for various samples of PGDMA. X denotes break point and defines both the ultimate elongation and ultimate tensile strength.

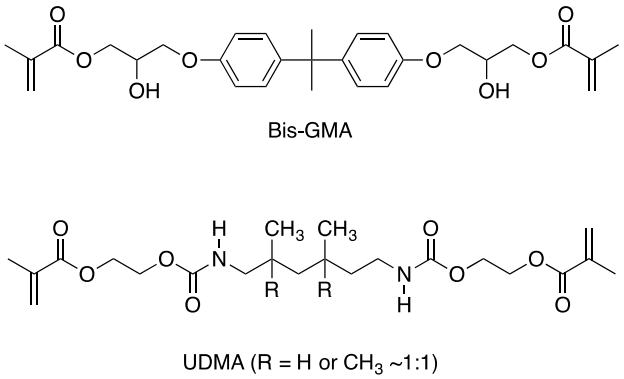

Figure 4.4. Commercially available rigid dimethacrylates bis-GMA and UDMA.

4.2.3 Degradation of PGDMA

The stability of PGDMA in aqueous environments was evaluated by submerging samples in neutral, acidic, and basic solutions and monitoring the mass of insoluble polymer over time (Figure 4.5). In 1 M NaOH, PGDMA samples readily degraded and became completely water soluble after 17 days. By contrast, PGDMA was stable in both DI H_2O and 1 M HCl. The loss of mass in basic conditions indicated that the crosslinked network eroded to yield water soluble degradation products. In acidic and neutral

conditions the final mass of PGDMA was over 100% due to swelling of the polymer network. To demonstrate the role of the dilactone in the degradation of PGDMA, the stability of poly(UDMA) (Figure 4.4) was also evaluated in the same environments. The commercially available monomer UDMA served as a structural analogue to GDMA without a dilactone core. The stability of poly(UDMA) at all conditions examined indicated the key role of the dilactone moiety in the degradation of PGDMA (and not the urethane linkage).

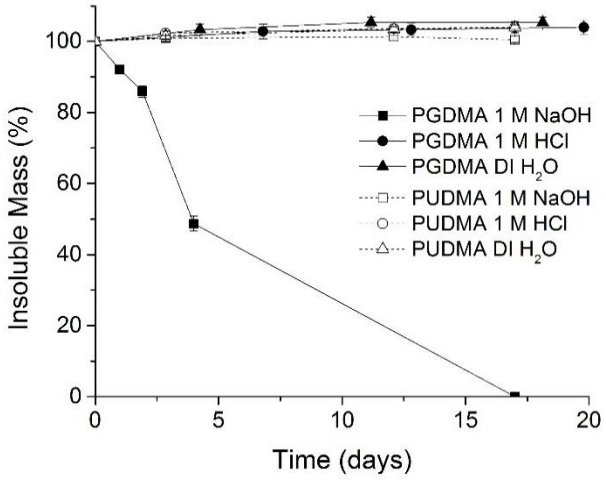

Figure 4.5. Stability of PGDMA and PUDMA in aqueous media.

To investigate the degradation products, PGDMA was degraded in 1 M NaOD/D_2O and analyzed by ^{1}H-NMR spectroscopy. Analysis of the crude degradation mixture showed the presence of 2-aminoethanol and methacrylic acid, as well as broad resonances corresponding to the methacrylic polymer backbone (Figure 4.6A). The integration area of vinyl protons from unreacted methacrylate groups compared to that of resonances corresponding to the polymer backbone gave an apparent p = 0.78. This value is higher than what was determined by FT-IR, possibly due to the remaining methacrylate groups

undergoing reaction during the degradation process. The resonances between 3.7 and 4.0 ppm are likely due to products from the degradation of the dilactone units, however the lack of resolution prevents any specific structural assignment.

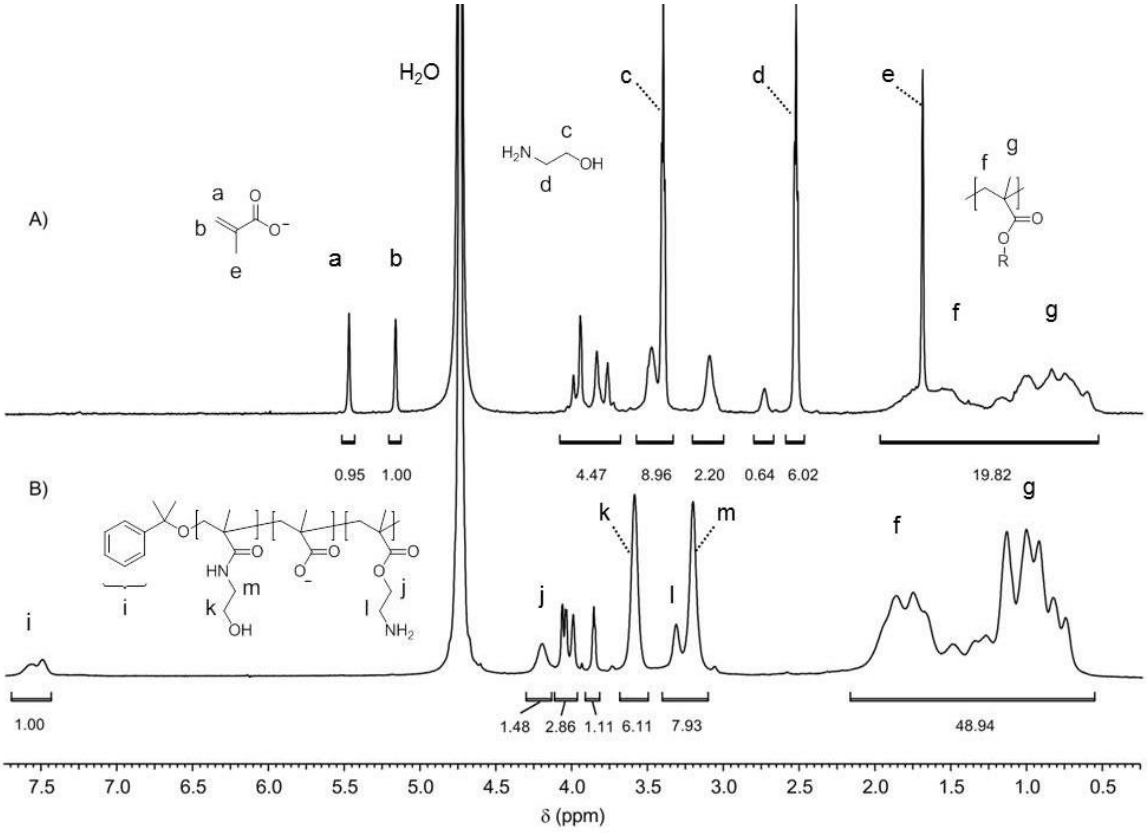

Figure 4.6. ^{1}H-NMR spectra of A) crude PGDMA degradation products (1 M NaOD, 500 MHz); B) high MW degradation products isolated by dialysis (MWCO 3.5 kg/mol) (D_2O, 500 MHz).

^{1}H-NMR data for the high molar mass component of degraded PGDMA isolated by dialysis indicates the presence of poly(2-aminoethyl methacrylate) (PAMA) and poly(2-hydroxyethyl methacrylamide) (PHEMa) repeat units (Figure 4.6B). A substoichiometric ratio of PAMA and PHEMa side chain resonances to that of the polymer backbone suggests partial hydrolysis of the methacrylate ester to a poly(methacrylic acid) (PMAA) repeat unit. Comparison of the areas for the aromatic protons of the DCP initiator fragment and the

polymer backbone gives a number average degree of polymerization (N_n) = 49. Based on these data, a proposed degradation pathway of PGDMA is outlined in Scheme 2. The degradation of the dilactone core likely proceeds by ring opening followed by scission of the urethane bond (Scheme 4.2A) analogous to that suggested by Hasimoto and co-workers.[14] As shown, the polymer structure afforded by removal of the dilactone and urethane units is PAMA. This polymer is known to degrade in basic conditions to give a combination of PHEMa, PMAA, and unaffected PAMA repeat units, as well as elimination of the small molecule 2-aminoethanol (Scheme 4.2B).[32] The presence of methacrylic acid in the crude degradation media is due to simple hydrolysis of unreacted methacrylate groups (Scheme 4.2C).

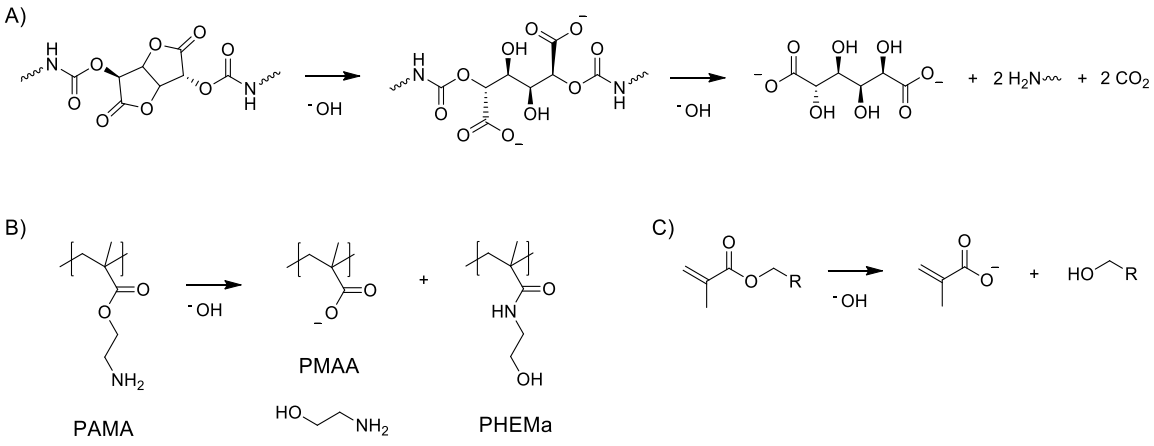

Scheme 4.2. Degradation pathways of PGDMA A) ring-opening of the dilactone followed by urethane scission, B) degradation of poly(aminoethyl methacrylate) via hydrolysis and intermolecular amidation, C) hydrolysis of unreacted methacrylate groups.

4.2.4 PGDMA and P(GDMA-*co*-MDMA) films

Given the selective degradability of PGDMA, we further investigated this material for potential film and microsphere applications. PGMDA films can be selectively degraded in base but remain stable in acidic and neutral conditions. Coatings that can be selectively

removed under specific conditions are useful in applications such as lithography and drug delivery.[28,33] Aside from using renewable feedstocks, a degradable film is appealing from a sustainability viewpoint since recycling films from consumer waste is a difficult and expensive process.[34] We initially attempted to fabricate PGDMA films by casting a solution of GDMA and DCP on to a substrate, followed by removal of the solvent and subsequent thermal curing. Conditions similar to those used for forming the bulk PGDMA material were chosen for film curing (135 °C, 20 minutes, Figure 4.10). While it was possible to fabricate PGDMA films in this manner, this approach was not ideal. For one, GDMA has poor solubility in most volatile organic solvents. Although it has good solubility in DMF and DMSO, the high boiling point of these solvents precluded their use. After screening a number of potential candidates, THF was the only suitable solvent that had a low boiling point and was capable of keeping GDMA in an amorphous state during the solvent removal stage. Also, PGDMA films exhibited slight yellowing when formed under the selected conditions (similar to the yellowing observed in the bulk PGDMA samples above). This was likely due to partial thermal decomposition of GDMA. Although the curing temperature of the PGDMA films is below the T_d of GDMA determined by TGA, it is possible that GDMA undergoes a decomposition process at elevated temperatures that is not accompanied by a loss of mass. GDL was previously reported to undergo thermal elimination in the melt at 130 °C to give the acids L-*threo*- and L-*erythro*-4-deoxyhex-4-enaro-6,3-lactone.[30] Furthermore, PGDMA film quality was variable and they often exhibited heterogeneities. This is likely due to the autopolymerization of GDMA upon melting. Differential scanning calorimetry (DSC) of GDMA without initiator

revealed a melting endotherm, followed immediately by an exotherm corresponding to polymerization (Figure 4.7). Simultaneous melting and polymerization could give rise to a heterogeneous film if unmelted fractions become entrapped by a cured polymer matrix.

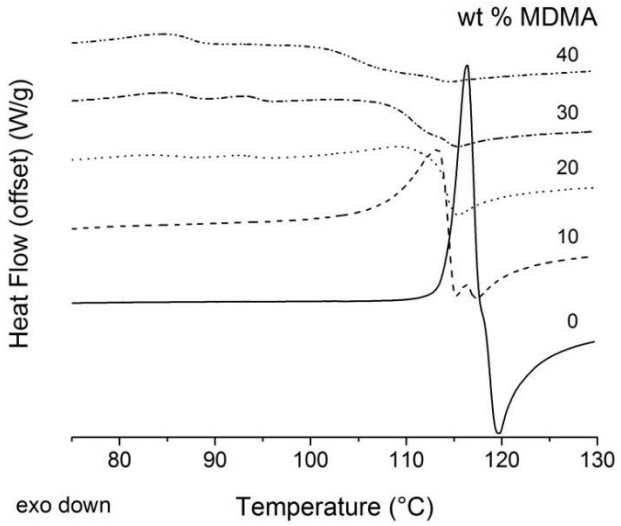

Figure 4.7. DSC traces of GDMA/MDMA mixtures ($\Delta T/t$ = 10 °C/min).

The use of a reactive diluent can address these issues above by suppressing crystallinity of the reaction mix and lowering the curing temperature. To this end, a mixture of GDMA and MDMA monomers were used for film generation. DSC traces of GDMA/MDMA mixtures show a dramatic suppression in both the melting point and the crystallinity with increasing MDMA content (Figure 4.7). At 40 wt% MDMA, the crystallinity of the mixture was almost completely suppressed and the melting point was lowered to 85 °C. Furthermore, there is baseline separation between the melting point of the mixture and the onset of autopolymerization. This indicated that a mixture of GDMA/MDMA in a 3:2 ratio could be used to make more homogeneous and clear films than those created by the homopolymerization of GDMA.

A temperature of 95 °C was selected for curing P(GDMA-*co*-MDMA) (3:2) films to ensure complete melting of the film while avoiding the onset of autopolymerization. The low crystallinity of the co-monomer mixture allowed for a wider range of appropriate casting solvents, with acetone and THF being most suitable. Due to the lower curing temperature, benzoyl peroxide (BPO) was found to be an appropriate substitute for DCP. Curing of the co-monomer films with 1.5 wt% BPO cast from acetone at 95 °C for 15 minutes gave clear homogeneous coatings without any noticeable yellowing. ATR-IR was used to determine *p* for the co-polymer films, employing the same process as used above for bulk PGDMA. Again, the values obtained using either the N-H bend or carbonyl stretch as internal standards were in good agreement, with an average value of $p = 0.50$. Although 50 % conversion is within the typical range for poly(dimethacrylates), this conversion value is noticeably lower than that observed for pure PGDMA samples. DSC modeling of the curing reaction indicated that this lower conversion value was not due to incomplete reaction time, as the exotherm of polymerization ends after approximately 8 minutes (Figure 4.8). The difference in *p* is at least partially due to the different reaction temperatures and radical initiators used to form PGDMA and the P(GDMA-*co*-MDMA) (3:2) films. Additionally, it has been shown that monomer composition can have a significant effect on the value of *p* obtained for poly(dimethacrylates).[22] Contact angle measurements indicated that the P(GDMA-*co*-MDMA) (3:2) films were moderately hydrophilic with $\theta = 78.4 \pm 0.6°$ (Figure 4.9).

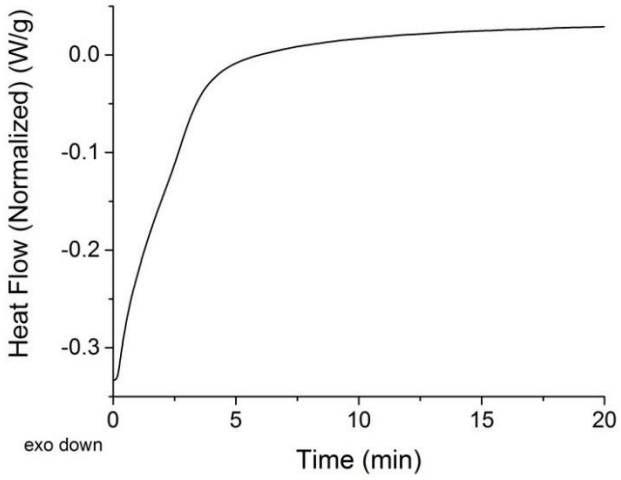

Figure 4.8. Isothermal DSC trace of GDMA:MDMA (3:2) mixture with 1.5 wt% BPO at 95 °C.

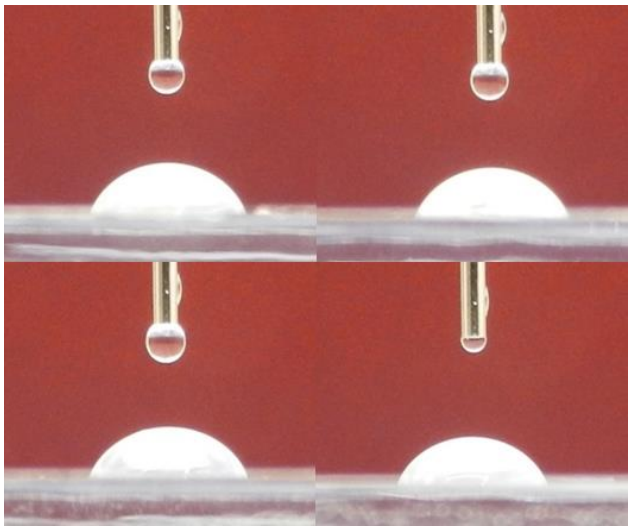

Figure 4.9. Contact angle measurements for P(GDMA-*co*-MDMA) films. Each image is of a different sample.

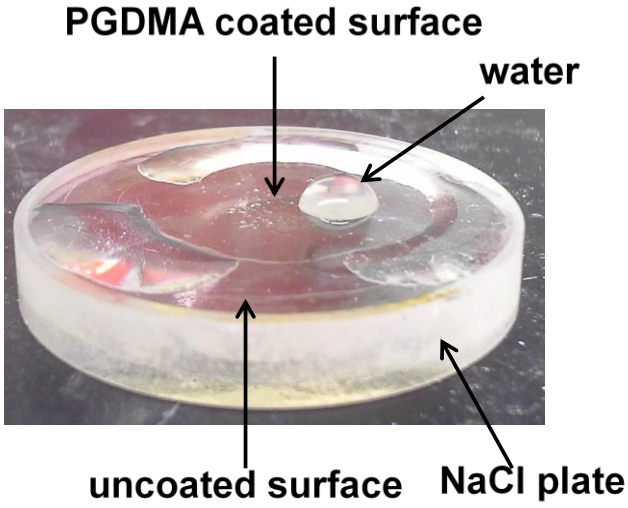

Figure 4.10. Image of a salt plate containing a PGDMA film (center circle of salt plate). The films derived from these sugar-based feedstocks demonstrate relatively clear and moderately hydrophilic coatings.

The degradability of the co-polymer films was evaluated in a similar manner to bulk PGDMA above. After being cast onto a glass slide and cured, the samples were immersed in 1 M HCl, DI H_2O, or 1 M NaOH solutions for 14 hours. The glass slides were then removed and evaluated. The co-polymer films are clear, thus, a red dye (Sudan III) was added to the solvent casting solution to aid in visual inspection of the films. After 14 hours, the samples immersed in 1 M HCl and DI H_2O remained adhered to the glass slide, while the sample immersed in 1 M NaOH completely degraded (Figure 4.11). Thus, the stability of the P(GDMA-*co*-MDMA) (3:2) films in aqueous environments was similar to that of bulk PGDMA.

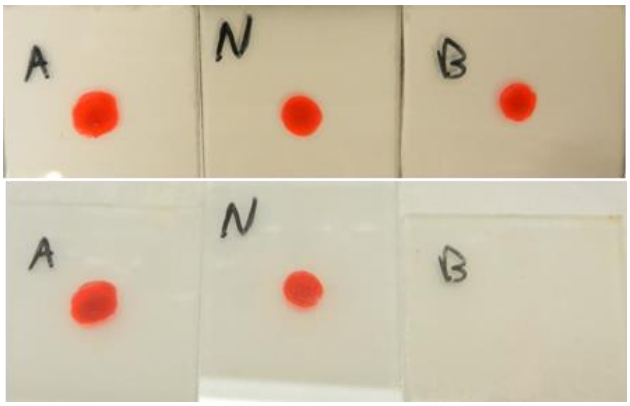

Figure 4.11. P(GDMA-*co*-MDMA) films with Sudan III dye before (top) and after (bottom) being immersed in an aqueous solution for 14 hours. A = 1 M HCl, N = DI H_2O, and B = 1 M NaOH.

4.2.5 PGDMA microspheres by precipitation polymerization

Polymer microparticles have a wide range of applications, including coatings, drug and gene delivery, biosensors, tissue engineering, nano-reactors, separations, waste water treatment, and enhanced oil recovery.[35,36] Degradable microparticles are of particular interest in the area of drug and gene delivery, whereby a therapeutic payload is released upon the removal of a polymeric carrier.[36,37] They are also useful as sacrificial templates for synthesis of more complex architectures (e.g., using a degradable core *en route* to a hollow microsphere).[36,38] Fabrication techniques for polymer microspheres include dispersion polymerization, emulsion polymerization, suspension polymerization and precipitation polymerization. The latter is an appealing option because it can afford clean, uniform polymer microspheres without the use of additives. Precipitation polymerization has been employed to fabricate a variety of microspheres with rather complex architectures.[36,39–41]

A typical formulation for a precipitation polymerization consists of a monofunctional monomer, a difunctional crosslinking monomer, radical initiator, and

solvent.[36] For thermally initiated precipitation polymerizations, particle formation is initiated by the aggregation of oligomers that form particles, which, due to the presence of difunctional monomer, have reactive vinyl groups. Subsequent particle growth occurs via the coupling of soluble radical oligomers onto the reactive surface of the growing polymer particle.[42] Since there are no ancillary components in the reaction medium during a precipitation polymerization, a variety of components affecting the solution conditions of the reaction medium must be carefully controlled, such as the ratio of monofunctional monomer to crosslinking agent, solvent composition, and monomer concentration. Polymer microspheres formed by this method are typically co-polymers, since precipitation polymerizations using only crosslinking monomer tend to give coagulum or irregular microparticles.[43–45] Although a wide range of monofunctional monomers have been used in precipitation polymerization, only very few difunctional crosslinking agents have been employed, namely divinyl benzene and ethylene glycol dimethacrylate.[36] To the best of our knowledge, no precipitation polymerization has been performed using a degradable crosslinking monomer.

To this end, we sought to fabricate polymer microspheres by precipitation polymerization using GDMA as the crosslinker. For this initial study, methyl methacrylate (MMA) was selected as the monofunctional co-monomer. THF was determined to be the best option due to its ability to solvate the monomers and avoid coagulation during the reaction. The reaction formulations are summarized in Table 4.1. All studies were performed at 70 °C without stirring in screw capped vials using AIBN as a source of free-radicals. Initial trials (entries 1–5) maintained a constant concentration of GDMA while

varying the ratio of GDMA:MMA. Reaction times greater than 3 hours under these conditions lead to coagulation, so the reaction time was limited to 2 hours. The microparticles were isolated as suspensions in THF after repeated cycles of centrifugation, decanting off the supernatant, and suspension in THF. Dynamic light scattering (DLS) results in THF show an increase in hydrodynamic diameter (D_h) with increasing MMA concentration up to 30 mol%. This trend reverses between MMA loadings of 30 and 40 mol% (trials 4 and 5), while MMA loadings of 50 mol% or greater lead to coagulum. A similar trend was previously reported for precipitation polymerizations using divinyl benzene and various monofunctional methacrylates.[44] The polydispersity index (PDI) values between 0.11 and 0.17 for trials 1-5 suggests that the particles were of relatively low dispersity. However, the irregular morphologies of these particles as determined by SEM prevented accurate size determination via imaging (Figure 4.12).

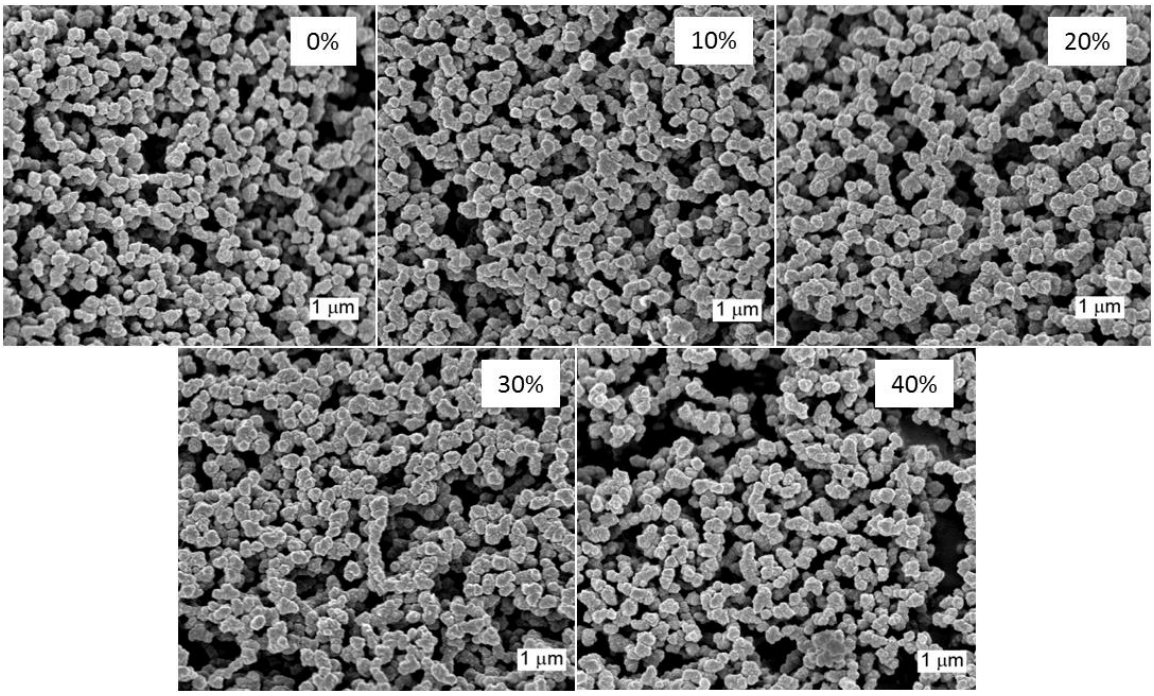

Figure 4.12. SEM images of P(GDMA-*co*-MMA) microparticles with varying mol% MMA (entries 1-5, Table 4.1).

Table 4.1. Formulations and characterization of P(GDMA-*co*-MMA) microspheres formed by precipitation polymerization.

Entry	Polym. time (h)	GDMA/MMA/AIBN mol ratio	[GDMA] (mM)	D_h [1] (nm)	D_n [2] (nm)	PDI [1]	CV [2] (%)
1	2	100/0/1.48	103	699	-	0.13	-
2	2	100/10/1.48	103	743	-	0.13	-
3	2	100/20/1.48	103	832	-	0.16	-
4	2	100/30/1.48	103	896	-	0.17	-
5	2	100/40/1.48	103	813	-	0.11	-
6 [3]	8	100/30/1.48	82.6	-	-	-	-
7	8	100/30/1.48	62.0	833	-	0.15	-
8	8	100/30/1.48	41.3	738	475	0.12	16
9	8	100/30/1.48	20.7	730	428	0.12	14

[1]Determined by DLS. [2]Coefficient of Variation, determined by SEM. [3]Coagulated by 8 h.

The irregular morphologies were likely due to the short reaction time, since longer reaction times typically give more spherically shaped particles for precipitation polymerizations.[36] However, longer reaction times lead to particle coagulation at [GDMA] = 103 mM. This issue was addressed by both lowering the concentration of monomers in solution and extending the reaction time (8 hours), while maintaining a constant ratio of GDMA:MMA of 10:3 (trials 6–9). Although a GDMA concentration of 83 mM lead to coagulation before 8 hours (trial 6), the reaction performed at GDMA concentrations of 62 mM (trial 7) gave discrete polymer microparticles. SEM images showed that these particles

had irregular morphologies similar to trials 1–5, albeit with smoother surfaces (Figure 4.13A). Further lowering the monomer concentration afforded microparticles with spherical morphologies (trials 8 and 9, Figures 4.13B and C, respectively). DLS results for trials 7–9 showed the D_h ranged from 730 to 833 nm with PDI values of 0.12–0.15, similar to what was observed for the microparticles formed at higher monomer concentrations. The diameter of the microspheres observed by SEM is significantly smaller than those determined by DLS. The difference is likely due to swelling of the microspheres in the presence of organic solvent, since DLS measurements were determined in THF while SEM was performed in the dry state. DSC of microspheres from trial 8 showed no significant thermal events, indicating that these particles are hard, rigid materials (Figure 4.14).

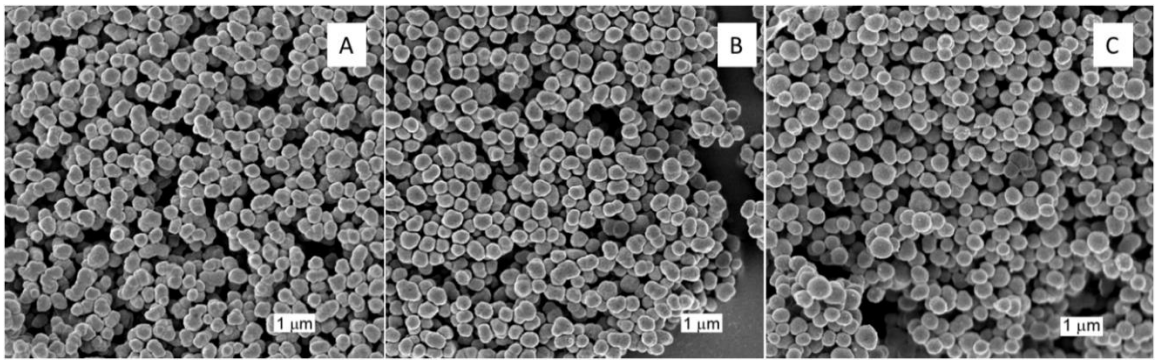

Figure 4.13. SEM images of P(GDMA-*co*-MMA) (10:3) microspheres formed at different monomer concentrations. (A) [GDMA] = 62 mM, (B) [GDMA] = 41.3 mM, (C), [GDMA] = 20.7 mM (Table 1 entries 7–9, respectively).

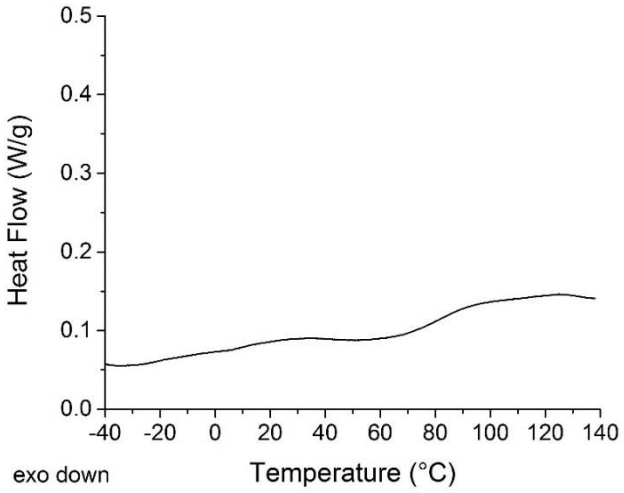

Figure 4.14. DSC of P(GDMA-*co*-MMA) microspheres (entry 8). Note scale of y-axis.

4.3 Conclusion

Herein, we have reported the synthesis of two new dimethacrylate monomers, GDMA and MDMA, containing sugar-derived dilactone cores. The route to GDMA was easily scalable and proceeded in a much higher overall yield than MDMA. Thermally initiated free radical polymerization of GDMA in the bulk yielded a highly crosslinked thermoset network, with mechanical properties comparable to reported values for commercially available stiff poly(dimethacrylates). It was shown that PGDMA degraded in a basic aqueous environment to give water soluble degradation products, but remained stable in acidic and neutral conditions. The utility of these two new monomers in coating and polymer microsphere applications was also demonstrated. For coatings, the suppression of crystallinity and melting point afforded by using a GDMA/MDMA admixture was found to be advantageous. Clear, homogenous P(GMDA-*co*-MDMA) (3:2) films were fabricated by casting a mixture of monomers and initiator in solution followed by solvent removal and thermal curing. The co-polymer films were found to have similar

degradability to that of the bulk PGDMA material. P(GDMA-*co*-MMA) microspheres were constructed via precipitation polymerization in THF. We demonstrated that a microsphere morphology could be achieved by using lower monomer concentrations and longer reaction times. Further investigation into microspheres incorporating GDMA and MDMA, including their degradation profiles, will be the focus of a future report.

4.4 Experimental

Unless otherwise noted, all chemicals were purchased from Aldrich and used without further purification. 2-isocyanatoethyl methacrylate (ICM) was purchased from TCI and used as received. GDL[30] and MDL[7,9,10] were synthesized according to previously reported procedures.

Characterization ^{1}H-NMR was performed on a Varian VI-500 and ^{13}C-NMR was performed on a Varian VI-300. FT-IR was performed on a Nicolet Magna-IR 750 spectrometer. ATR FT-IR was performed using a Bruker Alpha Platinum ATR spectrometer. High resolution mass spec was performed using a Bruker Bio-TOF II in positive mode ESI. A Perkin Elmer Pyris Diamond TG/DTA 6300 at a heating rate of 10 °C/min was used for TGA. DSC measurements were carried out using a TA Instruments Discovery DSC under N_2. Tensile testing was performed using a Minimat Tensile Tester on samples with a dog bone geometry (typical gauge dimensions 6.50x3.00x0.60 mm). SEM samples were coated with ~10 nm gold-palladium using a Denton DV-502A high vacuum deposition system and imaging was performed on a Hitachi S-900. DLS was performed using a Malvern Instrument Zetasizer Nano ZA at a concentration of ~0.1

mg/ml. Contact angle measurements were performed by imaging a drop of DI H_2O applied to a surface and measuring the contact angle using Adobe Photoshop.

D-2,5-di-O-(carbamate ethylene methacrylate)-1,4:6,3-glucarodilactone (GDMA) GDL (4.00 g, 23.0 mmol) was dissolved in dry THF (25 ml) in a flame dried flask. ICM (8.61 g, 55.6 mmol) and dibutyltin dilaurate (DBTDL) (27 μl, 46 μmol) were added to the flask. The mixture was stirred at room temperature for 4 hours, after which the precipitate was collected by filtration and thoroughly rinsed with Et_2O to give GDMA as a white crystalline powder (89%) m.p. 118 °C. ^{1}H-NMR (DMSO-d_6, 500 MHz): δ_{ppm}: 7.22 (t, *J* = 5.9 Hz, 1H), 7.17 (t, *J* = 5.6 Hz, 1H), 6.10 (d, *J* = 8.8 Hz, 2H), 5.62 (m, 2H), 5.51 (m, 2H), 5.41 (s, 1H), 4.96 (s, 1H), 4.20 (m, 4H), 3.48 (4H, multiplet), 1.90 (6H, s). ^{13}C-NMR (acetone-d_6, 90 MHz): δ_{ppm}: 171.46, 171.25, 167.53, 167.50, 156.17, 156.12, 137.20, 126.17, 126.14, 80.48, 75.89, 74.48, 68.74, 64.04, 63.96, 41.06, 40.99, 18.43. FT-IR (KBr pellet): $\upsilon_{cm^{-1}}$: 3369 (N-H), 2966 (C-H), 1783 (lactone C=O), 1733 (C=O), 1635 (methacrylate C=C), 1546 (N-H). MS (ESI-TOF, *m/z*) Calcd. for $C_{20}H_{24}N_2O_{12}$: 484.1329; found: 507.1243 ($M + Na^+$); error 4.3 ppm.

D-2,5-di-O-(carbamate ethylene methacrylate)-1,4:6,3-mannarodilactone (MDMA) MDL (332 mg, 1.91 mmol) was dissolved in a 50/50 (v/v) mix of DMF and THF (10 ml). ICM (2.0 ml, 14 mmol) and DBTDL (5 μl, 10 μmol) were added and the reaction was left to stir at room temperature for 24 hrs. The solvent was then removed under reduced pressure without heating and the crude product was recrystallized from an ethyl acetate/hexanes solvent pair to give a white crystalline powder (54%). ^{1}H-NMR (DMSO-d_6, 500 MHz): δ_{ppm}: 8.06 (t, *J* = 5.7 Hz, 2H), 6.07 (s, 2H), 5.94 (d, *J* = 6.1 Hz, 2H), 5.68 (s,

2H), 5.37 (d, *J* = 6.1 Hz, 2H), 4.11 (t, *J* = 8.5 Hz, 4H), 3.33 (t, *J* = 8.5 Hz, 4H), 1.88 (s, 6H). ^{13}C-NMR (acetone-d_6, 90 MHz): δ_{ppm}: 170.63, 167.50, 155.54, 137.22, 126.11, 75.89, 70.30, 64.11, 41.02, 18.43. MS (ESI-TOF, *m/z*) Calcd. for $C_{20}H_{24}N_2O_{12}$: 484.1329; found: 507.1221 ($M + Na^+$); error 1.2ppm.

Poly(GDMA) (PGDMA). GDMA and DCP (1.5 wt%) were dissolved in CH_2Cl_2 with stirring and the solvent was removed by rotary evaporation. The resulting powder (approx. 90 mg) was loaded into the stainless steel tensile bar mold between two Teflon inserts and heated in an oven at 135 °C. After 30 minutes, the sample was removed from the mold and allowed to cool. FT-IR (KBr pellet): $\upsilon_{cm^{-1}}$: 3376 (N-H), 2969 (C-H), 1805 (lactone C=O), 1735 (C=O), 1635 (C=C), 1537 (N-H).

P(GDMA-*co*-MDMA) (3:2) films. Polymer films were fabricated using a solvent casting method. A 3:2 mixture of GDMA:MDMA and benzoyl peroxide (1.5 wt%) were dissolved in acetone (0.10 g/ml). The solution was applied dropwise to a glass slide and the solvent was removed under reduced pressure. The film was then cured in an oven under ambient atmosphere and pressure at 95 °C for 20 min to give clear homogenous films. ATR-IR (neat): $\upsilon_{cm^{-1}}$: 3347 (N-H), 2956 (C-H), 1796 (lactone C=O), 1713 (C=O), 1635 (C=C), 1527 (N-H).

PGDMA microspheres by precipitation polymerization. A sample procedure is as follows: GDMA (10 mg) and AIBN (0.1 mg) were dissolved in dry THF (1 ml) in a 2 dram screw cap vial. The vial was then placed in thermostated sand bath at 70 °C and allowed to sit without stirring for an allotted amount of time. The milky white suspension was diluted with THF (5 ml), centrifuged (1 min @ 6500 rpm), and the supernatant removed by

decanting. Two more iterations of the dilution/centrifuge/decanting process were performed to remove any soluble impurities. ATR-IR (thin film THF): $\upsilon_{cm^{-1}}$: 3349 (N-H), 2949 (C-H), 1797 (lactone C=O), 1724 (C=O), 1630 (C=C), 1531 (N-H).

Hydrolytic stability. The stability of PGDMA in DI H_2O and 1M HCl and PUDMA in 1M NaOH was evaluated as follows: three parallel samples of polymer (typical dimensions 6.45x5.50x0.60 mm, ~50 mg) were immersed in the appropriate aqueous solution (10 ml) and allowed to sit undisturbed at room temperature. The samples were periodically removed, blotted dry, weighed, and reimmersed in the same solution.

For the stability of PGDMA in 1M NaOH, three parallel samples of PGDMA (typical dimensions 6.45x5.50x0.60 mm, ~50 mg) for each time point were immersed in solution (10 ml) and allowed to sit undisturbed at room temperature. At each time point the insoluble mass was collected by filtration, dried in a vacuum oven at 50 °C overnight and weighed. Degraded samples for NMR analysis were prepared by immersing PGDMA in a 1 M NaOD in D_2O solution until the mixture became homogeneous.

Crosslink density and network parameter. Three parallel samples of PGDMA (typical dimensions 6.45x5.50x0.60 mm, ~50 mg) were weighed (m_1) and subjected to soxhlet extraction by CH_2Cl_2 for 24 hours to remove the soluble fraction. The samples were then dried in a vacuum oven overnight at 50 °C and weighed (m_2). The crosslink density (a) and network parameter (M_c) were calculated according to equations 1 and 2,[22] where p is the fractional conversion determined by FT-IR and M_0 is the molecular weight of GDMA.

$$a = \frac{2pm_1 - m_2}{pm_1}$$ Eq. 1

$$M_c = M_0/a$$ Eq. 2

4.5 References

(1) Lichtenthaler, F. Carbohydrates as organic raw materials. *Ullmann's Encycl. Ind. Chem.* **2010**, 583–616.

(2) Fenouillot, F.; Rousseau, A.; Colomines, G.; Saint-Loup, R.; Pascault, J.-P. *Prog. Polym. Sci.* **2010**, *35*, 578–622.

(3) Scott, A. *Chem. Eng. News* **2012**, *90*, 27–29.

(4) Gandini, A. *Green Chem.* **2011**, *13*, 1061–1083.

(5) Werpy, T.; Petersen, G. *Top Value Added Chemicals from Biomass. Volume I—Results of Screening for Potential Candidates from Sugars and Synthesis Gas*; 2004.

(6) Hashimoto, K.; Okada, M.; Honjou, N. *Die Makromol. Chemie, Rapid Commun.* **1990**, *11*, 393–396.

(7) Hashimoto, K.; Wibullucksanakul, S.; Matsuura, M.; Okada, M. *J. Polym. Sci. Part A Polym. Chem.* **1993**, *31*, 3141–3149.

(8) Kiely, D.; Chen, L.; Lin, T. *J. Am. Chem. Soc.* **1994**, *116*, 571–578.

(9) Liu, Y.; Reineke, T. M. *J. Am. Chem. Soc.* **2005**, *127*, 3004–3015.

(10) Kiely, D. E.; Chen, L.; Lin, T. *J. Polym. Sci. Part A Polym. Chem.* **2000**, *38*, 594–603.

(11) Liu, Y.; Reineke, T. M. *Biomacromolecules* **2010**, *11*, 316–325.

(12) Wibullucksanakul, S.; Hashimoto, K.; Okada, M. *Macromol. Chem. Phys.* **1997**, *198*, 305–319.

(13) Wibullucksanakul, S.; Hashimoto, K.; Okada, M. *Macromol. Chem. Phys.* **1996**, *197*, 1865–1876.

(14) Hashimoto, K.; Wibullucksanakul, S.; Okada, M. *J. Polym. Sci. Part A Polym. Chem.* **1995**, *33*, 1495–1503.

(15) Kloosterboer, J. G. *Adv. Polym. Sci.* **1988**, *84*, 1–61.

(16) Vlakh, E. G.; Tennikova, T. B. *J. Chromatogr. A* **2009**, *1216*, 2637–2650.

(17) Sideridou, I. D.; Achilias, D. S.; Karava, O. *Macromolecules* **2006**, *39*, 2072–2080.

(18) Scranton, A. B.; Bowman, C. N.; Klier, J.; Peppas, N. A. *Polymer (Guildf).* **1992**, *33*, 1683–1689.

(19) Andrzejewska, E. *Prog. Polym. Sci.* **2001**, *26*, 605–665.

(20) Sideridou, I.; Tserki, V.; Papanastasiou, G. *Biomaterials* **2002**, *23*, 1819–1829.

(21) Bowman, C. N.; Peppas, N. A. *Macromolecules* **1991**, *24*, 1914–1920.

(22) Sideridou, I.; Tserki, V.; Papanastasiou, G. *Biomaterials* **2003**, *24*, 655–665.

(23) Kurdikar, D.; Peppas, N. *Macromolecules* **1994**, *27*, 4084–4092.

(24) Themistou, E.; Patrickios, C. S. *Macromolecules* **2007**, *40*, 5231–5234.

(25) De Clercq, R. R.; Goethals, E. J. *Macromolecules* **1992**, *25*, 1109–1113.

(26) Ogino, K.; Chen, J.-S.; Ober, C. K. *Chem. Mater.* **1998**, *10*, 3833–3838.

(27) Muggli, D.; Burkoth, A.; Keyser, S. *Macromolecules* **1998**, *98*, 4120–4125.

(28) Palmieri, F.; Adams, J.; Long, B.; Heath, W.; Tsiartas, P.; Willson, C. G. *ACS Nano* **2007**, *1*, 307–312.

(29) Anseth, K. S.; Quick, D. J. *Macromol. Rapid Commun.* **2001**, *22*, 564–572.

(30) Gehret, T. C.; Frobese, A. S.; Zerbe, J. S.; Chenault, H. K. *J. Org. Chem.* **2009**, *74*, 8373–8376.

(31) Barszczewska-Rybarek, I.; Gibas, M.; Kurcok, M. *Polymer (Guildf).* **2000**, *41*, 3129–3135.

(32) Thompson, K. L.; Read, E. S.; Armes, S. P. *Polym. Degrad. Stab.* **2008**, *93*, 1460–1466.

(33) Kim, B.; Park, S.; Hammond, P. *ACS Nano* **2008**, *2*, 386–392.

(34) Schmitz, P.; Siegfried, J. Films. *Ullmann's Encycl. Ind. Chem.* **2000**, 649–676.

(35) Thorne, J. B.; Vine, G. J.; Snowden, M. J. *Colloid Polym. Sci.* **2011**, *289*, 625–646.

(36) Li, G. L.; Möhwald, H.; Shchukin, D. G. *Chem. Soc. Rev.* **2013**, *42*, 3628–3646.

(37) Elsabahy, M.; Wooley, K. *Chem. Soc. Rev.* **2012**, *41*, 2545–2561.

(38) Fu, G.-D.; Li, G. L.; Neoh, K. G.; Kang, E. T. *Prog. Polym. Sci.* **2011**, *36*, 127–167.

(39) Li, W.; Stöver, H. *J. Polym. Sci. Part A Polym. Chem.* **1998**, *36*, 1543–1551.

(40) Li, W.; Stöver, H. *Macromolecules* **2000**, *33*, 4354–4360.

(41) Li, G.; Yang, X. *J. Phys. Chem. B* **2007**, *111*, 12781–12786.

(42) Downey, J.; Frank, R.; Li, W.; Stöver, H. *Macromolecules* **1999**, *32*, 2838–2844.

(43) Saraçoğlu, B.; Uğuzdoğan, E.; Gölgelioğlu, C.; Tuncel, A. *Ind. Eng. Chem. Res.* **2009**, *48*, 4844–4851.

(44) Li, W.; Stöver, H. *J. Polym. Sci. Part A Polym. Chem.* **1999**, *37*, 2899–2907.

(45) Jiang, J.; Zhang, Y.; Guo, X.; Zhang, H. *Macromolecules* **2011**, *44*, 5893–5904.

Bibliography

Abenhaïm, D.; Loupy, A.; Munnier, L.; Tamion, R.; Marsais, F.; Quéguiner, G. *Carbohydr. Res.* **1994**, *261* (2), 255–266.

Ahmed, I.; Khan, N. A.; Mishra, D. K.; Lee, J. S.; Hwang, J. S.; Jhung, S. H. *Chem. Eng. Sci.* **2013**, *93*, 91–95.

Andrzejewska, E. *Prog. Polym. Sci.* **2001**, *26*, 605–665.

Anseth, K. S.; Quick, D. J. *Macromol. Rapid Commun.* **2001**, *22*, 564–572.

Barrett, A.; Braddock, D. C. *Chem. Commun.* **1997**, *10*, 351–352.

Barszczewska-Rybarek, I.; Gibas, M.; Kurcok, M. *Polymer (Guildf).* **2000**, *41*, 3129–3135.

Bates, F. S.; Fredrickson, G. H. *Phys. Today* **1999**, *52* (2), 32–38.

Beghdadi, S.; Miladi, I. A.; Ben Romdhane, H.; Bernard, J.; Drockenmuller, E. *Biomacromolecules* **2012**, *13* (12), 4138–4145.

Blauer, R. *Sugar : World Markets and Trade*; 2014.

Benedek, I. *Pressure-Sensitive Adhesives and Applications*; CRC Press, 2004.

Berini, C.; Lavergne, A.; Molinier, V.; Capet, F.; Deniau, E.; Aubry, J.-M. *European J. Org. Chem.* **2013**, *2013* (10), 1937–1949.

Besset, C.; Pascault, J.-P.; Fleury, E.; Drockenmuller, E.; Bernard, J. *Biomacromolecules* **2010**, *11* (10), 2797–2803.

Besset, C.; Bernard, J.; Fleury, E.; Pascault, J. P.; Cassagnau, P.; Drockenmuller, E.; Williams, R. J. J. *Macromolecules* **2010**, *43*, 5672–5678.

Beyler, C. L.; Hirschler, M. M. In *SFPE Handbook of Fire Protection Engineering*; DiNenno, P. J., Ed.; 2001; pp 110–131.

Bowman, C. N.; Peppas, N. A. *Macromolecules* **1991**, *24*, 1914–1920.

Boyer, C.; Stenzel, M.; Davis, T. *J. Polym. Sci. Part A Polym. Chem.* **2011**, *49*, 551–595.

Brandrup, J.; Immergut, E.; Grulke, E.; Abe, A.; Bloch, D. *Polymer handbook*, 4th ed.;

1999; Vol. 49.

Cekovic, Z.; Tokic, Z. *Synthesis* **1989**, 610–612.

Chong, Y.; Krstina, J.; Le, T.; Moad, G. *Macromolecules* **2003**, *60*, 2256–2272.

Chrysanthos, M.; Galy, J.; Pascault, J. P. *Polymer* **2011**, *52* (16), 3611–3620.

Creton, C. *MRS Bull.* **2003**, *28* (06), 434–439.

De Clercq, R. R.; Goethals, E. J. *Macromolecules* **1992**, *25*, 1109–1113.

Delidovich, I.; Hausoul, P. J. C.; Deng, L.; Pfützenreuter, R.; Rose, M.; Palkovits, R. *Chem. Rev.* **2016**, *116* (3), 1540–1599.

Ding, K.; John, A.; Shin, J.; Lee, Y.; Quinn, T.; Tolman, W. B.; Hillmyer, M. a. *Biomacromolecules* **2015**, *85* (10), 150727093921007.

Downey, J.; Frank, R.; Li, W.; Stöver, H. *Macromolecules* **1999**, *32*, 2838–2844.

Dufour, B.; Koynov, K.; Pakula, T.; Matyjaszewski, K. *Macromol. Chem. Phys.* **2008**, *209*, 1686–1693.

Elias, H.-G.; Mülhaupt, R. In *Ullmann's Encyclopedia of Industrial Chemistry*; Wiley-VCH Verlag GmbH & Co. KGaA: Weinheim, Germany, 2015; Vol. 38, pp 1–70.

Elsabahy, M.; Wooley, K. *Chem. Soc. Rev.* **2012**, *41*, 2545–2561.

Favier, A.; Charreyre, M.; Chaumont, P.; Pichot, C. *Macromolecules* **2002**, *35* (22), 8271–8280.

Favier, A.; Charreyre, M.-T. *Macromol. Rapid Commun.* **2006**, *27* (9), 653–692.

Feng, X.; East, A. J.; Hammond, W. B.; Zhang, Y.; Jaffe, M. *Polym. Adv. Technol.* **2011**, *22* (1), 139–150.

Fenouillot, F.; Rousseau, A.; Colomines, G.; Saint-Loup, R.; Pascault, J. P. *Prog. Polym. Sci.* **2010**, *35* (5), 578–622.

Ferriol, M.; Gentilhomme, A.; Cochez, M.; Oget, N.; Mieloszynski, J. L. *Polym. Degrad. Stab.* **2003**, *79* (2), 271–281.

Fiebach, K.; Grimm, D. In *Ullmann's Encyclopedia of Industrial Chemistry*; Wiley-VCH Verlag GmbH & Co. KGaA: Weinheim, Germany, 2000; Vol. 9, pp 245–260.

Flèche, G.; Huchette, M. *Starch - Stärke* **1986**, *38* (1), 26–30.

Fu, G.-D.; Li, G. L.; Neoh, K. G.; Kang, E. T. *Prog. Polym. Sci.* **2011**, *36*, 127–167.

Fuji, M.; Akita, M.; Tanaka, T. Polycarbonate copolymer and method of producing the same. US20100190953 A1, 2010.

Galbis, J. A.; García-Martín, M. G. *Top. Curr. Chem.* **2010**, *295* (1), 147–176.

Gallagher, J. J.; Hillmyer, M. A.; Reineke, T. M. *ACS Sustain. Chem. Eng.* **2015**, *3* (4), 662–667.

Gandini, A. *Green Chem.* **2011**, *13* (5), 1061–1083.

Ge, J.; Trujillo, M.; Stansbury, J. *Dent. Mater.* **2005**, *21* (12), 1163–1169.

Gehret, T. C.; Frobese, A. S.; Zerbe, J. S.; Chenault, H. K. *J. Org. Chem.* **2009**, *74* (21), 8373–8376.

Gregory, A.; Stenzel, M. H. *Prog. Polym. Sci.* **2012**, *37* (1), 38–105.

Gu, C.; Dubay, M. R.; Severtson, S. J.; Gwin, L. E. *Ind. Eng. Chem. Res.* **2014**, *53* (27), 11000–11006.

Haloi, D. J.; Ata, S.; Singha, N. K.; Jehnichen, D.; Voit, B. *ACS Appl. Mater. Interfaces* **2012**, *4* (8), 4200–4207.

Hamada, K.; Ishiura, K.; Takahashi, T.; Sachie. PROCESS FOR POLYMERIZING A METHACRYLIC ESTER OR AN ACRYLIC ESTER. US 6,767,976 B2, 2004.

Hashimoto, K.; Wibullucksanakul, S.; Matsuura, M.; Okada, M. *J. Polym. Sci. Part A Polym. Chem.* **1993**, *31* (12), 3141–3149.

Hashimoto, K.; Okada, M.; Honjou, N. *Die Makromol. Chemie, Rapid Commun.* **1990**, *11*, 393–396.

Hashimoto, K.; Wibullucksanakul, S.; Okada, M. *J. Polym. Sci. Part A Polym. Chem.* **1995**, *33*, 1495–1503.

Hiemenz, P. C.; Lodge, T. P. *Polymer Chemistry, Second Edition*; Taylor & Francis, 2007.

Holmberg, A. L.; Reno, K. H.; Wool, R. P.; Epps Iii, T. H. *Soft Matter* **2014**, *10* (38), 7405–7424.

Hong, J.; Radojčić, D.; Ionescu, M.; Petrović, Z. S.; Eastwood, E. *Polym. Chem.* **2014**, *5*, 5360–5368.

Howard, S.; Hagberg, E.; Rockafellow, E. Method for quantitative analysis of sugars, sugar alcohols and related dehydration products. US 20130337570.

Ishihara, K.; Kubota, M.; Kurihara, H.; Yamamoto, H. *J. Am. Chem. Soc.* **1995**, *117* (15), 4413–4414.

Ishihara, K.; Kubota, M. *J. Org. Chem.* **1996**, *3263* (12), 4560–4567.

Isikgor, F. H.; C. Remzi Becer. *Polym. Chem.* **2015**, *6*, 4497–4559.

Jiang, J.; Zhang, Y.; Guo, X.; Zhang, H. *Macromolecules* **2011**, *44*, 5893–5904.

Kiely, D. E.; Chen, L.; Lin, T. *J. Polym. Sci. Part A Polym. Chem.* **2000**, *38*, 594–603.

Kiely, D.; Chen, L.; Lin, T. *J. Am. Chem. Soc.* **1994**, *116*, 571–578.

Kim, B.; Park, S.; Hammond, P. *ACS Nano* **2008**, *2*, 386–392.

Kloosterboer, J. G. *Adv. Polym. Sci.* **1988**, *84*, 1–61.

Kobayashi, H.; Yokoyama, H.; Feng, B.; Fukuoka, A. *Green Chem.* **2015**, *17* (5), 2732–2735.

Kola, R.; von Elsner, O.; Riepe, W.; Reuter, K. In *Ullmann's Encyclopedia of Industrial Chemistry*; Wiley-VCH Verlag GmbH & Co. KGaA: Weinheim,

Koyama, H.; Tsutsumi, K. Polymerizable monomer polymeric compound resin compositions for photoresist and method for producing semiconductor. wo 2004113404, 2004.

Krantz, J. C.; Carr, J. C.; Forman, S.; Ellis, F. W. *J. Pharmacol. Exp. Ther.* **1939**, *67*, 187–190.

Keddie, D. J. *Chem. Soc. Rev.* **2014**, *43* (2), 496–505.

Kobayashi, S.; Sugiura, M. *Chem. Rev.* **2002**, *102* (6), 2227–2302.

Kobayashi, S. *European J. Org. Chem.* **1999**, No. 1992, 15–27.

Kurdikar, D.; Peppas, N. *Macromolecules* **1994**, *27*, 4084–4092.

Lee, S.; Lee, K.; Kim, Y.-W.; Shin, J. *ACS Sustain. Chem. Eng.* **2015**, *3* (9), 2309–2320.

Lemieux, R.; McInnes, A. *Can. J. Chem.* **1960**, *38* (1), 136–140.

Li, G. L.; Möhwald, H.; Shchukin, D. G. *Chem. Soc. Rev.* **2013**, *42*, 3628–3646.

Li, W.; Stöver, H. *J. Polym. Sci. Part A Polym. Chem.* **1998**, *36*, 1543–1551.

Li, W.; Stöver, H. *Macromolecules* **2000**, *33*, 4354–4360.

Li, G.; Yang, X. *J. Phys. Chem. B* **2007**, *111*, 12781–12786.

Li, W.; Stöver, H. *J. Polym. Sci. Part A Polym. Chem.* **1999**, *37*, 2899–2907.

Lichtenthaler, F. Carbohydrates as organic raw materials. *Ullmann's Encycl. Ind. Chem.* **2010**, 583–616.

Liu, Y.; Reineke, T. M. *J. Am. Chem. Soc.* **2005**, *127* (9), 3004–3015.

Liufu, S.-C.; Xiao, H.-N.; Li, Y.-P. *Polym. Degrad. Stab.* **2005**, *87* (1), 103–110.

Mahalik, J. P.; Madras, G. *Ind. Eng. Chem. Res.* **2005**, *44* (12), 4171–4177.

Malic, N.; Evans, R. a. *Aust. J. Chem.* **2006**, *59* (10), 763–771.

Mansoori, Y.; Hemmati, S.; Eghbali, P.; Zamanloo, M. R.; Imanzadeh, G. *Polym. Int.* **2013**, *62* (2), 280–288.

Matyjaszewski, K. *Macromolecules* **2012**, *45* (10), 4015–4039.

Moad, G.; Rizzardo, E.; Thang, S. H. *Aust. J. Chem.* **2012**, *65* (8), 985.

Moineau, C.; Minet, M.; Teyssié, P.; Jérôme, R. *Macromolecules* **1999**, 8277–8282.

Motoyoshi, T.; Imazato, K.; Yamanaka, K. Polycarbonate resin. US 9096710 B2, 2015.

Muggli, D.; Burkoth, A.; Keyser, S. *Macromolecules* **1998**, *98*, 4120–4125.

Nakamura, Y.; Adachi, M.; Tachibana, Y.; Sakai, Y.; Nakano, S.; Fujii, S.; Sasaki, M.; Urahama, Y. *Int. J. Adhes. Adhes.* **2009**, *29* (8), 806–811.

Ogino, K.; Chen, J.-S.; Ober, C. K. *Chem. Mater.* **1998**, *10*, 3833–3838.

Ohara, T.; Sato, T.; Shimizu, N.; Prescher, G.; Schwind, H.; Weiberg, O.; Marten, K.;

Greim, H. *Ullmann's Encycl. Ind. Chem.* **2011**, *060* (10 C), 1–18.

Ono, A.; Toyohara, K.; Minematsu, H.; Kageyama, Y. Polycarbonate and process for producing the same. US 7,365,148 B2, 2008.

Oshita, S.; Chapman, B. K.; Hirata, K. J. *PSTC Tape Summit 2012*, Boston, May, 2012.

Palmieri, F.; Adams, J.; Long, B.; Heath, W.; Tsiartas, P.; Willson, C. G. *ACS Nano* **2007**, *1*, 307–312.

Perrier, S.; Barner-Kowollik, C.; Quinn, J. F.; Vana, P.; Davis, T. P. *Macromolecules* **2002**, *35* (22), 8300–8306.

Pion, F.; Reano, A. F.; Ducrot, P.-H.; Allais, F. *RSC Adv.* **2013**, *3* (23), 8988–8997.

Pu, G.; Hauge, D. A.; Gu, C.; Zhang, J.; Severtson, S. J.; Wang, W.; Houtman, C. J. *Macromol. React. Eng.* **2013**, *7* (10), 515–526.

Pu, G.; Dubay, M. R.; Zhang, J.; Severtson, S. J.; Houtman, C. J. *Ind. Eng. Chem. Res.* **2012**, *51* (37), 12145–12149.

Roquette. *ROQUETTE reinforces its position as world leader in ISOSORBIDE for the performance plastics and chemistry markets ROQUETTE*; 2015.

Rose, M.; Palkovits, R. *ChemSusChem* **2012**, *5* (1), 167–176.

Sadler, J. M.; Nguyen, A. P. T.; Toulan, F. R.; Szabo, J. P.; Palmese, G. R.; Scheck, C.; Lutgen, S.; La Scala, J. J. *J. Mater. Chem. A* **2013**, *1* (40), 12579–12586.

Saraçoğlu, B.; Uğuzdoğan, E.; Gölgelioğlu, C.; Tuncel, A. *Ind. Eng. Chem. Res.* **2009**, *48*, 4844–4851.

Sato, K.; Kodama, K. Positive-working far-UV photoresists. JP 2004341062, 2004.

Schmitz, P.; Siegfried, J. Films. *Ullmann's Encycl. Ind. Chem.* **2000**, 649–676.

Scott, A. *C&EN* **2014**, *90* (27), 16–17.

Scranton, A. B.; Bowman, C. N.; Klier, J.; Peppas, N. A. *Polymer (Guildf).* **1992**, *33*, 1683–1689.

Shaikh, A. L.; Kale, A. S.; Shaikh, M. A.; Puranik, V. G.; Deshmukh, A. R. A. S. *Tetrahedron* **2007**, *63* (16), 3380–3388.

Shearouse, W. C.; Lillie, L. M.; Reineke, T. M.; Tolman, W. B. *ACS Macro Lett.* **2015**, *4* (3), 284–288.

Shin, S.; Kim, B.-C. C.; Chang, E.; Cho, J. K.; Suh, D. H. *RSC Adv.* **2014**, *4* (12), 6226.

Shin, J.; Martello, M. T.; Shrestha, M.; Wissinger, J. E.; Tolman, W. B.; Hillmyer, M. A. *Macromolecules* **2011**, *44* (1), 87–94.

Sideridou, I. D.; Achilias, D. S.; Karava, O. *Macromolecules* **2006**, *39*, 2072–2080.

Sideridou, I.; Tserki, V.; Papanastasiou, G. *Biomaterials* **2002**, *23*, 1819–1829.

Sideridou, I.; Tserki, V.; Papanastasiou, G. *Biomaterials* **2003**, *24*, 655–665.

Stoss, P.; Merrath, P.; Schlüter, G. *Synthesis* **1987**, *1987* (2), 174–176.

Stoss, P. Process for the production of isosorbide-5-nitrate. US 4,371,703, 1983.

Themistou, E.; Patrickios, C. S. *Macromolecules* **2007**, *40*, 5231–5234.

Thompson, K. L.; Read, E. S.; Armes, S. P. *Polym. Degrad. Stab.* **2008**, *93*, 1460–1466.

Thorne, J. B.; Vine, G. J.; Snowden, M. J. *Colloid Polym. Sci.* **2011**, *289*, 625–646.

Tong, J. D.; Jerome, R. *Polymer* **2000**, *41*, 2499–2510.

Tullo, A. H. *Chem. Eng. News* **2013**, *91* (46), 18–19.

Tundo, P.; Aricò, F.; Gauthier, G.; Rossi, L.; Rosamilia, A. E.; Bevinakatti, H. S.; Sievert, R. L.; Newman, C. P. *ChemSusChem* **2010**, *3* (5), 566–570.

Van Buu, O. N.; Aupoix, A.; Hong, N. D. T.; Vo-Thanh, G. *New J. Chem.* **2009**, *33* (10), 2060–2072.

Vendamme, R.; Schüwer, N.; Eevers, W. *J. Appl. Polym. Sci.* **2014**, *131* (17), 8379–8394.

Vendamme, R.; Eevers, W. *Macromolecules* **2013**, *46* (9), 3395–3405.

Vlakh, E. G.; Tennikova, T. B. *J. Chromatogr. A* **2009**, *1216*, 2637–2650.

Werpy, T.; Petersen, G. *Top Value Added Chemicals from Biomass. Volume I—Results of Screening for Potential Candidates from Sugars and Synthesis Gas*; 2004.

Wibullucksanakul, S.; Hashimoto, K.; Okada, M. *Macromol. Chem. Phys.* **1997**, *198*,

305–319.

Willcock, H.; O'Reilly, R. K. *Polym. Chem.* **2010**, *1* (2), 149–157.

Xu, M.; Wang, W.; Xia, L.; Lin, G. *J. Org. Chem.* **2001**, *66* (11), 3953–3962.

Yamaguchi, A.; Sato, O.; Mimura, N.; Shirai, M. *Catal. Commun.* **2015**, *67* (2), 59–63.

Yang, H. W. H.; Chang, E.-P. *Trends Polym. Sci.* **1997**, *5* (11), 380–384.

Zhang, J.; Wang, L.; Liu, F.; Meng, X.; Mao, J.; Xiao, F.-S. *Catal. Today* **2015**, *242*, 249–254.

Zhang, J.; Li, J.; Wu, S.-B.; Liu, Y. *Ind. Eng. Chem. Res.* **2013**, *52* (34), 11799–

Global Ethylene Capacity and Capital Expenditure Outlook http://www.acutemarketreports.com/report/global-ethylene-capacity-and-capital-expenditure-outlook-rosneft-and-shell-lead-ethylene-capacity-growth (accessed Mar 23, 2016).

Global PET Supply to Exceed 24.39 Mln Tonnes in 2015 http://mcgroup.co.uk/news/20140117/global-pet-supply-exceed-2439-mln-tonnes-2015.html (accessed Mar 23, 2016).

Global Sorbitol Market http://www.transparencymarketresearch.com/sorbitol-market.html (accessed Mar 23, 2016).

The International Pharmacopoeia. 19th WHO Model List of Essential Medicines http://www.who.int/medicines/organization/par/edl/expcom13/eml13_en.pdf (accessed Mar 23, 2016).

Lactic Acid And Poly Lactic Acid (PLA) Market Analysis By Application (Packaging, Agriculture, Transport, Electronics, Textiles) And Segment Forecasts To 2020 http://www.grandviewresearch.com/industry-analysis/lactic-acid-and-poly-lactic-acid-market (accessed Mar 23, 2016).

Mitsubishi Chemical. World-First — DURABIO™, Bio-based Engineering Plastic from Mitsubishi Chemical, Used on the Front Panel of Sharp's New AQUOS CRYSTAL 2 Smartphone http://www.m-kagaku.co.jp/english/newsreleases/00258.html (accessed Jan 1, 2016).

Mitsubishi Chemical. New biobased engineering plastic "DURABIO" http://www.m-kagaku.co.jp/english/products/business/polymer/sustainable/details/1194667_3255.html (accessed Jan 1, 2016).

Natureworks. Product and Applications http://www.natureworksllc.com/Product-and-Applications (accessed Mar 23, 2016).

Roquette. Polycarbonates http://www.roquette-performance-plastics.com/polycarbonate/ (accessed Mar 23, 2016).

Appendix

A.1 AMI and AAI in unsaturated polyester and vinyl ester resins

The low volatility of AAI and AMI and the high T_g of their respective polymers make them promising candidates as styrene replacements in unsaturated polyester (UP) and vinyl ester (VE) resins (Figure A1). UP and VE resins are typically mixed with glass fiber fillers to prepare thermoset polymer composites for use in applications in automotive, marine, construction, and electrical industries.[1] These resins have a relatively high volatile organic content from their use of styrene as a reactive diluent. Therefore, the use of non-volatile alternatives would mitigate associated health and environmental hazards.[2,3]

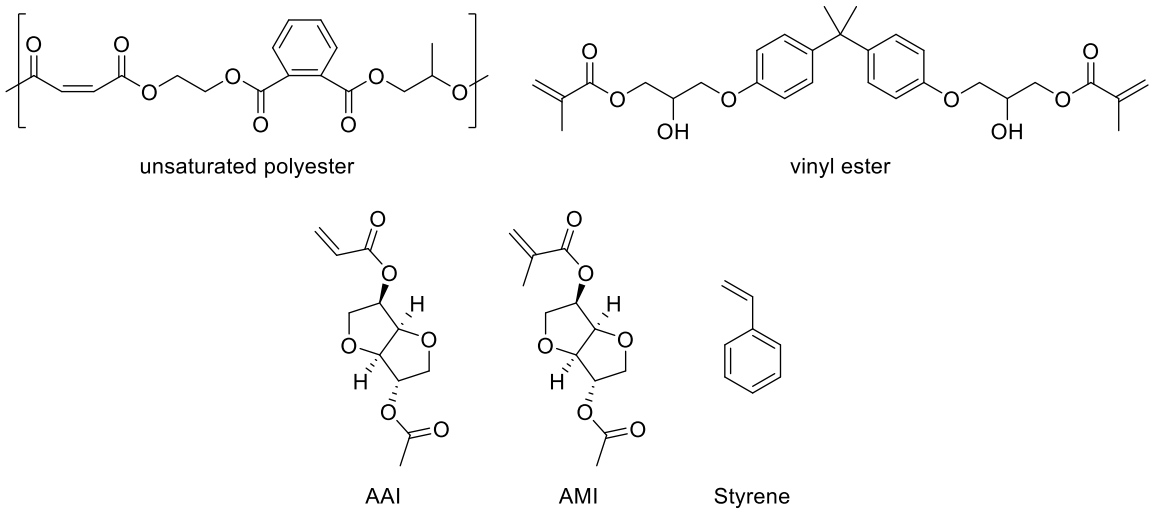

Figure A1. Unsaturated polyester, vinyl ester, and reactive monomers used in UP and VE resins.

Cured and post cured resins showed nearly full conversion of monomer by FT-IR with residual unreacted UP vinyl groups (Figure A2). Thermal characterization of the cured resin samples is summarized in Table A1. Values of T_d and T_g for AAI and styrene based samples were nearly identical, while those of the cured sample from AMI were all lower.

The samples differed noticeably in optical properties (Figure A3). Cured samples prepared with styrene and AAI did not exhibit any discoloration, while yellowing was observed in the samples prepared with AMI. The styrene based samples were slightly opaque while those from AAI were remarkably clear. A significant difference in resin viscosity was observed across the three samples. The resin formulated with AMI had a high viscosity and flowed very slowly at room temperature. The AAI based resin was tacky and did not flow at all at room temperature, possibly due to the crystallinity of AAI and low miscibility between AAI and the UP. This made preparing molded samples either very difficult in the case of AMI or nearly impossible in the case of AAI. As a result, mechanical testing was not practical.

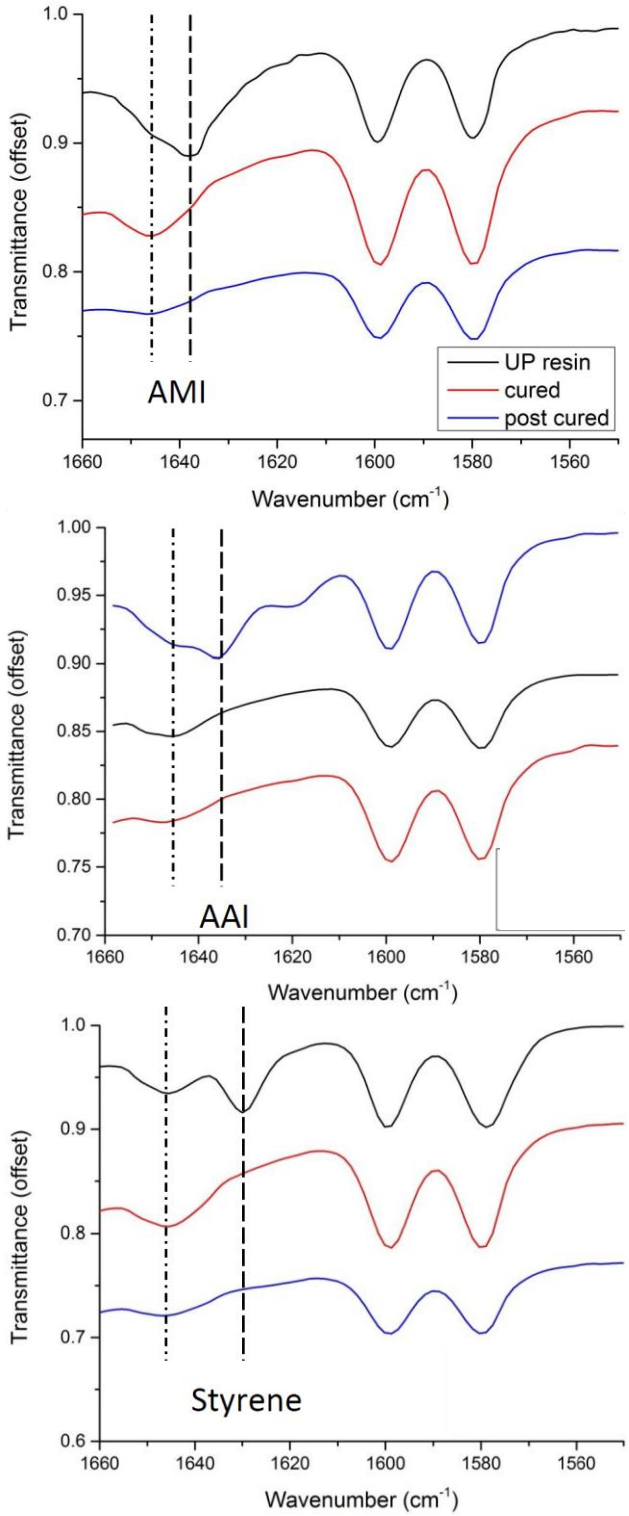

Figure A2. FT-IR spectra of UP resins with AMI, AAI, or styrene. Dashed line corresponds to the monomer vinyl stretch, dotted dashed line corresponds to unsaturated polyester vinyl stretch.

Table A1. Summary of cured UP resins.

Reactive monomer	Gel fraction[a]	T_d, air[b] (°C)	T_d, N_2[b] (°C)	T_g[c] (°C)
AMI	0.69	228	242	24
AAI	0.89	257	253	38
Styrene	0.71	253	227	38

[a]Determined by extraction with CH_2Cl_2 for 24 h, rinsing, and drying to constant mass. Values are averages of triplicate; [b]Determined by TGA, 5% mass loss, heating rate = 10 °C min^{-1}; [c]Determined by DSC, second heat, heating rate = 10 °C min^{-1}.

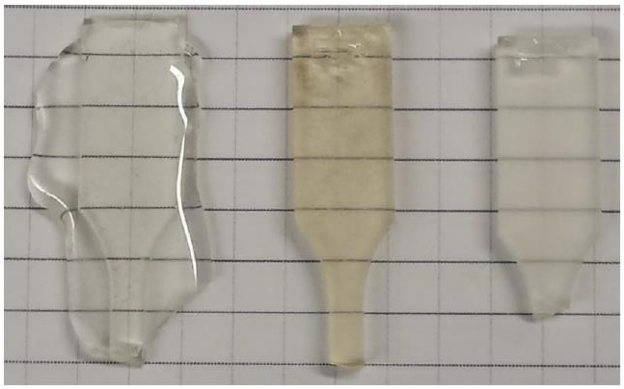

Figure A3. Cured UP resin samples prepared with (from left to right): AAI, AMI, and styrene.

AMI was also evaluated as a reactive monomer for VE resins. As was observed with UP resins, the viscosity of the VE resin prepared with AMI had a high viscosity and could not be processed at room temperature. A cured VE resin with AMI was prepared instead using the procedure for the UP resins. However, this approach was quickly abandoned as mixing the VE and AMI required the addition and subsequent removal of solvent which was deemed counterproductive in terms of reducing the volatile organic content of the resin. To address the issue of miscibility and viscosity of the AMI VE resin, a formulation was prepared with ethylene glycol dimethacrylate (EGDMA) as a reactive diluent (VE:EGDMA:AMI = 27.5:27.5:45 by weight). The resultant resin was easily

prepared without the need for added solvent and had a viscosity qualitatively similar to that of the styrene VE resin. Furthermore, EGDMA is not expected to contribute significantly to the volatile organic content of the resin as it has a reported boiling point of ~240–275 °C.

FT-IR of the cured VE resins showed nearly full conversion of monomer and VE (Figure A4). The properties of the cured VE resins are summarized in Table A2. T_d of the styrene based sample was significantly higher, likely due to the relatively low thermal stability of PAMI. The cured styrene based samples were remarkably robust and did not break under the tensile testing conditions used. Typical values of Young's modulus, stress at break, and strain at break for a cured VE resin sample are E = 3.2 GPa, δ_b = 86 MPa, and ε_b = 5%, respectively, according to the manufacturer. The cured AMI+EGDMA samples exhibited relatively lower modulus and stress at break than typically reported for cured styrene VE resins. Nevertheless, these results are encouraging as the values are on the same order of magnitude. It is expected that a similar approach of using a low viscosity reactive diluent could also be applied to the UP resins. In summary, AMI and AAI show promise as reactive monomers in UP and VE resins provided that issues with high resin viscosity can be overcome.

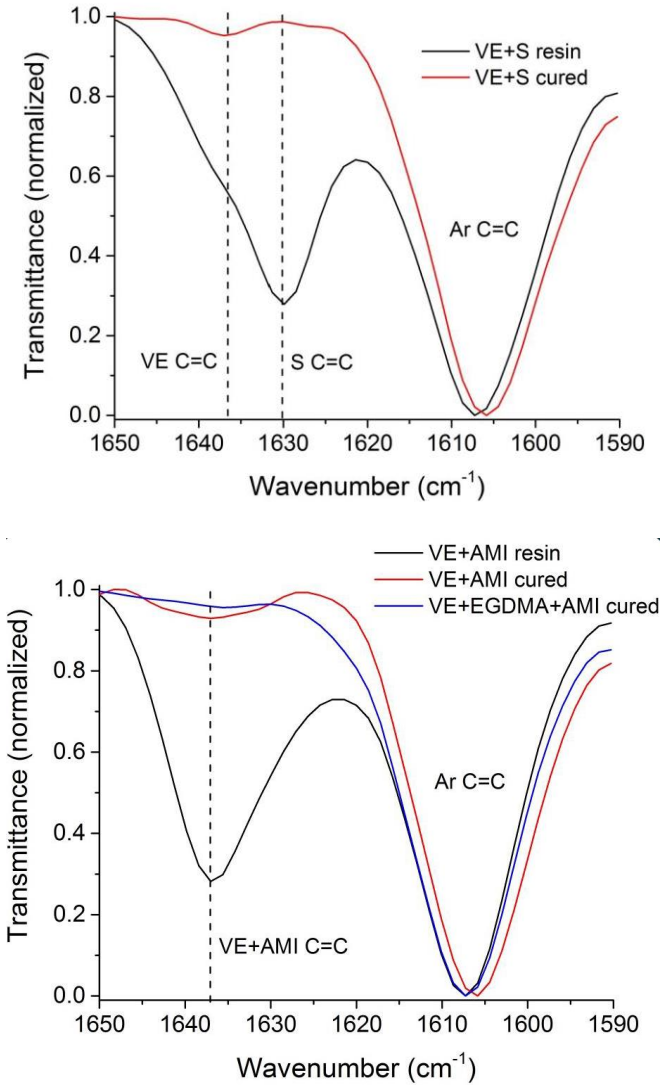

Figure A4. FT-IR spectra of vinyl ester resins with styrene or AMI.

Table A2. Summary of cured VE resins.

Reactive monomer	Gel fraction[a]	T_d, air[b] (°C)	T_g[c] (°C)	E (GPa)	δ_b (MPa)	ε_b %
AMI+EGDMA	1.02	267	n.o.	1.2 ± 0.1	41 ± 17	6.7 ± 4
styrene	1.03	341	106	>1.7*	>60*	n.o.

[a]Determined by extraction with CH_2Cl_2 for 24 h, rinsing, and drying to constant mass. Values are averages of triplicate; [b]Determined by TGA, 5% mass loss, heating rate = 10 °C min^{-1}; [c]Determined by DSC, second heat, heating rate = 10 °C min^{-1}; n.d. = not determined; n.o. = not observed; *samples did not break during tensile testing.

A.2 Experimental

VE and UP were provided by Ashland. AMI and AAI were prepared from *exo*-acetyl isosorbide according to the literature.[4,5] All other chemicals were purchased from Sigma and used without further purification.

Characterization. Gel fractions were determined in triplicate by extraction with CH_2Cl_2 for 24 h, rinsing, and drying to constant mass. FT-IR was performed using a Bruker Alpha Platinum ATR spectrometer. Thermogravimetric analysis (TGA) was performed on a TA Instruments Q500 at a heating rate of 10 °C min^{-1}. Differential scanning calorimetry (DSC) measurements were carried out using a TA Instruments Discovery DSC under N_2. T_g values were determined on the second heating at a heating rate of 10 °C min^{-1}. Tensile testing was performed on a Shimadzu ASGX at a strain rate of 5 mm min^{-1}.

UP resin curing. UP resins were prepared according to the following formula: 65:35 UP:monomer by weight, 1 parts per hundred resin (phr) benzoyl peroxide, 0.1 phr t-butyl peroxybenzoate. The resin was then poured into a silicone mold and cured for 2 h each at 49 °C, 71 °C, and 93 °C followed by post curing for 2 h at 138 °C.

VE resin curing. VE resins were prepared according to the following formula: 55:45 VE:monomer by weight, 0.46 phr cobalt naphthenate (6% in mineral spirits), 1.94 phr 2-butanone peroxide (Luperox® DDM 9, ~35 wt% solution). The resin was poured to a silicone mold and allowed to cure under ambient conditions for 24 h followed by 2 h at 120 °C under vacuum.

A.3 References

(1) Krämer, H. In *Ullmann's Encyclopedia of Industrial Chemistry*; Wiley-VCH Verlag GmbH & Co. KGaA: Weinheim, Germany, 2000; pp 623–649.

(2) Cousinet, S.; Ghadban, A.; Fleury, E.; Lortie, F.; Pascault, J. P.; Portinha, D. *Eur. Polym. J.* **2015**, *67*, 539–550.

(3) Sadler, J. M.; Nguyen, A. P. T.; Toulan, F. R.; Szabo, J. P.; Palmese, G. R.; Scheck, C.; Lutgen, S.; La Scala, J. J. *J. Mater. Chem. A* **2013**, *1* (40), 12579–12586.

(4) Gallagher, J. J.; Hillmyer, M. A.; Reineke, T. M. *ACS Sustainable Chem. Eng.* **2015**, *3* (4), 662–667.

(5) Gallagher, J. J.; Hillmyer, M. A.; Reineke, T. M. *ACS Sustainable Chem. Eng.* **2016**, *Just accepted*. DOI: 10.1021/acssuschemeng.6b00455